**Title**
Supernovae as Dark Matter Signals



**Author**
Janish, Ryan

**Publication Date**
2020

Peer reviewed|Thesis/dissertation

# Supernovae as Dark Matter Signals

by

Ryan Janish

A dissertation submitted in partial satisfaction of the

requirements for the degree of

Doctor of Philosophy

in

Physics

in the

Graduate Division

of the

University of California, Berkeley

Committee in charge:

Professor Surjeet Rajendran, Co-chair
Professor Lawrence J. Hall, Co-chair
Professor Hitoshi Murayama
Professor Chung-Pei Ma

Spring 2020

Supernovae as Dark Matter Signals

Abstract

Supernovae as Dark Matter Signals

by

Ryan Janish

Doctor of Philosophy in Physics

University of California, Berkeley

Professor Surjeet Rajendran, Co-chair

Professor Lawrence J. Hall, Co-chair

The empirical study of ultraheavy dark matter (DM) requires astrophysical probes. We present here a detailed study of DM-induced type Ia supernovae as one such probe. Dark matter may heat a small region in a white dwarf (WD) sufficient to trigger runaway fusion and ignite a supernova. We consider DM candidates that heat through the production of high-energy standard model (SM) particles, and show that such particles efficiently thermalize the WD medium and ignite supernovae. Based on the existence of long-lived WDs and the observed supernovae rate, we put new constraints on ultra-heavy DM candidates with masses above $10^{16}$ GeV that produce SM particles through annihilation, decay, and DM-SM scattering in the stellar medium. As a concrete example, this rules out supersymmetric Q-ball DM in parameter space complementary to terrestrial bounds. We further consider the possibility of DM capture by WDs, leading to the formation and self-gravitational collapse of a DM core within the star. This process allows two additional mechanisms for DM-induced particle heating, which we study here. For asymmetric DM, such a core may form a black hole that ignites a supernovae via Hawking radiation. For DM with a sufficiently small but nonzero annihilation cross section the core may cause ignition via a burst of annihilation during gravitational collapse. These processes are sensitive to much less massive candidates, down to $10^7$ GeV, than are the mechanisms involving a single DM particle. It is also intriguing that these DM-induced ignition scenarios provide an alternative mechanism of triggering supernovae from sub-Chandrasekhar mass progenitors.

To my grandparents,
Gary, Nancy, George, and Etta

# Contents

# List of Figures

# Acknowledgments

I want to thank my advisor, Surjeet Rajendran, for always encouraging my creativity and exploration of new ideas. His example as a researcher has shaped my development as a physicist for the better, and his advice and guidance have been invaluable. I also want to thank Chung-Pei Ma, my advisor during my first few years of graduate school. I learned a tremendous amount working with her in astronomy, and gained a perspective that has been consistently useful in my current work in particle phenomenology. There are many other professors whose guidance I have benefited from here at Berkeley, and I am grateful to them all. I am particularly indebted to Lawrence Hall for his generous advice and assistance, and to Hitoshi Murayama and Dan McKinsey for serving on my committee. I am also deeply grateful to Anne Takizawa, Donna Sakima, Joelle Miles, LaVern Navarro, and the entire staff of the Physics Department for all of their generous support over the years.

Much of my work in graduate school has been done in collaboration with Paul Riggins and Vijay Narayan. Working with them has been a joy and a privilege, and I will remember fondly the many hours we struggled and laughed together. There are many other collaborators and friends that I am grateful to have met at Berkeley. I have learned much from working alongside post-docs and my fellow students, and their conversation and camaraderie has enriched my time here. I am particular grateful to have collaborated with Harikrishnan Ramani, who has truly helped me to grow as a physicist. And I am deeply thankful to have met Kaylan and Sean Burleigh in my first year, whose friendship has been a constant blessing to me and my family.

I want to thank my parents for their tireless work in raising me and for the encouragement they have given me throughout my life, without which I likely would never have begun graduate school. I also want to thank my wife's parents, whose visits have brightened our time here. I am supremely grateful for my daughter Eleanor, and I thank her for the many late night opportunities she graciously provided for me to think about physics while rocking and feeding. Her very existence has brought so much joy and clarity to my life, and I will always remember this place not just as my home during graduate school but as the place of her birth. And above all, I want to thank my wife Amanda. None of this work would have been possible without her, and I am forever grateful for her love and support. This journey has been much happier for having shared it with her.

# Chapter 1

# Introduction

The unknown nature of Dark Matter (DM) remains, in my view, the most pressing and interesting unresolved question in physics. After decades of work there is much that we do understand of both its interactions and history, yet there remains many unknowns. We do not know if DM has any non-gravitational interactions with Standard Model (SM) particles, and we do not know if DM consists of a single elementary particle species or a complex array of particles with their own rich structure of interactions and bound states. Perhaps the most striking quantitative statement of our ignorance is in the unknown value of the mass of DM, which is only constrained to be within a range of roughly 88 orders of magnitude [1] [2].

The best strategy for detecting DM has been to postulate candidate models which satisfy all known observational constraints, identify empirical signatures of the candidate models, and then search for those signatures. The best-known of these candidates are perhaps the weakly interacting massive particle (WIMP) and the QCD axion, for which extensive, unsuccessful searches have been made [3] [4]. Detection efforts for these and other candidates continue, and while we may remain optimistic, it is perhaps not surprising in light of the vast possible variety of allowed DM candidates that direct detection has remained elusive. The candidates are many, but the searches are few.

A particularly challenging possibility is that of ultraheavy DM. Because the average DM mass density is known, the corresponding number density must scale inversely with candidate DM mass. For sufficiently large masses, the local flux of DM is low enough that terrestrial searches are ineffective and the only observable DM signals are astrophysical. To empirically test this scenario, it is thus important to understand the possible phenomena arising from DM interactions in astrophysical systems and whether observations of these phenomena may be used to constrain or detect ultraheavy DM.

This dissertation focuses on one such phenomenon, the ignition of type Ia supernovae by DM-induced particle heating. Chapter 2, which is adapted from the paper [5] written in collaboration with Peter W. Graham, Vijay Narayan, Surjeet Rajendran, and Paul Riggins, focuses on the ignition mechanism of particle heating. We consider the possibility that DM may, through some interaction with a white dwarf (WD), produce high-energy standard model particles within the star. We study the scattering of those particles with the stellar

medium of the WD and its associated energy transfer, identifying the conditions under which they heat the medium sufficient to trigger runaway thermonuclear fusion and produce a type Ia supernova. We identify several means by which a single DM particle may produce a supernova in this manner, and then use the observations of supernovae and the ages of WDs to place limits on the non-gravitational interactions of ultraheavy DM.

Chapter 3, adapted from the paper [6] written in collaboration with Vijay Narayan and Paul Riggins, continues the study of DM-induced particle heating by introducing several new mechanisms by which DM may produce high-energy SM particles. We study the generic possibility that DM is captured in a WD and forms a central DM core which eventually collapses under self-gravity. The collapsing core may then produce SM particles via a burst of DM-DM annihilations, or by forming a black hole which emits SM particles as Hawking radiation. In these mechanisms, the energy available for heating the stellar medium is given by the total accumulated mass of DM rather than that of a single transiting DM particle. This allows constraints to be placed on DM candidates of much smaller mass than those considered in [5].

# Chapter 2

# White Dwarfs as Dark Matter Detectors

Dark matter that is capable of sufficiently heating a local region in a white dwarf will trigger runaway fusion and ignite a type Ia supernova. This was originally proposed by Graham et al. and used to constrain primordial black holes which transit and heat a white dwarf via dynamical friction. In this paper, we consider dark matter (DM) candidates that heat through the production of high-energy standard model (SM) particles, and show that such particles will efficiently thermalize the white dwarf medium and ignite supernovae. Based on the existence of long-lived white dwarfs and the observed supernovae rate, we derive new constraints on ultra-heavy DM with masses greater than $10^{16}$ GeV which produce SM particles through DM-DM annihilations, DM decays, and DM-SM scattering interactions in the stellar medium. As a concrete example, we place bounds on supersymmetric Q-ball DM in parameter space complementary to terrestrial bounds. We put further constraints on DM that is captured by white dwarfs, considering the formation and self-gravitational collapse of a DM core which heats the star via decays and annihilations within the core. It is also intriguing that the DM-induced ignition discussed in this work provide an alternative mechanism of triggering supernovae from sub-Chandrasekhar, non-binary progenitors.

## 2.1 Introduction

Identifying the nature of dark matter (DM) remains one of the clearest paths beyond the Standard Model (SM) and it is thus fruitful to study the observable signatures of any yet-allowed DM candidate. Many direct detection experiments are designed to search for DM, e.g. [7, 8], yet these lose sensitivity to heavier DM due to its diminished number density. Even for a strongly-interacting candidate, if the DM mass is above $\sim 10^{22}$ GeV a terrestrial detector of size $\sim (100\text{ m})^2$ will register fewer than one event per year. While these masses are large compared to those of fundamental particles, it is reasonable to suppose that DM may exist as composite states just as the SM produces complex structures with mass much

larger than fundamental scales (e.g., you, dear reader). Currently there is a wide range of unexplored parameter space for DM candidates less than $\sim 10^{48}$ GeV, above which the DM will have observable gravitational microlensing effects [9]. For such ultra-heavy DM, indirect signatures in astrophysical systems are a natural way forward. One such signal first proposed in [10] is that DM can trigger runaway fusion and ignite type Ia supernovae (SN) in sub-Chandrasekhar white dwarf (WD) stars.

In addition to constraining the properties of DM, this raises the intriguing possibility that DM-induced runaway fusion is responsible for a fraction of observed astrophysical transients. The progenitors of type Ia SN are not fully understood [11], and recent observations of sub-Chandrasekhar [12, 13], hostless [14], and unusual type Ia SN [15] suggest that multiple progenitor systems and ignition mechanisms are operative. Other suspected WD thermonuclear events, such as the Ca-rich transients [16], are also poorly understood. While mechanisms for these events have been proposed [17, 18, 19, 20], the situation is yet unclear and it is worthwhile to consider new sources of thermonuclear ignition.

Runaway thermonuclear fusion requires both a heating event and the lack of significant cooling which might quench the process. The WD medium is particularly suited to this as it is dominated by degeneracy pressure and undergoes minimal thermal expansion, which is the mechanism that regulates fusion in main sequence stars. Thermal diffusion is the primary cooling process in a WD, and it can be thwarted by heating a large enough region. The properties of a localized heating necessary to trigger runaway fusion were computed in [21]. Consequently, it was realized [10] that if DM is capable of sufficiently heating a WD in this manner, it will result in a SN with sub-Chandrasekhar mass progenitor. This was used to place limits on primordial black holes which transit a WD and cause heating by dynamical friction, although the authors of [10] identify several other heating mechanisms which may be similarly constrained. Note that the idea of using observations of WDs to constrain DM properties has been pursued before, e.g. through an anomalous heating of cold WDs [22, 23] or a change in the equilibrium structure of WDs with DM cores [24]. These are quite distinct from the observational signature considered in this work, which is the DM trigger of a type Ia SN (although see [25] for a related analysis).

In this paper, we examine DM candidates which have additional non-gravitational interactions and are thus capable of heating a WD and igniting a SN through the production of SM particles. An essential ingredient in this analysis is understanding the length scales over which SM particles deposit energy in a WD medium. We find that most high energy particles thermalize rapidly, over distances shorter than or of order the critical size for fusion. Particle production is thus an effective means of igniting WDs. Constraints on these DM candidates come from either observing specific, long-lived WDs or by comparing the measured rate of type Ia SN with that expected due to DM. It is important to note that these constraints are complementary to direct searches—it is more massive DM that is likely to trigger SN, but also more massive DM that has low terrestrial flux. The WD detector excels in this regime due to its large surface area $\sim (10^4 \text{ km})^2$, long lifetime $\sim$ Gyr, and high density. We demonstrate these constraints for generic classes of DM models that produce SM particles via DM-SM scattering, DM-DM collisions, or DM decays, and consider the significantly en-

hanced constraints for DM that is captured in the star. For these cases, we are able to place new bounds on DM interactions for masses greater than $m_\chi \gtrsim 10^{16}$ GeV. As a concrete example we consider ultra-heavy Q ball DM as found in supersymmetric extensions of the SM.

The rest of the paper is organized as follows. We begin in Section 2.2 by reviewing the mechanism of runaway fusion in a WD. In Section 2.3 we study the heating of a WD due to the production of high-energy SM particles. Detailed calculations of the stopping of such particles are provided in Appendix A. In Section 2.4 we parameterize the explosiveness and event rate for generic classes of DM-WD encounters, and in Section 2.5 we derive schematic constraints on such models. The details of DM capture in a WD are reserved for Appendix B. Finally we specialize to the case of Q-balls in Section 2.6, and conclude in Section 2.7.

## 2.2 White Dwarf Runaway Fusion

We first review the conditions for which a local energy deposition in a WD results in runaway fusion. Any energy deposit will eventually heat ions within some localized region—parameterize this region by its linear size $L_0$, total kinetic energy $\mathcal{E}_0$ and typical temperature $T_0$. These scales evolve in time, but it will be useful to describe a given heating event by their initial values.

The fate of a heated region is either a nonviolent diffusion of the excess energy across the star, or a runaway fusion chain-reaction that destroys the star. The precise outcome depends on $L_0$, $\mathcal{E}_0$ and $T_0$. There is a critical temperature $T_f$, set by the energy required for ions to overcome their mutual Coulomb barrier, above which fusion occurs. For carbon burning, $T_f \sim$ MeV [26]. Any heated region $T_0 > T_f$ will initially support fusion, although this is not sufficient for runaway as cooling processes may rapidly lower the temperature below $T_f$. This cooling will not occur if the corresponding timescale is larger than the timescale at which fusion releases energy. Cooling in a WD is dominated by thermal diffusion, and the diffusion time increases as the size of the heated region. However, the timescale for heating due to fusion is independent of region size. Thus, for a region at temperature $\gtrsim T_f$, there is a critical size above which the heated region does not cool but instead initiates runaway. For a region at the critical fusion temperature $T_f$, we call this critical size the *trigger size* $\lambda_T$. The value of $\lambda_T$ is highly dependent on density, and in a WD is set by the thermal diffusivity of either photons or degenerate electrons. This critical length scale has been computed numerically in [21] for a narrow range of WD densities and analytically scaled for other WD masses in [10]. As in [10], we will restrict our attention to carbon-oxygen WDs in the upper mass range $\sim 0.85 - 1.4\ M_\odot$ (these will yield the most stringent constraints on DM). This corresponds to a central number density of ions $n_{\rm ion} \sim 10^{30} - 10^{32}$ cm$^{-3}$ and a trigger size of $\lambda_T \sim 10^{-3} - 10^{-5}$ cm.

If a heated region is smaller than the trigger size, its thermal evolution is initially dominated by diffusion. However, this will still result in runaway fusion if the temperature is of order $T_f$ by the time the region diffuses out to the trigger size. For our purposes it is more

natural to phrase this in terms of the total energy $\mathcal{E}_0$ deposited during a heating event. Of course, the relation between energy $\mathcal{E}_0$ and temperature $T_0$ depends on the rate at which WD constituents—ions, electrons, and photons—thermalize with each other within the region size $L_0$. Given that the different species thermalize rapidly, the excess energy required to raise the temperature to $T_f$ in a volume $V$ is given by a sum of their heat capacities

$$\frac{\mathcal{E}_0}{V} \gtrsim \int_0^{T_f} dT(n_{\rm ion} + n_e^{2/3}T + T^3), \tag{2.1}$$

where $n_e$ is the number density of electrons. Note that we use the heat capacity of a degenerate gas of electrons, since the Fermi energy $E_F \gtrsim$ MeV for the densities we consider. The minimum energy deposit necessary to trigger runaway fusion is simply

$$\mathcal{E}_{\rm boom} \sim \lambda_T^3(n_{\rm ion}T_f + n_e^{2/3}T_f^2 + T_f^4) \approx 10^{16} - 10^{23}\ \text{GeV}. \tag{2.2}$$

$\mathcal{E}_{\rm boom}$ is shown over the range of WD masses in Figure 2.1, where we have employed a numerical formulation of the WD mass-density relation as given by [27]. Once again, for a given WD density the critical energy threshold is primarily set by $\lambda_T$—this length scale has been carefully computed and tabulated in [21], along with the attendant assumptions. In any case, we expect the simplified expression (2.2) to be accurate at the order of magnitude level, and we refrain from a more detailed analysis here. Thus for a heating event characterized by its $L_0$, $\mathcal{E}_0$, and $T_0 \gtrsim T_f$, there is an *ignition condition*:

$$\mathcal{E}_0 \gtrsim \mathcal{E}_{\rm boom} \cdot \max\left\{1, \frac{L_0}{\lambda_T}\right\}^3. \tag{2.3}$$

Any $\mathcal{E}_0$ satisfying this condition is minimized for $L_0$ less than the trigger size, where it is also independent of the precise value of $L_0$. For broader deposits, the necessary energy is parametrically larger than $\mathcal{E}_{\rm boom}$ by a volume ratio $(L_0/\lambda_T)^3$. As a result, understanding the $L_0$ for different kinds of heating events in a WD is critical to determining whether or not they are capable of destroying the star.

## 2.3 Particle Heating of White Dwarfs

Production of high-energy SM particles in a WD will result in heating of the stellar medium. The critical quantity to understand is the length scale over which such heating occurs—this scale determines the efficiency of the heating event in triggering runaway fusion, as described by condition (2.3). Note that this is a question of purely SM physics. The unknown physics of DM will serve only to set the initial properties of the SM particles.

We find that SM particles efficiently heat the WD regardless of species or energy (neutrinos are a slight exception)—the heating length is typically less than or of order the trigger size $\lambda_T$. This is accomplished primarily through hadronic showers initiated by collisions with carbon ions. In some cases electromagnetic showers are important, however at high energies

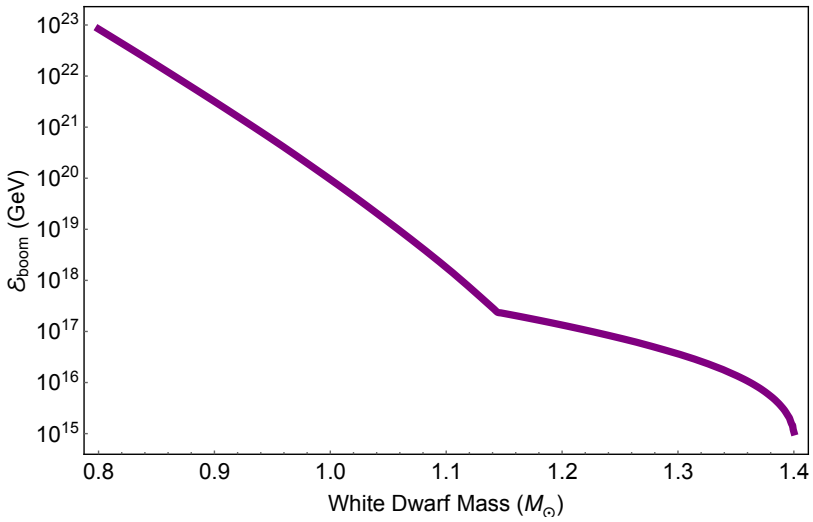


Figure 2.1: The minimum energy deposit (2.2) necessary to trigger runaway fusion, based on numerical results for $\lambda_T$ [21] and the WD mass-density relation [27]

.

these are suppressed by density effects and even photons and electrons are dominated by hadronic interactions. These showers rapidly stop high-energy particles due to their logarithmic nature, transferring the energy into a cloud of low-energy particles which heat the medium through elastic scatters. A schematic for the flow of energy during deposition is given in Figure 2.2. In this light, the WD operates analogously to a particle detector, including hadronic and electromagnetic "calorimeter" components. Runaway fusion provides the necessary amplification to convert a detected event into an observable signal.

The remainder of this section will discuss the above heating process in more detail. We summarize the dominant source of energy loss and the resulting stopping lengths $\lambda$ for SM particles of incident kinetic energy $\epsilon$. The total path length traveled by a particle before depositing $\mathcal{O}(1)$ of its energy is approximately

$$R_{\rm SP} \sim \frac{\epsilon}{dE/dx}, \tag{2.4}$$

where $dE/dx$ is the stopping power in the WD medium. If the mean free path to hard scatter $\lambda_{\rm hard}$ is smaller than this path length $R_{\rm SP}$, then the particle undergoes a random walk with $N_{\rm hard}$ scatters, and the net displacement is reduced by $\sqrt{N_{\rm hard}}$. We therefore approximate the stopping length as

$$\lambda \sim \min\left\{R_{\rm SP}, \sqrt{R_{\rm SP}\lambda_{\rm hard}}\right\} \tag{2.5}$$

This random walk behavior is relevant for low-energy elastic scatters.

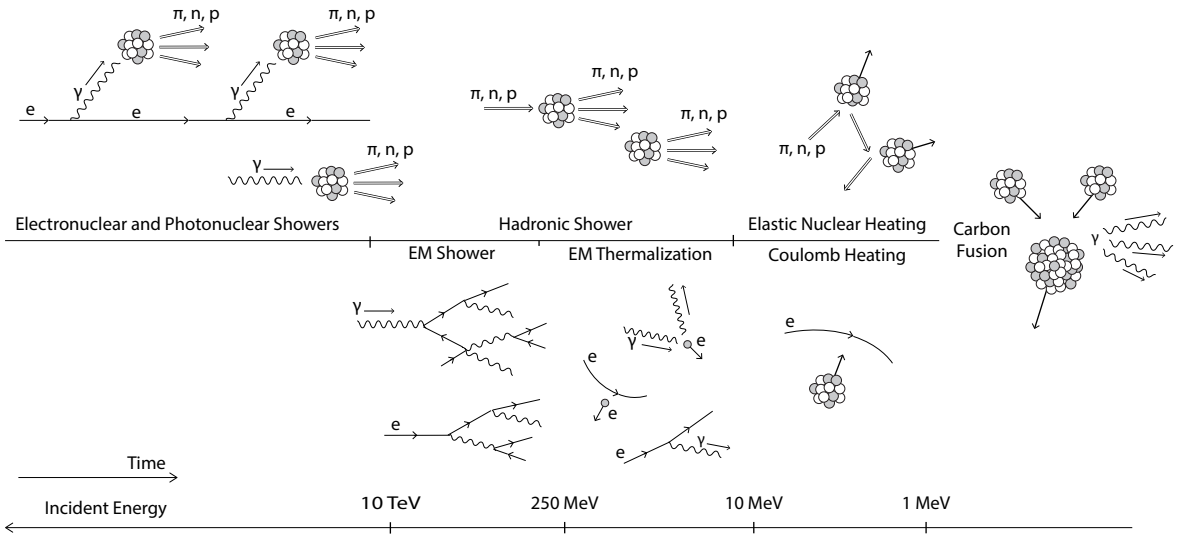


Figure 2.2: Dominant energy loss and thermalization processes in the WD as a function of energy, with energy decreasing towards the right. Hadronic processes are shown in the upper panel and EM processes in the lower panel. High energy particles will induce showers that terminate into elastic thermalization of the WD ions, moving from left to right in the diagram. The quoted energies are for a $\sim 1.37\, M_\odot$ WD, although the cartoon is qualitatively the same for all densities.

Stopping lengths are plotted in Figures 2.3 and 2.4, and a detailed treatment of the stopping powers is given in Appendix A. We will consider incident light hadrons, photons, electrons, and neutrinos—as we are concerned with triggering runaway fusion, we restrict our attention to energies $\epsilon \gg T_f \sim$ MeV.

## High-Energy Showers

**Hadronic Showers.** Incident hadrons with kinetic energy larger than the nuclear binding scale $\sim 10$ MeV will undergo violent inelastic collisions with carbon ions resulting in an $\mathcal{O}(1)$ number of secondary hadrons. This results in a roughly collinear shower of hadrons of size

$$X_{\rm had} \sim \frac{1}{n_{\rm ion}\sigma_{\rm inel}} \log\left(\frac{\epsilon}{10\ {\rm MeV}}\right) \approx 10^{-6}\ {\rm cm} \left(\frac{10^{32}\ {\rm cm}^{-3}}{n_{\rm ion}}\right).$$

where the inelastic nuclear cross section is $\sigma_{\rm inel} \approx 100$ mb and we have taken the logarithm to be $\sim 10$. The shower terminates into pions and nucleons of energy $\sim 10$ MeV, whose cooling is discussed below. Note that neutral pions of energy $10 - 100$ MeV have a decay length to photons of $\delta_{\pi^0} \sim 10^{-6}$ cm. Hadronic showers will therefore generate an electromagnetic component carrying an $\mathcal{O}(1)$ fraction of the energy.

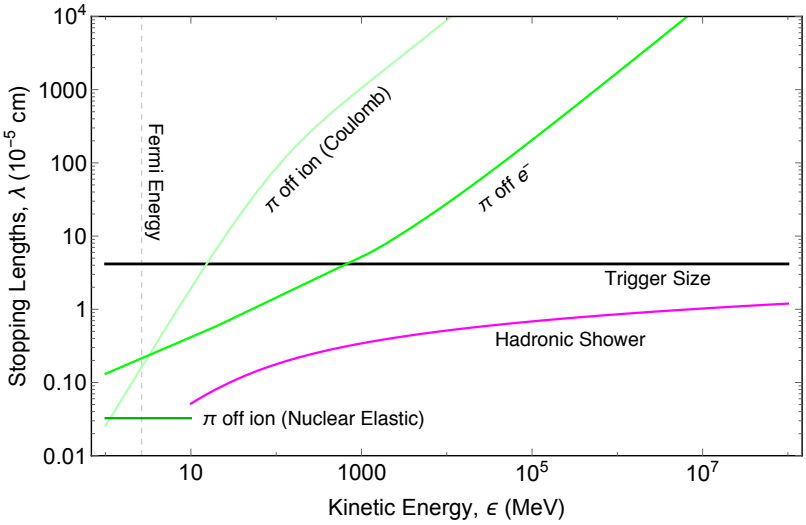


Figure 2.3: Stopping lengths for incident hadrons as a function of kinetic energy in a WD of density $n_{\rm ion} \sim 10^{31}$ cm$^{-3}$ ($\approx 1.25\ M_\odot$), including the hadronic shower length (magenta). Any discontinuities in the stopping lengths are due to approximate analytic results in the different energy regimes. See Appendix A for calculation details.

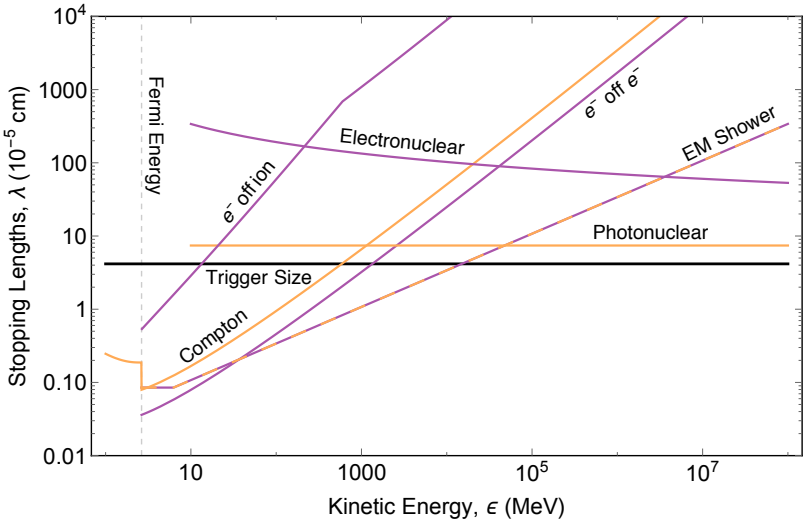


Figure 2.4: Stopping lengths of incident photons (orange) and electrons (purple) as a function of kinetic energy in a WD of density $n_{\rm ion} \sim 10^{31}$ cm$^{-3}$ ($\approx 1.25\ M_\odot$), including the EM shower length (dashed). Any discontinuities in the stopping lengths are due to approximate analytic results in the different energy regimes. See Appendix A for calculation details.

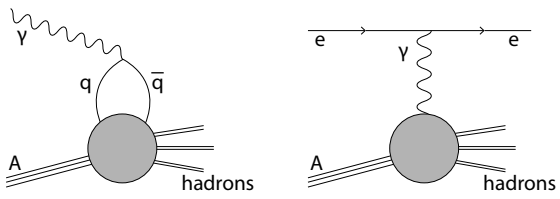


Figure 2.5: Photonuclear (left) and Electronuclear (right) interactions. The shaded region contains, at high energies, the familiar point-like processes of deep inelastic scattering and for energies below $\Lambda_{\rm QCD}$ is best described by exchange of virtual mesons.

**Photonuclear and Electronuclear Showers.** A photon or electron can directly induce hadronic showers via production of a quark-antiquark pair, depicted in Figure 2.5. The LPM effect, discussed below, ensures that these process dominate the stopping of photons and electrons at high energies, $\epsilon \gtrsim 10^4 - 10^6$ GeV.

The only substantial difference between photonuclear showers and purely hadronic ones is that they require a longer distance to initiate. Roughly, the photonuclear cross section is suppressed relative to the hadronic inelastic cross section $\sigma_{\rm inel}$ by a factor of $\alpha$, and so the photon range is

$$\lambda_{\gamma A} \approx 10^{-5}\ \text{cm} \left( \frac{10^{32}\ \text{cm}^{-3}}{n_{\rm ion}} \right). \tag{2.6}$$

Here $\lambda_{\gamma A}$ is the distance to initiate a hadronic shower, whereas the shower itself extends a distance $X_{\rm had}$. Note that $\lambda_{\gamma A}$ is of order the trigger size.

The electronuclear showers are qualitatively different, as the electron survives the interaction. This process is best described as a continuous energy loss of the electron, due to radiation of virtual photons into hadronic showers. The stopping power is again radiative, which gives the constant stopping length

$$\lambda_{eA} \approx 10^{-4}\ \text{cm} \left( \frac{10^{32}\ \text{cm}^{-3}}{n_{\rm ion}} \right). \tag{2.7}$$

This is suppressed by an additional factor of $\alpha$ relative to the photonuclear interaction, although a full calculation also yields an $\mathcal{O}(10)$ logarithmic enhancement. We see that the electronuclear length scale $\lambda_{eA}$ is at most larger than the trigger size by an order of magnitude.

**Electromagnetic Showers.** Of course, electrons and photons can also shower through successive bremsstrahlung and pair-production. An electromagnetic shower proceeds until a critical energy $\sim 100$ MeV, at which point these radiative processes become subdominant to elastic Coulomb and Compton scattering. Below this scale radiation can still be important,

though electromagnetic showers do not occur. Note that bremsstrahlung and pair-production are strictly forbidden for incident energies below the Fermi energy $E_F$.

At sufficiently high electron/photon energies and nuclear target densities, electromagnetic showers are elongated due to the Landau-Pomeranchuk-Migdal (LPM) effect. High-energy radiative processes necessarily involve small momentum transfers to nuclei. These soft virtual photons cannot be exchanged with only a single ion, but rather interact simultaneously with multiple ions. This generates a decoherence, suppressing bremsstrahlung/pair-production above an energy $E_{\rm LPM}$ which scales inversely with density:

$$E_{\rm LPM} \approx 1 \text{ MeV} \left( \frac{10^{32} \text{ cm}^{-3}}{n_{\rm ion}} \right). \tag{2.8}$$

The corresponding shower lengths are

$$X_{\rm EM} \approx X_0 \cdot \begin{cases} \left(\frac{\epsilon}{E_{\rm LPM}}\right)^{1/2} & \epsilon > E_{\rm LPM} \\ 1 & \epsilon < E_{\rm LPM} \end{cases} \tag{2.9}$$

where

$$X_0 \approx 10^{-7} \text{ cm} \left( \frac{10^{32} \text{ cm}^{-3}}{n_{\rm ion}} \right) \tag{2.10}$$

is the unsuppressed EM shower length. See Appendix A.3 for details. At the highest WD densities radiative processes are always LPM-suppressed, while at lower densities we observe both regimes. We emphasize that for all densities, throughout the energy range where it is relevant, the length of electromagnetic showers is never parametrically larger than the trigger size.

**Neutrinos.** Neutrinos scatter off nuclei with a cross section that increases with energy. In these interactions, an $\mathcal{O}(1)$ fraction of the neutrino energy is transferred to the nucleus with the rest going to produced leptons—this is sufficient to start a hadronic shower [28, 29]. At an energy of $\sim 10^{11}$ GeV, [28] calculates the neutrino-nuclear cross section to be $\sim 10^{-32}$ cm$^2$. Conservatively assuming this value for even higher energies, we find a neutrino mean free path in a WD of order $\sim 10$ cm. Therefore, any high-energy neutrino released in the WD will (on average) only interact after traveling a distance $\gg \lambda_T$. As per the discussion above, this makes the heating of a WD via the release of multiple neutrinos highly inefficient due to the (enormous) volume dilution factor in (2.3). Interestingly, a *single* high-energy neutrino with energy greater than $\mathcal{E}_{\rm boom}$ will still be able to efficiently heat the star and trigger a runaway. This is because the neutrino mean free path is simply a displacement after which a compact shower of size $X_{\rm had}$ occurs. If the energy contained in a single shower is large enough, then the heating caused by this single neutrino can effectively be considered as a separate and efficient heating event.

## Low-Energy Elastic Heating

The showers of high-energy particles described above terminate in a cloud of low-energy $\epsilon \sim 10$ MeV neutrons, protons, and charged pions, and $\epsilon \sim 10 - 100$ MeV electrons and photons. Of course, particles at these energies may also be directly produced by the DM. At these energies, elastic nuclear, Coulomb, and Compton scatters dominate and eventually lead to the thermalization of ions. Once again, the physical expressions for all computed stopping powers and stopping lengths are given in Appendix A whereas we simply quote the relevant numerical values here.

**Hadrons.** Neutral hadrons are the simplest species we consider, interacting at low-energies only through elastic nuclear scatters with cross section $\sigma_{\rm el} \approx 1$ b, where 1 b $= 10^{-24}$ cm$^2$. Note that the large ion mass requires $\sim 10 - 100$ hard scatters to transfer the hadron's energy in the form of a random-walk. This elastic heating range is

$$\lambda_{\rm el} \approx 10^{-7}\ {\rm cm} \left( \frac{10^{32}\ {\rm cm}^{-3}}{n_{\rm ion}} \right), \tag{2.11}$$

and is always less than the trigger size.

Charged hadrons are also subject to Coulomb interactions, which would provide the dominant stopping in terrestrial detectors. In this case, however, Coulomb scatters off degenerate WD electrons are strongly suppressed and charged hadrons predominantly undergo elastic nuclear scatters like their neutral brethren. This suppression is due to (1) motion of the electrons, which fixes the relative velocity to be $\mathcal{O}(1)$ and removes the enhancement of Coulomb stopping usually seen at low velocity, and (2) Pauli blocking, which forces the incident particle to scatter only electrons near the top of the Fermi sea. For an incident particle with velocity $v_{\rm in} \ll 1$, the first effect suppresses the stopping power by a factor of $v_{\rm in}^2$ relative to that off stationary, non-degenerate electrons and the second by an additional factor of $v_{\rm in}$. Note that there is a small range of energies in which Coulomb scatters off ions dominate the stopping of charged hadrons—either way, both length scales are well below the trigger size.

**Electrons and Photons.** For electrons and photons below $\sim 100$ MeV the dominant interactions are Coulomb scatters off WD electrons and Compton scatters, respectively. The length scale of these processes is smaller than any interaction with ions, and so these electrons and photons will thermalize into a compact electromagnetic "gas" with a size set by the radiative length scale $X_{\rm EM}$. The EM gas will cool and diffuse to larger length scales, eventually allowing thermalization with nuclei via the subdominant Coulomb scatters of electrons off ions. The photons of the EM gas will not undergo photonuclear showers here, as the gas will cool below $\sim 10$ MeV by the time it diffuses out to a size $\lambda_{\gamma A}$. This gas temperature is initially at most $\sim 100$ MeV. At these temperatures the heat capacity is dominated by photons, so as the gas diffuses to a size $\lambda_{\gamma A}$ it cools by a factor $(X_{\rm EM}/\lambda_{\gamma A})^{3/4} \sim 10^{-2} - 10^{-1}$. Note that for temperatures $T$ less than $E_F$, the electrons are partially degenerate

and heating proceeds via the thermal tail with kinetic energies $\epsilon \sim E_F + T$. Therefore, the relevant thermalization process is Coulomb scattering of electrons off ions.

Like the hadronic elastic scatters, an electron Coulomb scattering off ions will occasionally hard scatter, and thus deposit its energy along a random walk. This reduces the stopping length at low energies, yielding

$$\lambda_{\rm coul} \approx 10^{-6}\ {\rm cm} \left(\frac{\epsilon}{10\ {\rm MeV}}\right)^{3/2} \left(\frac{10^{32}\ {\rm cm}^{-3}}{n_{\rm ion}}\right) \tag{2.12}$$

which is below the trigger size.

## 2.4 Dark Matter-Induced Ignition

Any DM interaction that produces SM particles in a WD has the potential to ignite the star, provided that sufficient SM energy is produced. The distribution in space, momentum, and species of these SM products is dependent on unknown DM physics and is needed to determine the rate of DM-induced ignition. This can be done precisely for a specific DM model, as we do for Q-balls in Section 2.6. In this Section, however, we study some general features of DM-WD encounters involving DM that possesses interactions with itself and the SM. We collect below the basic formulas relating DM model parameters to ignition criteria, SN rate, etc.

DM can generically heat a WD through three basic processes: DM-SM scattering, DM-DM collisions, and DM decays. For ultra-heavy DM, these processes can be complicated events involving many (possibly dark) final states, analogous to the interactions of heavy nuclei. In the case of DM-SM scattering, we consider both elastic and inelastic DM scatters off WD constituents, e.g. carbon ions. We classify DM candidates into three types according to the interaction that provides the dominant source of heating, and refer to these as scattering, collision, and decay candidates. We also make the simplifying assumption that the above events are "point-like", producing SM products in a localized region (smaller than the heating length) near the interaction vertex. Where this is not the case (as in our elastic scattering and Q-ball constraints, see Sections 2.5 and 2.6), then the same formalism applies but with the event size added to the stopping length.

The SN rate may be greatly enhanced if DM is captured in the star, so we also consider separately "transiting DM" and "captured DM". In general, there is some loss of DM kinetic energy in the WD. In the transit scenario, this energy loss is negligible and the DM simply passes through the star. In the capture scenario, the energy loss is not directly capable of ignition but is sufficient to stop the DM and cause it to accumulate in the star. Energy loss may be due to a variety of processes, but for simplicity we will focus on an DM-nuclei elastic scattering. Of course, due to the velocity spread of DM in the rest frame of a WD, there will necessarily be both transiting and captured DM populations in the star.

## DM Transit

**DM-SM Scattering.** Runaway fusion only occurs in the degenerate WD interior where thermal expansion is suppressed as a cooling mechanism. The outer layers of the WD, however, are composed of a non-degenerate gas and it is therefore essential that a DM candidate penetrate this layer in order to ignite a SN. We parameterize this by a DM stopping power $(dE/dx)_{\rm SP}$, the kinetic energy lost by the DM per distance traveled in the non-degenerate layer, and demand that

$$\left(\frac{dE}{dx}\right)_{\rm SP} \ll \frac{m_\chi v_{\rm esc}^2}{R_{\rm env}}, \tag{2.13}$$

where $R_{\rm env}$ is the nominal size of the non-degenerate WD envelope and $v_{\rm esc} \sim 10^{-2}$ is the escape velocity of the WD, at which the DM typically transits the star.

DM-SM scattering will result in a continuous energy deposit along the DM trajectory (if the interaction is rare enough for this not to be true, then the encounter is analogous to the case of DM decay). This is best described by a linear energy transfer $(dE/dx)_{\rm LET}$, the kinetic energy of SM particles produced per distance traveled by the DM. If these products have a heating length $L_0$ then the energy deposit must at minimum be taken as the energy transferred along a distance $L_0$ of the DM trajectory. Importantly, as per the ignition condition (2.3), such a deposition is *less* explosive unless $L_0$ is smaller than the trigger size $\lambda_T$. We thus consider the energy deposited over the larger of these two length scales. Assuming the energy of the DM is roughly constant during this heating event, the ignition condition is:

$$\left(\frac{dE}{dx}\right)_{\rm LET} \gtrsim \frac{\mathcal{E}_{\rm boom}}{\lambda_T} \cdot \max\left\{\frac{L_0}{\lambda_T}, 1\right\}^2. \tag{2.14}$$

Note that the DM stopping power $(dE/dx)_{\rm SP}$ and the linear energy transfer $(dE/dx)_{\rm LET}$ are related in the case of elastic scatters, but in general the two quantities may be controlled by different physics. In addition, a transit event satisfying condition (2.13) will have negligible energy loss over the parametrically smaller distances $\lambda_T$ or $L_0$, validating (2.14).

The above condition sums the individual energy deposits along the DM trajectory as though they are all deposited simultaneously. This is valid if the DM moves sufficiently quickly so that this energy does not diffuse out of the region of interest before the DM has traversed the region. We therefore require that the diffusion time $\tau_{\rm diff}$ across a heated region of size $L$ at temperature $T_f$ be larger than the DM crossing-time:

$$\tau_{\rm diff} \sim \frac{L^2}{\alpha(T_f)} \gg \frac{L}{v_{\rm esc}}, \tag{2.15}$$

where $\alpha(T)$ is the temperature-dependent diffusivity. This condition is more stringent for smaller regions, so we focus on the smallest region of interest, $L = \lambda_T$. Then (2.15) is equivalent to demanding that the escape speed is greater than the conductive speed of the

fusion wave front, $v_{\rm cond} \sim \alpha(T_f)/\lambda_T$. Numerical calculations of $v_{\rm cond}$ are tabulated in [21], and indeed condition (2.15) is satisfied for all WD densities.

The rate of transit events is directly given by the flux of DM through a WD

$$\Gamma_{\rm trans} \sim \frac{\rho_\chi}{m_\chi} R_{\rm WD}^2 \left(\frac{v_{\rm esc}}{v_{\rm halo}}\right)^2 v_{\rm halo}, \tag{2.16}$$

where $\rho_\chi$ is the DM density in the region of the WD, and $R_{\rm WD}$ is the WD radius. Here $v_{\rm halo} \sim 10^{-3}$ is the virial velocity of our galactic halo. Note the $(v_{\rm esc}/v_{\rm halo})^2 \sim 100$ enhancement due to gravitational focusing.

We will not consider here captured DM that heats the star via scattering events, as such heating will typically cause ignition before capture occurs. However, it is possible to cause ignition after capture if the collection of DM leads to an enhanced scattering process.

**DM-DM Collisions and DM Decays.** For a point-like DM-DM collision or DM decay event releasing particles of heating length $L_0$, ignition will occur if the total energy in SM products satisfies condition (2.3). Such an event will likely result in both SM and dark sector products, so we parameterize the resulting energy in SM particles as a fraction $f_{\rm SM}$ of the DM mass. For non-relativistic DM, the DM mass is the dominant source of energy and therefore $f_{\rm SM} \lesssim 1$ regardless of the interaction details. A single DM-DM collision or DM decay has an ignition condition:

$$m_\chi f_{\rm SM} \gtrsim \mathcal{E}_{\rm boom} \cdot \max\left\{\frac{L_0}{\lambda_T}, 1\right\}^3. \tag{2.17}$$

Thus the WD is sensitive to annihilations/decays of DM masses $m_\chi \gtrsim 10^{16}$ GeV.

DM that is not captured traverses the WD in a free-fall time $t_{\rm ff} \sim R_{\rm WD}/v_{\rm esc}$, and the rate of DM-DM collisions within the WD parameterized by cross section $\sigma_{\chi\chi}$ is:

$$\Gamma_{\rm SN}^{\rm ann} \sim \left(\frac{\rho_\chi}{m_\chi}\right)^2 \sigma_{\chi\chi} \left(\frac{v_{\rm esc}}{v_{\rm halo}}\right)^3 v_{\rm halo} R_{\rm WD}^3. \tag{2.18}$$

Similarly the net DM decay rate inside the WD parameterized by a lifetime $\tau_\chi$ is:

$$\Gamma_{\rm SN}^{\rm decay} \sim \frac{1}{\tau_\chi}\frac{\rho_\chi}{m_\chi}\left(\frac{v_{\rm esc}}{v_{\rm halo}}\right) R_{\rm WD}^3. \tag{2.19}$$

## DM Capture

**Review of DM Capture.** We first summarize the capture and subsequent evolution of DM in the WD, ignoring annihilations or decays—see Appendix B for details. Consider a spin-independent, elastic scattering off carbon ions with cross section $\sigma_{\chi A}$. The rate of DM capture in gravitating bodies is of course very well-studied [30, 31]. However, this rate must

be modified when the DM requires multiple scatters to lose the necessary energy for capture. Ultimately, for ultra-heavy DM the capture rate is of the form

$$\Gamma_{\rm cap} \sim \Gamma_{\rm trans} \cdot \min\left\{1, \overline{N}_{\rm scat} \frac{m_{\rm ion} v_{\rm esc}^2}{m_\chi v_{\rm halo}^2}\right\}, \tag{2.20}$$

where $\overline{N}_{\rm scat} \sim n_{\rm ion}\sigma_{\chi A} R_{\rm WD}$ is the average number of DM-carbon scatters during one DM transit. For the remainder of this Section, all results are given numerically assuming a WD central density $n_{\rm ion} \sim 10^{31}$ cm$^{-3}$. The relevant parametric expressions are presented in further detail in Appendix B.

Once DM is captured, it eventually thermalizes with the stellar medium at velocity $v_{\rm th} \sim (T_{\rm WD}/m_\chi)^{1/2}$, where $T_{\rm WD}$ is the WD temperature. The dynamics of this process depend on the strength of the DM-carbon interaction, namely on whether energy loss to carbon ions provides a small perturbation to the DM's gravitational orbit within the star or whether DM primarily undergoes Brownian motion in the star due to collisions with carbon. For simplicity, we will focus here only on the former case, corresponding roughly to interactions

$$\sigma_{\chi A} \lesssim \frac{m_\chi}{\rho_{\rm WD} R_{\rm WD}} \sim 10^{-26}\ {\rm cm}^2 \left(\frac{m_\chi}{10^{16}\ {\rm GeV}}\right) \tag{2.21}$$

where the DM is able to make more than a single transit through the star before thermalizing. Note that the opposite regime indeed also provides constraints on captured DM and is unconstrained by other observations, see Figure 2.9, however the resulting limits are similar to those presented here.

In the limit (2.21), captured DM will thermalize by settling to a radius $R_{\rm th}$ given by the balance of gravity and the thermal energy $T_{\rm WD}$,

$$R_{\rm th} \approx 0.1\ {\rm cm} \left(\frac{m_\chi}{10^{16}\ {\rm GeV}}\right)^{-1/2}. \tag{2.22}$$

This settling proceeds in two stages. Captured DM will initially be found on a large, bound orbit that exceeds the size of the WD, decaying after many transits of the star until the orbital size is fully contained within the WD. This occurs after a time

$$t_1 \approx 7 \times 10^{16}\ {\rm s} \left(\frac{m_\chi}{10^{16}\ {\rm GeV}}\right)^{3/2} \left(\frac{\sigma_{\chi A}}{10^{-35}\ {\rm cm}^2}\right)^{-3/2}. \tag{2.23}$$

The DM then completes many orbits within the star until its orbital size decays to the thermal radius, occurring after a further time

$$t_2 \approx 10^{14}\ {\rm s} \left(\frac{m_\chi}{10^{16}\ {\rm GeV}}\right) \left(\frac{\sigma_{\chi A}}{10^{-35}\ {\rm cm}^2}\right)^{-1}. \tag{2.24}$$

Note that the difference in scalings between $t_1$ and $t_2$ is due to the fact that, while the two times are ultimately determined by scattering in the star, the dynamics of the settling DM

are quite distinct in each case. $t_1$ is dominated by the time spent on the largest orbit outside the WD (which additionally depends on $\sigma_{\chi A}$) while $t_2$ is dominated by the time spent near the thermal radius. Subsequently the DM will begin steadily accumulating at $R_{\rm th}$, with the possibility of self-gravitational collapse if the collected mass of DM exceeds the WD mass within this volume. This occurs after a time

$$t_{\rm sg} \approx 10^9 \text{ s} \left(\frac{m_\chi}{10^{16} \text{ GeV}}\right)^{-1/2} \left(\frac{\sigma_{\chi A}}{10^{-35} \text{ cm}^2}\right)^{-1}. \tag{2.25}$$

Of course, not all of these stages may be reached within the age of the WD $\tau_{\rm WD}$. The full time to collect and begin self-gravitating is $t_1 + t_2 + t_{\rm sg}$.

At any point during the above evolution, captured DM has the potential to trigger a SN. We will consider ignition via either the decay or annihilation of captured DM. Of particular interest are events occurring within a collapsing DM core, as such cores have the additional ability to ignite a WD for DM masses less than $\mathcal{E}_{\rm boom}$, either via multiple DM annihilations or by the formation of a black hole. This is discussed in detail in [6]. In the following, we restrict attention to the limit (2.21) and require DM masses sufficiently large so that a single collision or decay will ignite the star, and give only a quick assessment of DM core collapse.

**Captured DM-DM Collisions.** We now turn to the rate of DM-DM collisions for captured DM. Of course, the thermalizing DM constitutes a number density of DM throughout the WD volume. Assuming that $t_1 + t_2 < \tau_{\rm WD}$, the total rate of annihilations for this "in-falling" DM is peaked near the thermal radius and is of order:

$$\Gamma_{\rm infall} \sim \frac{(\Gamma_{\rm cap} t_2)^2}{R_{\rm th}^3} \sigma_{\chi\chi} v_{\rm th}. \tag{2.26}$$

If $\Gamma_{\rm infall} t_2 > 1$, then a SN will be triggered by the in-falling DM population. Otherwise if $\Gamma_{\rm infall} t_2 < 1$, the DM will start accumulating at the thermal radius. If $t_{\rm sg} \ll t_2$ (as expected for such heavy DM masses) there will be no collisions during this time and thus a collapse will proceed. For a DM sphere consisting of $N$ particles at a radius $r$, the rate of annihilations is

$$\Gamma_{\rm collapse} \sim \frac{N^2}{r^3} \sigma_{\chi\chi} v_\chi, \quad v_\chi \sim \sqrt{\frac{GNm_\chi}{r}}. \tag{2.27}$$

Of course, there may be some stabilizing physics which prevents the DM from collapsing and annihilating below a certain radius, such as formation of a black hole or bound states. To illustrate the stringent nature of the collapse constraint we will simply assume some benchmark stable radius, as in Figure 2.10. We assume that the timescale for collapse at this radius is set by DM cooling $t_{\rm cool}$, which is related to $t_2$. Note that if a single collision has not occurred during collapse, one may additionally examine annihilations of the subsequent in-falling DM down to the stable radius—for simplicity, we do not consider this scenario.

**Captured DM Decays.** Lastly, we compute the rate of decays for captured DM, which is simply proportional to the number of DM particles in the WD available for decay at any given instance. In the transit scenario (2.19), this rate is $\Gamma \sim \tau_\chi^{-1}\Gamma_{\rm trans}t_{\rm ff}$. In the capture scenario, this number is instead determined by the thermalization time within the WD $\Gamma \sim \tau_\chi^{-1}\Gamma_{\rm cap}t_2$, conservatively assuming that after a thermalization time, the DM quickly collapses and stabilizes to an "inert" core incapable of further decay. If this is not the case, then the captured DM decay rate is given by $\Gamma \sim \tau_\chi^{-1}\Gamma_{\rm cap}\tau_{\rm WD}$.

## 2.5 Dark Matter Constraints

We now constrain some generic DM candidates which will ignite a WD via one of the processes parameterized in Section 2.4. These release SM particles that deposit their energy and thermalize ions within a distance described in Section 2.3. First, however, we review how WD observables constrain DM candidates capable of triggering SN.

### Review of WD Observables

Following the discussion of [10], our constraints come from (1) the existence of heavy, long-lived white dwarfs, or (2) the measured type Ia SN rate. The ages of WD can be estimated by measuring their temperature and modeling their cooling over time, and we take the typical age of an old WD to be of order $\sim$ Gyr [32]. RX J0648.04418 is one such nearby star and one of the heavier known WDs, with a mass $\sim 1.25\ M_\odot$ [33] and local dark matter density which we take to be $\rho_\chi \sim 0.4$ GeV/cm$^3$. Of course, this is not the only known heavy WD—the Sloan Digital Sky Survey [34] has found 20+ others. The NuStar collaboration has also recently uncovered evidence for the likely existence of heavy WDs near the galactic center [35], where the DM density is assumed to be much greater $\rho_\chi \gtrsim 10^3$ GeV/cm$^3$ [36]. Such heavy candidates are particularly suited for our constraints as the energy deposit necessary to trigger SN (2.3) is a decreasing function of WD mass. However, less dense white dwarfs are significantly more abundant in the galaxy. Thus, even if a sufficiently massive DM is unable to trigger a violent heating event within the lifetime of a WD, it could still ignite enough lighter WDs to affect the measured SN rate of $\sim 0.3$ per century. The DM-induced SN rate is estimated using the expected number of white dwarfs per galaxy $\sim 10^{10}$ and their mass distribution [34]. Simulations indicate that only WD masses heavier than $\sim 0.85\ M_\odot$ will result in optically visible SN [10]. Therefore, most of the stars exploded in this manner will be in the mass range $\sim 0.85 - 1\ M_\odot$, resulting in weaker SN than expected of typical Chandrasekhar mass WDs.

To summarize, a bound on DM parameters can be placed if either a single explosive event occurs during the lifetime of an observed star such as RX J0648.04418, or the SN rate due to such DM events throughout the galaxy exceeds the measured value. Note that for low-mass WDs dominated by photon diffusion, $\mathcal{E}_{\rm boom}$ is a strong function of WD density. The average density for WDs is typically a factor $\sim 10^{-2} - 10^{-1}$ less than the central density, although

it is found that the WD density only changes by an $\mathcal{O}(1)$ fraction from the central value up to a distance $\sim R_{\rm WD}/2$ [37]. Therefore the central density is a valid approximation as long as we consider heating events within this "modified" WD volume. For simplicity, we employ this approach.

## Scattering Constraints

In order to constrain a DM model with a scattering interaction, we require that it satisfy the ignition condition (2.14). This is given in terms of an LET, which parameterizes the ability for DM to release sufficient energy to the star in the form of SM particles. Here we consider a DM elastic scattering off carbon ions with cross section $\sigma_{\chi A}$, which has an LET:

$$\left(\frac{dE}{dx}\right)_{\rm LET} \sim n_{\rm ion}\sigma_{\chi A} m_{\rm ion} v_{\rm esc}^2. \tag{2.28}$$

This can be expressed in terms of the cross section per nucleon $\sigma_{\chi n}$—see Appendix B Each elastic scatter transfers an energy of order $m_{\rm ion}v_{\rm esc}^2 \approx 1-10$ MeV to the target nuclei, thus enabling fusion reactions. Note that the stopping power of the DM in the non-degenerate envelope is of the same form, but with the density replaced by its diminished value in this region. It is interesting that combining the ignition condition (2.14) with the requirement that the DM adequately penetrates the non-degenerate layer (2.13) yields a lower bound on DM mass.

$$m_\chi > \mathcal{E}_{\rm boom}\left(\frac{R_{\rm env}}{\lambda_T}\right)\left(\frac{\rho_{\rm env}}{\rho_{\rm WD}}\right)\frac{1}{v_{\rm esc}^2}, \tag{2.29}$$

where $\rho_{\rm WD}$ is the central density of the WD. Here $R_{\rm env} \approx 50$ km is the width of a non-degenerate WD envelope—the density in this region $\rho_{\rm env}$ is typically a small fraction $\sim 10^{-3}$ of the central density [32]. We conservatively take the envelope to be composed of carbon ions; if it were primarily hydrogen or helium, then the condition for penetration is weakened by 4 orders of magnitude due to the reduced energy transfer and cross section for scattering. We find that the DM must be heavier than $\sim 10^{28}$ GeV to ensure an explosive transit of a 1.25 $M_\odot$ WD *and* minimal loss of kinetic energy in the non-degenerate layer. For the sake of comparison this corresponds to a macroscopic DM mass of order $\sim 20$ kg.

Of course, this bound is only applicable if the energy input to the WD is solely coming from DM kinetic energy. We may also consider DM inelastic scattering off carbon ions which transfer more than $\sim$ MeV per collision. Examples of such a process include baryon-number violating interactions which can release the nucleon mass energy $\sim$ GeV per collision. This is similar to Q-balls, which absorb the baryon number of nuclear targets and liberate binding energy rather than transferring kinetic energy—this interaction is examined in Section 2.6. Note that the assumption of a "point-like" interaction requires that the physical size of the DM is much smaller than $\lambda_T$—this is sensible up to masses of order $\sim 10^{47}$ GeV, at which point the gravitational radius of the DM exceeds $\lambda_T$.

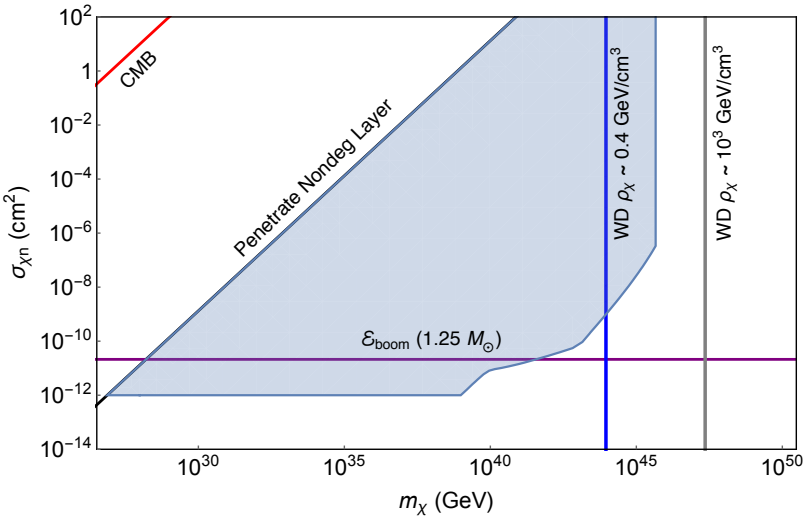


Figure 2.6: Constraints on DM-carbon elastic scattering cross section. Bounds come from demanding that the DM transit triggers runaway fusion (2.14) and occurs at a rate (2.16) large enough to either ignite a 1.25 $M_\odot$ WD in its lifetime or exceed the measured SN rate in our galaxy (blue shaded). We also demand that the DM penetrates the non-degenerate stellar envelope, taken at the highest densities, without losing appreciable kinetic energy. Constraints from the CMB/large-scale structure [38] are depicted as well.

In Figure 2.6 we constrain the DM elastic scattering cross section per nucleon $\sigma_{\chi n}$ as a function of DM mass $m_\chi$ using the different classes of observables described above. Note that the scattering cross sections constrained here are incredibly large $\gtrsim 10^{-10}$ cm$^2$—however, the constraints from WDs reach to very large masses for which no other constraints exist. At these masses, the most stringent limits on DM elastic scattering are from CMB and Lyman-$\alpha$ spectrum analysis [38], which constrain $\frac{\sigma_{\chi n}}{m_\chi} < \frac{10^{-3}\text{b}}{\text{GeV}}$. These cross sections also require that the DM involved be macroscopically large, of order or larger than the trigger size, and so the interaction is decidedly not "point-like." This fact does not weaken our constraints, however, since the energy transferred to each ion in the DM's path is greater than $\sim$ MeV.

## Collision and Decay Constraints

In order to constrain a DM model through its annihilations or decays within a WD, we require that it satisfy the ignition condition (2.17). Consider a single annihilation or decay with $f_{\rm SM} = 1$ that releases a spectrum of SM particles. As shown in Section 2.3, the constraint has minimal dependence on the released species if the typical energy $\epsilon$ of secondary products is greater than an MeV. In the case of neutrinos, we may simply demand that $\epsilon$ is sufficiently large that a single neutrino can ignite the star. With this schematic for the DM interaction, we can constrain the cross section for collision $\sigma_{\chi\chi}$ and lifetime $\tau_\chi$. This is done in Figures 2.7

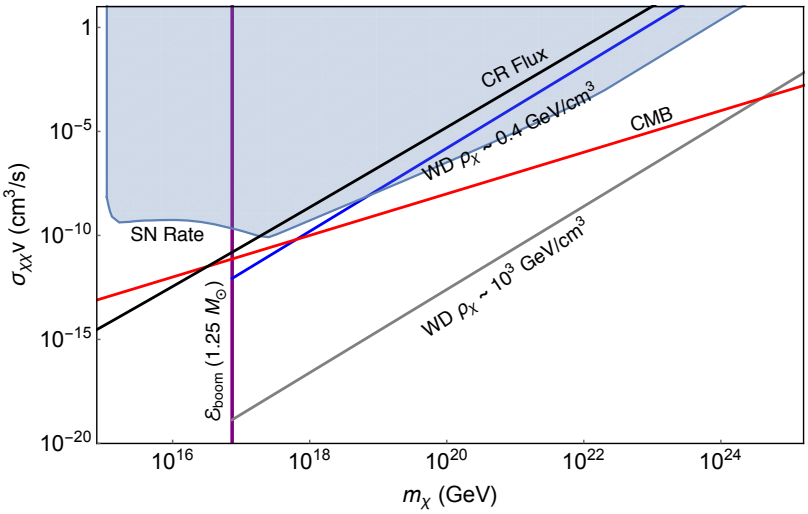


Figure 2.7: Constraints on DM-DM collision cross section to SM products of energy $\epsilon \gg$ MeV. Bounds come from demanding that the DM transit interaction triggers runaway fusion (2.17) and occurs at a rate (2.18) large enough to either ignite an observed 1.25 $M_\odot$ WD in its lifetime or exceed the measured SN rate in our galaxy (blue shaded). Also shown are the CMB [39] (red) and CR flux (black) constraints on DM annihilations.

and 2.8 in the case of transiting DM using the different classes of observables for DM-DM collisions and DM decays, respectively.

Of course there are existing limits on DM annihilations and decays, complementary to the ones placed from WDs. DM annihilations/decays inject energy and affect the ionization history of our universe, which can be probed by measurements of the CMB temperature and polarization angular spectrum [41, 39, 40]. These constraints are of order $\sigma_{\chi\chi} v < 10^{-27}\ \frac{\rm cm^3}{\rm s} \left(\frac{m_\chi}{10\ \rm GeV}\right)$ for annihilations, and $\tau_\chi > 10^7$ Gyr for decay. There are also constraints on DM annihilation/decays in our halo from the cosmic ray (CR) flux seen in large terrestrial detectors. Here we provide a crude estimate of the expected constraints from CRs in the case of DM annihilation (decays are qualitatively similar). A more detailed analysis is beyond the scope of this work. The Pierre Auger Observatory [42] has detected the flux of $E_{\rm th} \sim 10^{11}$ GeV cosmic rays with an exposure of order $A_{\rm PA} \sim 40000$ km$^2$ sr yr. Ultra-heavy DM annihilations $m_\chi > 10^{16}$ GeV will generally produce secondary particles of energy $\epsilon \gtrsim E_{\rm th}$ via final-state radiation. For a simple 2-2 process (e.g. $\chi\chi \to qq$), the expected number of final-state particles radiated at $E_{\rm th}$ due to QCD showers is approximated by the Sudakov double logarithm

$$N_{\rm rad} \sim \frac{4\alpha_s}{\pi} \log\left(\frac{m_\chi}{\Lambda_{\rm QCD}}\right) \log\left(\frac{m_\chi}{E_{\rm th}}\right) \approx 100, \tag{2.30}$$

where $\alpha_s$ is the QCD coupling constant. Similarly, the estimated number of final-state

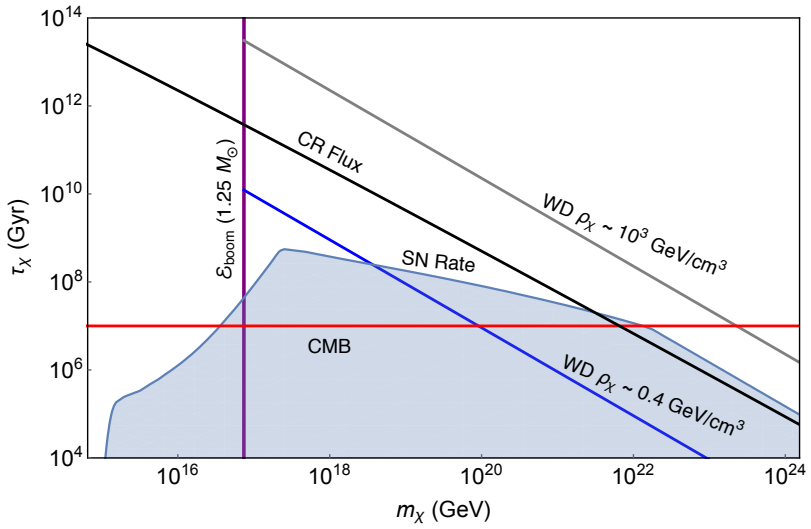


Figure 2.8: Constraints on DM decay to SM products of energy $\epsilon \gg$ MeV. Bounds come from demanding that the DM transit interaction triggers runaway fusion (2.17) and occurs at a rate (2.19) large enough to either ignite an observed 1.25 $M_\odot$ WD in its lifetime or exceed the measured SN rate in our galaxy (blue shaded). Also shown are the CMB [40] (red) and CR flux (black) constraints on DM lifetime.

particles at $E_{\rm th}$ due to EW showers is $\approx 50$. We expect that CRs at this energy originating in our galaxy will be able to strike the earth unattenuated. Thus, such events would affect the measured CR flux of Pierre Auger unless

$$\left(\frac{\rho_\chi}{m_\chi}\right)^2 \sigma_{\chi\chi} v \frac{R_{\rm halo}}{4\pi} N_{\rm rad} \times A_{\rm PA} \lesssim 1. \tag{2.31}$$

Here we assume an average value for DM density $\rho_\chi \approx 0.4$ GeV/cm$^3$ as a reasonable approximation to the integral over our galactic halo volume. Surprisingly, the above CR constraints are (within a few orders of magnitude) comparable to the constraints due to the observation of long-lived WDs. This is actually due to a coincidence in the effective "space-time volumes" of the two systems. A terrestrial CR detector such as Pierre Auger sees events within a space-time volume ($R_{\rm det}^2 R_{\rm halo} \times t_{\rm det}$), where $R_{\rm det} \sim 50$ km, $R_{\rm halo} \sim 10$ kpc, and $t_{\rm det} \sim 10$ yr. This is similar in magnitude to the WD space-time volume ($R_{\rm WD}^3 \times \tau_{\rm WD}$).

It is important to note that there is a large parameter space in $\sigma_{\chi n}$ which will lead to DM capture, thermalization, and core collapse in a WD. This is depicted in Figure 2.9, along with the existing constraints on DM elastic scattering. As detailed in [43], direct detection experiments such as Xenon 1T [44] are only sensitive to DM masses $m_\chi < 10^{17}$ GeV. For even larger masses $m_\chi < 10^{26}$ GeV there are constraints from the MACRO experiment [45] and from ancient excavated mica. The latter has been studied in [46]. We have similarly estimated the bounds from MACRO assuming a detectable threshold of $\sim 5$ MeV/cm [45].

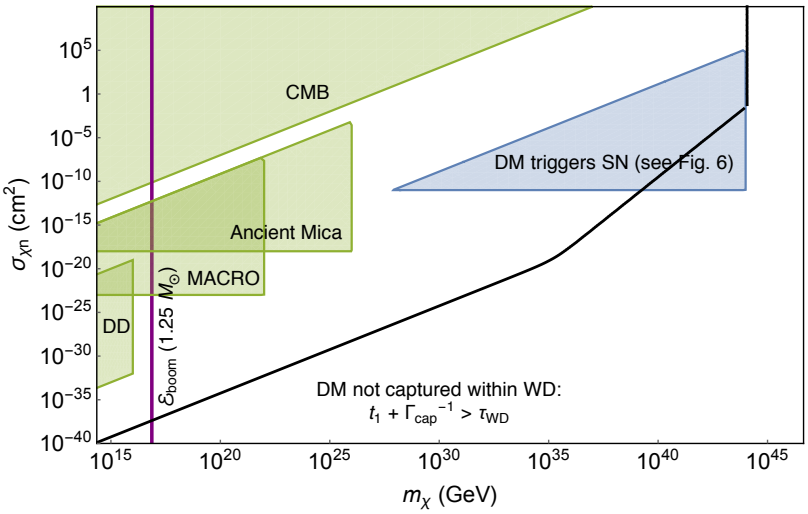


Figure 2.9: Viable parameter space (above the black line) in which DM-nucleon elastic scattering leads to DM capture in a 1.25 $M_\odot$ WD. All of this space is subject to constraints on DM decay and DM-DM annihilation analogous to those given in Figures 2.11 and 2.10. Note the blue region, reproducing Figure 2.6, indicates DM which causes SN via elastic heating. We also indicate here estimates of the scattering constraints from cosmology, direct detection, MACRO, and ancient mica [46].

In the case of captured DM, we show the constraints on $\sigma_{\chi\chi}$ and $\tau_\chi$ assuming a benchmark value of the elastic scattering cross section $\sigma_{\chi n} = 10^{-32}$ cm$^2$. With regards to DM-DM collisions, we also assume a stabilizing radius for the collapsing DM sphere. This is done in Figures 2.10 and 2.11—for simplicity, here we only show the constraints from the existence of nearby, heavy WDs.

## 2.6 Q-balls

Having derived constraints on generic models of ultra-heavy DM, we turn towards a concrete example. In various supersymmetric extensions of the SM, non-topological solitons called Q-balls can be produced in the early universe [47, 48]. If these Q-balls were stable, they would comprise a component of the DM today. For gauge-mediated models with flat scalar potentials, the Q-ball mass and radius are given by

$$M_Q \sim m_S Q^{3/4}, \quad R_Q \sim m_S^{-1} Q^{1/4}, \tag{2.32}$$

where $m_S$ is related to the scale of supersymmetry breaking, and $Q$ is the global charge of the Q-ball—in our case, baryon number. The condition $M_Q/Q < m_p$ ensures that the Q-ball is stable against decay to nucleons. The interaction of relic Q-balls with matter depends on its

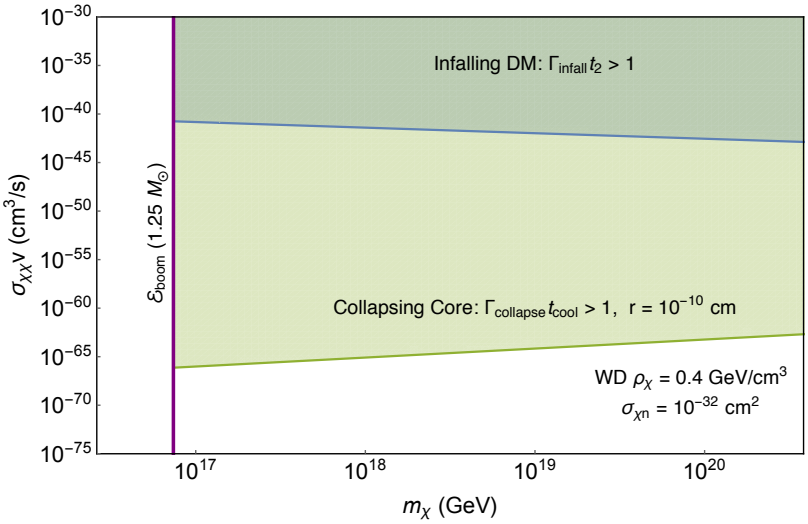


Figure 2.10: Constraints on DM-DM collision cross section to SM products of energy $\epsilon \gg$ MeV, assuming DM is captured with an elastic scattering cross section $\sigma_{\chi n} = 10^{-32}$ cm$^2$. Bounds come from the observation of 1.25 $M_\odot$ WDs in local DM density. We consider the annihilation rate during the in-falling thermalization stage (2.26) (blue shaded) and during self-gravitational collapse (2.27) to a stable radius $r = 10^{-10}$ cm (green shaded). See text for details.

ability to retain electric charge [49]. We restrict our attention to electrically neutral Q-balls, which induce the dissociation of incoming nucleons and in the process absorb their baryonic charge. During this proton decay-like process (see Figure 2.12), excess energy of order $\Lambda_{\rm QCD}$ is released via the emission of 2–3 pions. We assume that for each Q-ball inelastic collision, there is equal probability to produce $\pi^0$ and $\pi^\pm$ under the constraint of charge conservation. The cross section for this interaction is approximately geometric

$$\sigma_Q \sim \pi R_Q^2, \tag{2.33}$$

and thus grows with increasing $Q$. Note that a sufficiently massive Q-ball will become a black hole if $R_Q \lesssim G M_Q$. In the model described above, this translates into a condition $(M_{\rm pl}/m_S)^4 \lesssim Q$.

We now determine the explosiveness of a Q-ball transit. This process is described by a linear energy transfer

$$\left(\frac{dE}{dx}\right)_{\rm LET} \sim n_{\rm ion} \sigma_Q N_\pi \epsilon, \tag{2.34}$$

where the nuclear interaction results in $N_\pi \approx 30$ pions released, each with kinetic energy $\epsilon \approx 500$ MeV. These pions induce hadronic showers which terminate in low-energy hadrons that rapidly transfer their energy to ions via elastic scatters, as discussed in Section 2.3.

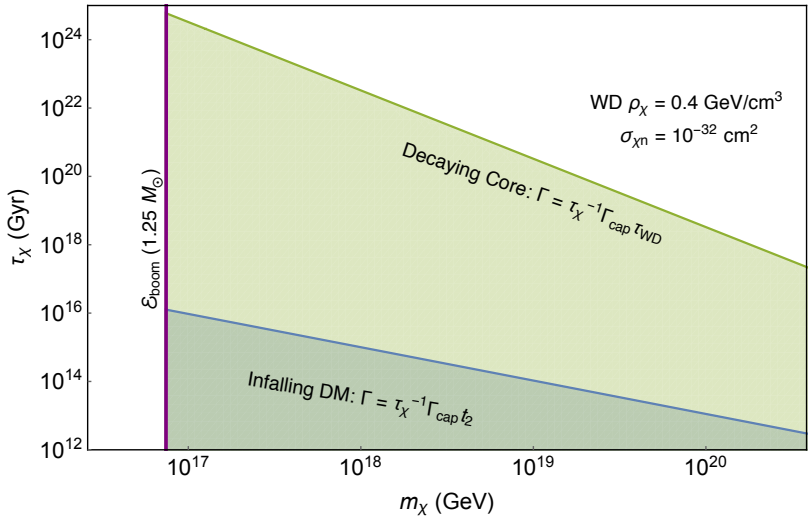


Figure 2.11: Constraints on DM decay to SM products of energy $\epsilon \gg$ MeV, assuming DM is captured with an elastic scattering cross section $\sigma_{\chi n} = 10^{-32}$ cm$^2$. Bounds come from the observation of 1.25 $M_\odot$ WDs in local DM density. We consider the rate of decays during the in-falling thermalization stage (blue shaded) and for a decaying DM core (green shaded). See text for details.

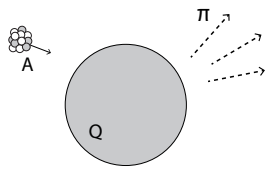


Figure 2.12: Interaction of a baryonic Q-ball with a nucleus $A$. The Q-ball destroys the nucleus and absorbs its baryonic charge, while the excess energy is radiated into roughly $A$ outgoing pions of energy $\Lambda_{\rm QCD}$.

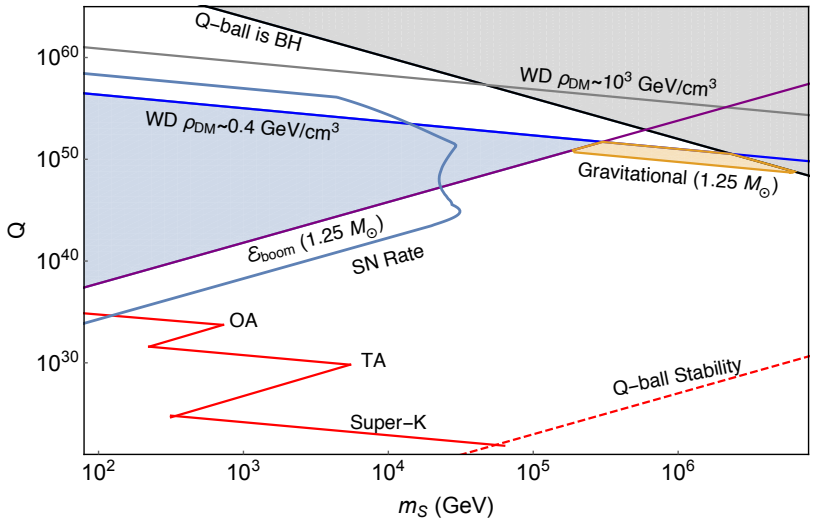


Figure 2.13: Constraints on Q-ball DM. Bounds come from demanding that the Q-ball interaction during a DM transit is capable of igniting WDs, occurring at a rate large enough to either ignite a single observed 1.25 $M_\odot$ WD in its lifetime (WD in local DM density is blue shaded) or exceed the measured SN rate in our galaxy. Also shown is the corresponding constraint from gravitational heating of WDs (orange shaded), and existing limits from terrestrial detectors (red) [50].

The pions have a heating length $X_{\rm had} \lesssim \lambda_T$; however, we will see the Q-ball has a finite size $R_Q \gtrsim X_{\rm had}$ in the region we are able to constrain. So, as mentioned in Section 2.4, we take the heating length to be $L_0 \sim R_Q + X_{\rm had} \sim R_Q$. The ignition condition is then given by equations (2.14) and (2.34):

$$R_Q^2 \gtrsim \frac{1}{n_{\rm ion}} \frac{\mathcal{E}_{\rm boom}}{\lambda_T} \max\left\{\frac{R_Q}{\lambda_T}, 1\right\}^2 \left(\frac{1}{10\ \text{GeV}}\right). \tag{2.35}$$

This implies $\sigma_Q \gtrsim 10^{-12}$ cm$^2$ is sufficient to ignite a 1.25 $M_\odot$ WD, which corresponds to a charge $Q \gtrsim 10^{42}\ (m_S/\text{TeV})^4$. Note that for sufficiently large $Q$, the radius will grow larger than $\lambda_T$. This situation still results in ignition, however, as the energy $\sim 10$ GeV released per ion is much larger than the $\sim$ MeV needed per ion for fusion. Note finally that the Q-ball interaction described above results in minimal slowing for Q-balls this massive, so transits will easily penetrate the non-degenerate WD envelope (2.13).

The existing limits on Q-balls primarily come from Super-Kamiokande and air fluorescence detectors of cosmic rays (OA, TA) [50]. However, the constraints that come from considering the ignition of WDs are in a fundamentally new and complementary region of parameter space. These are plotted in Figure 2.13. We have also included the constraints that result from gravitational heating of a WD during a Q-ball transit, as in [10].

## 2.7 Discussion

The detection of ultra-heavy DM is an open problem which will likely require a confluence of astrophysical probes. Here we present a guide to constraining these candidates through DM-SM scatters, DM-DM annihilations, and DM decays inside a WD that release sufficient SM energy to trigger runaway fusion. In particular, we calculate the energy loss of high-energy particles due to SM interactions within the WD medium and determine the conditions for which a general energy deposition will heat a WD and ignite SN. Ultra-heavy DM that produces greater than $10^{16}$ GeV of SM particles in a WD is highly constrained by the existence of heavy WDs and the measured SN rate. The formalism provided will enable WDs to be applied as detectors for any DM model capable of heating the star through such interactions. We have done so for baryonic Q-balls, significantly constraining the allowed parameter space in a complementary way to terrestrial searches.

We have explored briefly the application of this WD instability to self-gravitational collapse of DM cores, which has very interesting possibilities. The decay or annihilation of DM which is captured by a WD and forms a self-gravitating core is highly constrained for DM with mass greater than $10^{16}$ GeV. In addition, such collapsing cores can provide enough heating via multiple annihilations to ignite the star for much smaller DM masses than those considered here, e.g. $10^7$ GeV, and can induce SN through other means such as the formation and evaporation of mini black holes. This is addressed in Chapter 5.

Finally, in addition to the constraints mentioned above, the general phenomenology of these DM-induced runaways will be the ignition of sub-Chandrasekhar mass WDs, possibly with no companion star present. Some of the mechanisms considered above are also likely to initiate fusion far from the center of the star. This is in contrast with conventional single-degenerate and double-degenerate mechanisms, which require a companion star and ignite fusion near the center of a super-Chandrasekhar mass WD [11]. This raises the tantalizing possibility that DM encounters with WDs provide an alternative explosion mechanism for type Ia SN or similar transient events, and that these events may be distinguishable from conventional explosions. Understanding and searching for possible distinguishing features of DM-induced events is an important follow-up work.

# Chapter 3

# Type Ia Supernovae from Dark Matter Core Collapse

Dark matter (DM) which sufficiently heats a local region in a white dwarf will trigger runaway fusion, igniting a type Ia supernova (SN). In a companion paper, this instability was used to constrain DM heavier than $10^{16}$ GeV which ignites SN through the violent interaction of one or two individual DM particles with the stellar medium. Here we study the ignition of supernovae by the formation and self-gravitational collapse of a DM core containing many DM particles. For non-annihilating DM, such a core collapse may lead to a mini black hole that can ignite SN through the emission of Hawking radiation, or possibly as a by-product of accretion. For annihilating DM, core collapse leads to an increasing annihilation rate and can ignite SN through a large number of rapid annihilations. These processes extend the previously derived constraints on DM to masses as low as $10^5$ GeV.

## 3.1 Introduction

Dark matter (DM) accounts for over 80% of the matter density of the Universe, but its identity remains unknown. While direct detection [3] is a promising approach to identifying the nature of DM, searches for indirect signatures of DM interactions in astrophysical systems is also fruitful, particularly if the unknown DM mass happens to be large.

It was recently suggested [10] that white dwarfs (WD) act as astrophysical DM detectors: DM may heat a local region of a WD and trigger thermonuclear runaway fusion, resulting in a type Ia supernova (SN). DM ignition of sub-Chandrasekhar WDs was further studied in a companion paper [5], where we showed that generic classes of DM capable of producing high-energy standard model (SM) particles in the star can be constrained, e.g., by DM annihilations or decay to SM products. As an illustrative example, [5] placed new constraints on ultra-heavy DM with masses greater than $10^{16}$ GeV for which a single annihilation or decay is sufficient to ignite a SN.

Here we examine the possibility of igniting SN by the formation and self-gravitational

collapse of a DM core. We study two novel processes by which a collapsing DM core in a WD can ignite a SN—these were first pointed out in [5], and are studied here in more detail. If the DM has negligible annihilation cross section, collapse may result in a mini black hole (BH) that can ignite a SN via the emission of energetic Hawking radiation or possibly as it accretes. If the DM has a small but non-zero annihilation cross section, collapse can dramatically increase the number density of the DM core, resulting in SN ignition via a large number of rapid annihilations. Both of these processes extend the previously derived constraints on DM in [5], notably to masses as low as $10^5$ GeV.

A number of potential observables of DM cores in compact objects have been considered in the literature. These include: (1) gravitational effects of DM cores on the structure of low-mass stars [51, 52, 53, 54, 55], WDs [24], and neutron stars (NS) [56, 57, 58, 59], (2) BH formation and subsequent destruction of host NSs [60, 61, 62, 63, 64, 65, 66, 67, 68, 69, 70, 71, 72, 73, 74], and (3) anomalous heating from DM annihilations or scatters in WDs and NSs [75, 76, 77, 78, 79, 80, 81, 82]. See also [83, 84] for unique astroseismology signatures of possible low-mass bosonic DM cores. We emphasize that the signature of a DM core igniting a type Ia SN is distinct from these, and thus the constraints derived here are complementary. For instance, while it has been known that DM cores which form evaporating mini BHs are practically unobservable in a NS, this is decidedly not the case in a WD where (as we show) such BHs will typically ignite a SN. Note that [25] considers DM cores in WDs which inject heat and ignite SN through elastic DM-nuclear scatters—we discuss this process in more detail later as it pertains to our new constraints.

The paper is organized as follows. In Sec. 3.2, we review the triggering of runaway fusion by localized energy deposition in a WD. In Sec. 3.3, we summarize the necessary conditions for DM core collapse and discuss the generic end-states of such collapse. In Sec. 3.4 and Sec. 3.5, we derive constraints on DM cores which would ignite SN by the processes described above, namely black hole formation and DM-DM annihilations. We conclude in Sec. 3.6.

## 3.2 Triggering thermonuclear runaway

Thermonuclear runaway in a carbon WD generally occurs when the cooling timescale of a hot region exceeds the fusion timescale. Cooling is dominated by the thermal diffusion of either photons or degenerate electrons, while the highly exothermic fusion of carbon ions is unsuppressed at temperatures greater than their Coulomb threshold $\approx$ MeV. Crucially, the diffusion time increases with the size $L$ of the heated region while the fusion time is independent of $L$. This defines a critical trigger size and temperature for ignition:

$$L \gtrsim \lambda_T \quad \text{and} \quad T \gtrsim \text{MeV} \;\Rightarrow \text{ignite supernova.} \tag{3.1}$$

$\lambda_T$ was numerically computed in [21] and is $\lambda_T \approx 10^{-5}$ cm at a number density $n_{\text{ion}} \approx 10^{32}$ cm$^{-3}$.

One can also consider, as in [5], the critical energy $\mathcal{E}_{\text{boom}}$ required to heat an entire trigger region $\lambda_T^3$ to an MeV. $\mathcal{E}_{\text{boom}} \approx 10^{16}$ GeV for $n_{\text{ion}} \approx 10^{32}$ cm$^{-3}$ and sharply increases

at lower WD densities—this agrees with the expectation that WDs grow closer to instability as they approach the Chandrasekhar mass. Of course to trigger runaway fusion, an energy in excess of $\mathcal{E}_{\rm boom}$ must also be deposited sufficiently rapidly. The relevant timescale is the characteristic diffusion time $\tau_{\rm diff}$ across a region of size $\lambda_T$ at a temperature $\approx$ MeV. This diffusion time is also computed in [21] to be $\tau_{\rm diff} \approx 10^{-12}$ s at densities $n_{\rm ion} \approx 10^{32}$ cm$^{-3}$. Therefore a total energy $\mathcal{E}$, specifically deposited within a trigger region $\lesssim \lambda_T^3$ and a diffusion time $\lesssim \tau_{\rm diff}$, will ignite a SN if:

$$\mathcal{E} \gtrsim \mathcal{E}_{\rm boom} \;\Rightarrow \text{ignite supernova.} \tag{3.2}$$

One possibility is that the necessary energy (3.2) is deposited directly to carbon ions, e.g., by a transiting primordial BH [10]. It is also possible to deposit this energy indirectly, e.g., by DM interactions releasing SM particles into the stellar medium [5]. To this end the stopping distances of high-energy ($\gg$ MeV) particles in a WD was calculated in [5], where it was shown that hadrons, photons and electrons all transfer their energies to the stellar medium within a distance of order $\lambda_T$ (the sole exception being neutrinos). We thus safely presume that any $\mathcal{E} \gtrsim \mathcal{E}_{\rm boom}$ released into these SM products inside $\lambda_T^3$ will be efficiently deposited and thermalized within this region as well.

In summary, the rate of any process which deposits an energy $\mathcal{E}$ (defined to be localized spatially within $\lambda_T^3$ and temporally within $\tau_{\rm diff}$) that satisfies (3.2) can be constrained. This is done by either demanding that a single explosive event not occur during the lifetime of an observed heavy $\gtrsim 1.2\ M_\odot$ WD[1], or that the occurrence of many such events throughout the galaxy in predominantly lower mass WDs not affect the observed SN rate. For simplicity we just utilize the former here and the existence of a WD with properties:

$$\begin{aligned} n_{\rm ion} &\approx 10^{31}\ \text{cm}^{-3}, \quad \rho_{\rm WD} \approx 3 \cdot 10^8\ \frac{\text{g}}{\text{cm}^3}, \\ M_{\rm WD} &\approx 1.25\ M_\odot, \quad R_{\rm WD} \approx 3000\ \text{km}. \end{aligned} \tag{3.3}$$

Here $n_{\rm ion}$ and $\rho_{\rm WD}$ refer to the central density of the WD, and we relate this to its mass and radius using the equation of state formulated in [27]. While the average density is smaller by a factor $\sim 10^{-1}$, $n_{\rm ion}$ only changes by $\mathcal{O}(1)$ from the central value out to distances $\sim R_{\rm WD}/2$ [37]. For such a WD, the relevant trigger scales are of order:

$$\lambda_T \approx 4 \cdot 10^{-5}\ \text{cm}, \quad \mathcal{E}_{\rm boom} \approx 7 \cdot 10^{16}\ \text{GeV}, \quad \tau_{\rm diff} \approx 4 \cdot 10^{-11}\ \text{s}. \tag{3.4}$$

These values are approximate, but we expect they are accurate at the order of magnitude level, as are the ensuing constraints. Finally, we assume the WD has a typical interior temperature $T_{\rm WD} \approx$ keV and lifetime $\tau_{\rm WD} \approx 5$ Gyr [32].[2]

[1] For instance, the Sloan Digital Sky survey has cataloged $> 10$ such heavy WDs [34].

[2] The age of a WD is typically estimated by measuring its temperature and modeling the cooling over time.

## 3.3 Dark matter core collapse

Here we review the conditions for DM capture, collection, and self-gravitational collapse in a WD. As much of this discussion is already present in the literature, in what follows we simply quote the relevant results. We assume throughout that the DM loses energy primarily by short-range nuclear scatters. While other dissipation mechanisms are certainly possible (such as exciting dark states or emitting radiation) we will not treat these here.

Consider DM with mass $m_\chi \gg 10$ GeV and scattering cross section off ions $\sigma_{\chi A}$. For spin-independent interactions, $\sigma_{\chi A}$ is related to the DM-nucleon cross section $\sigma_{\chi n}$ by

$$\sigma_{\chi A} = A^2 \left(\frac{\mu_{\chi A}}{\mu_{\chi n}}\right)^2 F^2(q)\sigma_{\chi n} \sim A^4 F^2(q)\sigma_{\chi n}, \tag{3.5}$$

where $F^2(q)$ is the Helm form factor [85], and $q \sim m_{\rm ion} v_{\rm rel} \sim m_{\rm ion}\max[v, v_{\rm ion}]$ is the momentum transfer between the DM at velocity $v$ and a nuclear target. Currently the most stringent constraints on $\sigma_{\chi n}$ come from Xenon 1T [3]:

$$\sigma_{\chi n} < 10^{-45}\ {\rm cm}^2 \left(\frac{m_\chi}{\rm TeV}\right), \tag{3.6}$$

It is also possible for DM to have spin-dependent interactions (e.g., Majorana DM) which does not benefit from a $A^2$ coherent enhancement and is less constrained by direct detection [86]. WDs predominantly consist of spin-zero nuclei ($^{12}$C, $^{16}$O), though as pointed out by [62] DM capture/thermalization can proceed by scattering off a lower density of non-zero spin nuclei (e.g., a small fraction of $^{13}$C). For simplicity, we will restrict our attention here only to spin-independent interactions.

### Core formation

DM capture in compact objects has a long history [30, 31], though the usual formulae must be modified to account for heavy DM requiring multiple scatters to be captured (e.g., see [5]). DM transits the WD at a rate

$$\Gamma_{\rm trans} \sim \frac{\rho_\chi}{m_\chi} R_{\rm WD}^2 \left(\frac{v_{\rm esc}}{v_{\rm halo}}\right)^2 v_{\rm halo}, \tag{3.7}$$

where $v_{\rm esc} \approx 2 \cdot 10^{-2}$ is the escape velocity and $v_{\rm halo} \approx 10^{-3}$ is the virial velocity of our galactic halo. $\rho_\chi$ is the DM density in the region of the WD—we may consider either nearby WDs [34] with $\rho_\chi \approx 0.4\ \frac{\rm GeV}{\rm cm^3}$ or WDs close to the galactic center [35] where it is expected that $\rho_\chi \gtrsim 10^3\ \frac{\rm GeV}{\rm cm^3}$ [36]. Meanwhile, DM is captured by the WD at rate that is parametrically

$$\Gamma_{\rm cap} \sim \Gamma_{\rm trans} \cdot \min\left[1,\ \frac{N_{\rm scat}}{N_{\rm cap}(v_{\rm halo})}\right]. \tag{3.8}$$

$N_{\rm scat} \sim n_{\rm ion}\sigma_{\chi A}R_{\rm WD}$ is the average number of DM scatters during a single transit, and $N_{\rm cap}(v) \sim \frac{m_\chi v^2}{m_{\rm ion}v_{\rm esc}^2}$ is roughly the number of scatters needed for DM with velocity $v$ asymptotically far away from star to become gravitationally bound, though with a necessary minimum of $N_{\rm cap} \geq 1$. More properly, $\Gamma_{\rm cap}$ should be numerically calculated [87], though the expression in (3.8) is parametrically correct. Based on the assumed WD parameters (3.3), we find $N_{\rm cap}(v_{\rm halo}) > 1$ for DM masses $m_\chi > 10$ TeV; in this regime, the capture rate scales as $\Gamma_{\rm cap} \propto \frac{\sigma_{\chi A}}{m_\chi^2}$ as opposed to the usual $\Gamma_{\rm cap} \propto \frac{\sigma_{\chi A}}{m_\chi}$ result that is often used.

We now turn to DM thermalization. This may proceed in either of two qualitatively different regimes, orbital decay or terminal drift, depending on the strength of dissipation. For simplicity we compute detailed constraints only for the case of orbital decay, which is applicable in the case of sufficiently small DM-nuclei cross section $\sigma_{\chi A}$, though we also briefly comment on the dynamics of DM terminal drift.

In the limit of orbital decay, DM within the WD follows gravitational orbits which gradually shrink as the DM dissipates energy. We require here that the timescale of energy loss is much slower than the DM orbital period, which is simply the gravitational free-fall time in the star

$$t_{\rm ff} \sim \sqrt{\frac{1}{G\rho_{\rm WD}}} \approx 0.1 \text{ s}. \tag{3.9}$$

The rate of energy loss due to nuclear scatters is given by

$$\frac{dE}{dt} \sim \rho_{\rm WD}\sigma_{\chi A}v^2 \max[v, v_{\rm ion}], \tag{3.10}$$

where $v_{\rm ion} \sim \sqrt{\frac{T_{\rm WD}}{m_{\rm ion}}} \approx 4 \cdot 10^{-4}$ is the thermal ion velocity and $v$ is the velocity of the "infalling" DM. The *max* function distinguishes between the regimes of "inertial" and "viscous" drag, with the latter being relevant once $v$ drops below $v_{\rm ion}$. This dissipation is always small on orbital timescales provided $\sigma_{\chi A}$ is below a critical cross section

$$\sigma_{\rm ff} \sim \frac{m_\chi}{\rho_{\rm WD}v_{\rm esc}t_{\rm ff}} \approx 3 \cdot 10^{-38} \text{ cm}^2 \left(\frac{m_\chi}{\text{TeV}}\right). \tag{3.11}$$

In addition to the drag force of (3.10), nuclear scatters will inflict a slight Brownian motion on the DM trajectory, though this only becomes important at cross sections well above $\sigma_{\rm ff}$. An individual nuclear scatter will transfer a small amount of momentum $\delta p \ll m_\chi v$ to the DM,

$$\delta p \sim m_{\rm ion} \max[v, v_{\rm ion}], \tag{3.12}$$

which is set by the ion momentum in the rest frame of the DM and is roughly constant for hard scatters. Over the course of one orbit, an accumulation of momentum transfers will yield a net change $\Delta p$. This accumulation is a Brownian process as each scatter transfers momentum of roughly the same magnitude $\delta p$ (3.12) but with a random direction, giving

$\Delta p \sim \delta p \cdot N^{1/2}$ where $N \sim n_{\rm ion}\sigma_{\chi A}\max[v, v_{\rm ion}]\, t_{\rm ff}$ is the number of scatters occurring during an orbit. We find that $\Delta p$ is small compared to the DM momentum $m_\chi v$ provided that $\sigma_{\chi A} < \sigma_{\rm ff}$. Thus the DM undergoes negligible deflection during an orbit, and Brownian motion may indeed be ignored for the case of orbital decay.

Thermalization in the orbital decay limit proceeds in three stages (e.g., see [62] for a detailed derivation). First, the DM will pass through the star many times on a wide elliptic orbit of initial size $R_i \gg R_{\rm WD}$ set by the number of scatters during the first stellar transit:

$$R_i \sim R_{\rm WD}\left(\frac{m_\chi}{m_{\rm ion}}\right)\frac{1}{\max[N_{\rm scat}, 1]}. \tag{3.13}$$

The time for the DM orbital size to become contained within the WD is then:

$$t_1 \sim \frac{m_\chi}{\rho_{\rm WD}\sigma_{\chi A} v_{\rm esc}}\left(\frac{R_i}{R_{\rm WD}}\right)^{1/2}, \quad (R_i \to R_{\rm WD}). \tag{3.14}$$

Note that $t_1$ is parametrically shorter if the DM scatters multiple times in a single transit $N_{\rm scat} > 1$ (see (3.13)), corresponding to cross sections $\sigma_{\chi n} > 10^{-41}$ cm$^2$. This results in a change of slope at $10^{-41}$ cm$^2$ in the constraints shown in Fig. 3.1, 3.4, and 3.5. Subsequently the DM completes many orbits within the star, losing energy according to (3.10). Eventually the DM reaches velocities $v_{\rm th}$ and settles at a radius $R_{\rm th}$ where its kinetic energy is of order $T_{\rm WD}$ and balances the gravitational potential of the enclosed WD mass:

$$v_{\rm th} \sim \sqrt{\frac{T_{\rm WD}}{m_\chi}} \approx 10^{-7}\left(\frac{m_\chi}{10^8\ {\rm GeV}}\right)^{-1/2}, \tag{3.15}$$

$$R_{\rm th} \sim \left(\frac{T_{\rm WD}}{G m_\chi \rho_{\rm WD}}\right)^{1/2} \approx 500\ {\rm cm}\left(\frac{m_\chi}{10^8\ {\rm GeV}}\right)^{-1/2}. \tag{3.16}$$

The DM first slows to $v_{\rm ion}$ in a time

$$t_2 \sim \frac{m_\chi}{\rho_{\rm WD}\sigma_{\chi A} v_{\rm ion}}, \quad (v_{\rm esc} \to v_{\rm ion}). \tag{3.17}$$

and then to $v_{\rm th}$ in a time that is logarithmically greater:

$$t_3 \sim t_2 \log\left(\frac{m_\chi}{m_{\rm ion}}\right), \quad (v_{\rm ion} \to v_{\rm th}). \tag{3.18}$$

A DM core will thus form within the age of the WD for $\sigma_{\chi A} < \sigma_{\rm ff}$ if

$$t_1 + t_2 + t_3 < \tau_{\rm WD} \quad \text{(form DM core)}. \tag{3.19}$$

We now consider $\sigma_{\chi A} > \sigma_{\rm ff}$, the regime of terminal drift, in which case the condition for core formation is parametrically different than (3.19). In particular, the time required for DM to settle to $R_{\rm th}$ increases with increasing $\sigma_{\chi A}$, which sets an upper bound $\sigma_{\rm max}$ on the

cross sections for which a DM core can form within the age of a WD. In this scenario, $\mathcal{O}(1)$ of the DM kinetic energy is rapidly lost in the first pass through the star. The dynamics are then dominated by the drag force corresponding to (3.10)

$$F_A \sim \rho_{\rm WD}\sigma_{\chi A} v \, \max[v, v_{\rm ion}], \tag{3.20}$$

and the DM will fall towards $R_{\rm th}$ on a predominantly radial trajectory with the infall velocity given by the terminal speed at which $F_A$ balances gravity. To estimate $\sigma_{\rm max}$, we consider the extreme case of large $\sigma_{\chi A}$ and a radial infall. Here $F_A$ takes the linear form as $v$ is small, and the DM drifts always with the local terminal speed, yielding a drift time

$$t_{\rm drift} \sim \frac{t_{\rm ff}^2}{t_2} \, \log\left(\frac{R_{\rm WD}}{R_{\rm th}}\right). \tag{3.21}$$

Core formation occurs if $t_{\rm drift} < \tau_{\rm WD}$, which sets an upper bound $\sigma_{\rm max} \sim 10^{16}\ \sigma_{\rm ff}$. Finally, with $\sigma_{\chi A} > \sigma_{\rm ff}$, the Brownian nature of nuclear scatters may become important before a DM particle reaches $R_{\rm th}$, and its motion will then be a random walk with an inward gravitational drift. Indeed, the terminal velocity may fall below $v_{\rm th}$ as the DM approaches the center of the star, at which point the DM becomes thermal even outside of $R_{\rm th}$ and equilibrates with the stellar medium. The DM then settles into a Boltzmann distribution of temperature $T_{\rm WD}$, in this case a Gaussian density profile with size $R_{\rm th}$ in the center of the star. The relevant core formation timescale is now the time required for thermal DM particles located at some $r > R_{\rm th}$ to settle into this distribution. But, such a biased random walk proceeds precisely as Brownian motion about a center which drifts inward at the terminal speed—thus the timescale for infall is just (3.21) and the bound $\sigma_{\rm max}$ is valid regardless of the onset of Brownian motion.

## Asymmetric DM Collapse

First consider the evolution of a core of non-annihilating DM, herein referred to as asymmetric DM [88, 89]. Upon formation, the DM core will steadily collect at $R_{\rm th}$ at a rate $\Gamma_{\rm cap}$. If its density ever exceeds the WD density $\rho_{\rm WD}$, then the core will become self-gravitating. The critical number of DM particles needed for the onset of self-gravitation is

$$N_{\rm sg} \sim \frac{\rho_{\rm WD} R_{\rm th}^3}{m_\chi} \approx 5 \cdot 10^{32} \left(\frac{m_\chi}{10^8\ {\rm GeV}}\right)^{-5/2}, \tag{3.22}$$

while the total number of DM particles that can possibly be collected within $\tau_{\rm WD}$ is simply:

$$N_{\rm life} \sim \Gamma_{\rm cap}\tau_{\rm WD}. \tag{3.23}$$

Thus self-gravitational collapse requires

$$N_{\rm sg} < N_{\rm life}, \quad \text{(core self-gravitates)}. \tag{3.24}$$

This sets an upper limit on the DM mass that can form a self-gravitating core $m_\chi \gtrsim 100$ TeV (or $R_{\rm th} \lesssim 0.1$ km), taking the maximum possible capture rate $\Gamma_{\rm cap} = \Gamma_{\rm trans}$ and $\rho_\chi = 0.4\ \frac{\rm GeV}{\rm cm^3}$.

Of course, this assumes that the DM core obeys Maxwell-Boltzmann statistics throughout the collection phase. In general, the quantum statistics of DM with velocity $v$ in a core of size $N$ becomes important once the de Broglie wavelength of individual DM particles exceeds their physical separation in the core. For the thermal DM population at $R_{\rm th}$, this occurs after it has collected a number:

$$N_{\rm QM,\ th} \sim (m_\chi T_{\rm WD})^{3/2} R_{\rm th}^3 \sim \frac{T_{\rm WD}^3}{(G\rho_{\rm WD})^{3/2}} \approx 10^{52}, \tag{3.25}$$

which is greater than $N_{\rm sg}$ for all DM masses $m_\chi \gtrsim$ GeV. In the case of bosonic DM, if the core reaches $N_{\rm QM,\ th}$ before the onset of self-gravitation it will begin populating a Bose-Einstein condensate (BEC). A more compact BEC could then self-gravitate earlier, as considered by [60, 64, 63] in a NS. We find this is not possible in a WD, namely $N_{\rm QM,\ th} \gg N_{\rm life}$ even for light bosonic DM $m_\chi \lesssim$ GeV. Thus the condition for core collapse is indeed (3.24).

For simplicity, we focus on DM which scatters infrequently with the medium, $\sigma_{\chi A} < \sigma_{\rm ff}$, see (3.11). The orbital timescale of the constituents of a collapsing core decreases faster than the timescale of energy loss due to nuclear scatters, so in this regime the DM trajectories will continue to have the form of slowly decaying orbits during the entire collapse.

In summary, the conditions (3.19) and (3.24) on $\{m_\chi, \sigma_{\chi n}\}$ parameter space for which a DM core forms and collapses in a WD are depicted in Fig. 3.1. One can check that for DM masses and scattering cross sections satisfying (3.24), the left-hand side of the core formation condition (3.19) is ultimately dominated by $t_1$. We also show a rough amalgamation (e.g., see [43]), extending to large DM masses and cross sections, of the constraints from underground direct detection experiments including Xenon 1T [3].

We now turn to the dynamics of collapse. In order for a self-gravitating DM core to shrink, it must lose the excess gravitational potential energy. The "cooling" timescale $t_{\rm col}$ (leading to gravitational heating of the DM) is initially independent of DM velocity but hastens once the DM velocity exceeds $v_{\rm ion}$. For a collapsing DM core with a number of particles $N_{\rm col}$, the velocity and characteristic collapse time at size $r$ is:

$$\begin{aligned} v_{\rm col}(r) &\sim \sqrt{\frac{G N_{\rm col} m_\chi}{r}}, \\ t_{\rm col}(r) &\sim \frac{m_\chi v_{\rm col}^2}{dE/dt(v_{\rm col})} \sim t_2 \min\left[1,\ \frac{v_{\rm ion}}{v_{\rm col}}\right], \end{aligned} \tag{3.26}$$

where we have used elastic scatters (3.10) as the dominant dissipation mechanism. This should be modified once $v_{\rm col} \gtrsim 2 \cdot 10^{-2}$ and the momentum transfer becomes $\sim \Lambda_{\rm QCD}$. At this point the interaction is not described by elastic scattering off nuclei, but an inelastic scattering off constituent quarks. This is a non-perturbative QCD process that will result in the release of pions. Since the typical momentum transfer here saturates at $\sim \Lambda_{\rm QCD}$, the energy transfer per scatter scales linearly with velocity and is roughly of order $\sim \Lambda_{\rm QCD} v_{\rm col}$.

For simplicity, we assume that the cross section for this inelastic interaction is also of order $\sigma_{\chi A}$ (with the form factor (3.5) set to $A^{-2}$). The rate of energy loss in this regime is parametrically

$$\frac{dE}{dt} \sim \Lambda_{\rm QCD} n_{\rm ion} \sigma_{\chi A} v_{\rm col}^2. \tag{3.27}$$

Thus at velocities $v_{\rm col} \gtrsim 2 \cdot 10^{-2}$, the characteristic core collapse time saturates to $t_{\rm col} \sim \frac{m_\chi}{n_{\rm ion}\sigma_{\chi A}\Lambda_{\rm QCD}}$. One can also check that $t_{\rm col}$ is always greater than the (decreasing) dynamical time $\sim r/v_{\rm col}$.

We emphasize that while cooling by nuclear scatters during core collapse is the minimal assumption, other dissipation mechanisms (e.g., radiating as a blackbody) could become efficient due to the increasing DM density, as considered by [60]. However since this is more model-dependent, we do not consider any such additional cooling mechanisms here.

Actually, the initial number of collapsing particles can be parametrically greater than the critical self-gravitation number $N_{\rm col} \gg N_{\rm sg}$ As discussed in [5], this occurs when the time to capture a self-gravitating number is much less than the time for the DM core to collapse, i.e., when $N_{\rm sg} < \Gamma_{\rm cap} t_{\rm col}$. We find this is relevant for DM masses $m_\chi \gtrsim 10^{14}$ GeV. Here the collapsing core will inevitably "over-collect" to a much larger number until these two timescales become comparable $N_{\rm col} \sim \Gamma_{\rm cap} t_{\rm col}$, although the density profile of the core at this point is highly non-trivial. It is worth noting that the collapsing core would likely be non-uniform even in the absence of over-collection, as emphasized in [66]—realistically, the core might develop a "cuspy" profile similar to the formation of galactic DM halos. In either case, a precise understanding of the DM core density profile is beyond the scope of this work. For simplicity we will assume a core of *uniform* density with a number of collapsing particles

$$N_{\rm col} = \max[N_{\rm sg},\ \Gamma_{\rm cap} t_{\rm col}]. \tag{3.28}$$

However, this assumption of a uniform density core is likely a conservative one with regards to our constraints. For asymmetric DM, a density peak within the collapsing core (e.g. due to over-collection) would collapse to BHs of smaller mass than otherwise assumed and (as we show) would still ignite a SN. For annihilating DM, a density peak may have a greater rate of annihilations depending on the density profile which would ignite a SN sooner than otherwise assumed.

Though irrelevant prior to self-gravitation, QM effects may become important during the collapse itself. For a number of collapsing particles $N_{\rm col} = N_{\rm sg}$, this occurs once the de Broglie wavelengths of DM particles in the core begin overlapping: $\frac{1}{m_\chi v_{\rm col}(r)} \sim \frac{r}{N_{\rm sg}^{1/3}}$. That is, once the core has shrunk to a size

$$R_{\rm QM} \sim \frac{1}{G m_\chi^3 N_{\rm sg}^{1/3}} \approx 3 \cdot 10^{-11}\ {\rm cm} \left(\frac{m_\chi}{10^8\ {\rm GeV}}\right)^{-13/6}, \tag{3.29}$$

and has a density

$$\rho_{\rm QM} \sim \frac{N_{\rm sg} m_\chi}{R_{\rm QM}^3} \sim \frac{m_\chi^5 T_{\rm WD}^3}{\rho_{\rm WD}} \approx 10^{72} \frac{\rm GeV}{\rm cm^3} \left(\frac{m_\chi}{10^8\ {\rm GeV}}\right)^5. \tag{3.30}$$

Of course this assumes that the core has not already formed a BH $GN_{\rm sg}m_\chi \lesssim R_{\rm QM}$. This means that QM collapse is only relevant for DM masses:

$$m_\chi \lesssim \frac{\rho_{\rm WD}}{T_{\rm WD}^3} \approx 10^9 \text{ GeV}, \quad \text{(QM affects collapse)}, \tag{3.31}$$

for which it is indeed the case that $N_{\rm col} = N_{\rm sg}$. Note that the extreme densities of the DM core (3.30) are not necessarily problematic as we always assume the DM is point-like with no substructure; however, with an explicit model one should be wary of higher dimension operators modifying the collapse dynamics by potentially triggering new interactions.

**Fermionic DM** If DM is a fermion, (3.29) is precisely the radius of stabilization due to degeneracy pressure. A degenerate DM core will sit at $R_{\rm QM}$ until it collects an additional number of particles $N \gg N_{\rm sg}$ and subsequently shrinks as $r \sim \frac{1}{Gm_\chi^3 N^{1/3}}$. Note that additional captured DM particles are still able to dissipate energy and decrease their orbital sizes below the thermal radius under the gravitational influence of the compact core. For DM masses (3.31) the collection time $\frac{N}{\Gamma_{\rm cap}}$ is always far greater than the cooling time $t_{\rm col}$ (3.26), and thus the shrinking proceeds adiabatically at a rate $\Gamma_{\rm cap}$.

Fermi pressure is capable of supporting a self-gravitating degenerate DM core until it exceeds the Chandrasekhar limit

$$N_{\rm Cha}^{\rm f} \sim \frac{M_{\rm pl}^3}{m_\chi^3} \approx 2 \cdot 10^{33} \left(\frac{m_\chi}{10^8 \text{ GeV}}\right)^{-3}. \tag{3.32}$$

Thus the fermi degenerate core will collapse to a BH as long as

$$N_{\rm Cha}^{\rm f} < N_{\rm life}, \quad \text{(BH from degenerate core)}, \tag{3.33}$$

which is the case for $m_\chi \gtrsim 10^6$ GeV, assuming $\Gamma_{\rm cap} = \Gamma_{\rm trans}$ and $\rho_\chi = 0.4 \frac{\rm GeV}{\rm cm^3}$. We note that the presence of attractive e.g., Yukawa-type DM self-interactions can drastically reduce the critical number required to overcome Fermi pressure (see [70]), though we do not consider this possibility here.

**Bosonic DM** If DM is a boson, once the DM core collapses to (3.29) it starts populating a BEC. Further collapse results in increasing the number of particles in the BEC, with the density of the non-condensed particles fixed at $\rho_{\rm QM}$, see [66] for details. The size of the BEC is initially set by the gravitational potential of the enveloping self-gravitating sphere, and particles in the BEC have a velocity set by the uncertainty principle:

$$\begin{aligned} r_{\rm BEC} &\sim \left(\frac{1}{G\rho_{\rm QM}m_\chi^2}\right)^{1/4} \approx 10^{-16} \text{ cm} \left(\frac{m_\chi}{10^8 \text{ GeV}}\right)^{-7/4}, \\ v_{\rm BEC} &\sim \frac{1}{m_\chi r_{\rm BEC}} \approx 10^{-6} \left(\frac{m_\chi}{10^8 \text{ GeV}}\right)^{3/4}. \end{aligned} \tag{3.34}$$

The BEC sits at $r_{\rm BEC}$ until it becomes self-gravitating at a number:

$$N_{\rm BEC,\ sg} \sim \frac{\rho_{\rm QM} r_{\rm BEC}^3}{m_\chi} \approx 2 \cdot 10^{16} \left(\frac{m_\chi}{10^8\ {\rm GeV}}\right)^{-5/4}. \tag{3.35}$$

A self-gravitating BEC will continue to add particles, and in the process shrink as $r_{\rm BEC} \sim \frac{1}{G m_\chi^3 N}$. The rate at which DM particles are added to the BEC is set by the rate at which the non-condensed DM core sheds the excess gravitational energy. The time to condense a number of particles $N \ll N_{\rm sg}$ is:

$$t_{\rm BEC}(N) \sim \frac{N}{N_{\rm sg}} t_{\rm col}(R_{\rm QM}). \tag{3.36}$$

Note that the typical DM velocity in the non-condensed DM sphere at this stage is:

$$v_{\rm col}(R_{\rm QM}) \sim \sqrt{\frac{G N_{\rm sg} m_\chi}{R_{\rm QM}}} \approx 0.3 \ \left(\frac{m_\chi}{10^8\ {\rm GeV}}\right)^{1/3}. \tag{3.37}$$

The pressure induced by the uncertainty principle is capable of supporting the self-gravitating sphere of DM particles until it exceeds the so-called bosonic Chandrasekhar limit:

$$N_{\rm Cha}^{\rm b} \sim \frac{M_{\rm pl}^2}{m_\chi^2} \approx 10^{22} \left(\frac{m_\chi}{10^8\ {\rm GeV}}\right)^{-2}, \tag{3.38}$$

which is far less than $N_{\rm sg}$ for all DM masses (3.31). Interestingly, this limit is dramatically affected by even the presence of miniscule DM self-interactions [90]. These may be a generic expectation given the already assumed scattering cross section off nucleon, as emphasized in [69]. In the case of a repulsive $\lambda|\chi|^4$ interaction potential where $\lambda > 0$, no stable configuration exists beyond a critical number

$$N_{\rm Cha,\ self}^{\rm b} \sim \frac{M_{\rm pl}^2}{m_\chi^2} \left(1 + \frac{\lambda}{32\pi} \frac{M_{\rm pl}^2}{m_\chi^2}\right)^{1/2}. \tag{3.39}$$

We find that $N_{\rm Cha,\ self}^{\rm b}$ is still less than $N_{\rm sg}$ as long as $\lambda \lesssim 10^{-2}$. An attractive self-interaction could reduce the necessary critical limit, although this is highly model-dependent. From here on, we will use (3.38) as the relevant critical limit.

## Annihilating DM Collapse

Now consider the case of DM with an annihilation cross section $\sigma_{\chi\chi}$ into SM products, e.g., quarks. We will restrict our attention here to DM masses $m_\chi \ll \mathcal{E}_{\rm boom}$ such that multiple annihilations are necessary to ignite a SN. As in the asymmetric case, for simplicity we focus on DM which scatters infrequently, $\sigma_{\chi A} < \sigma_{\rm ff}$.

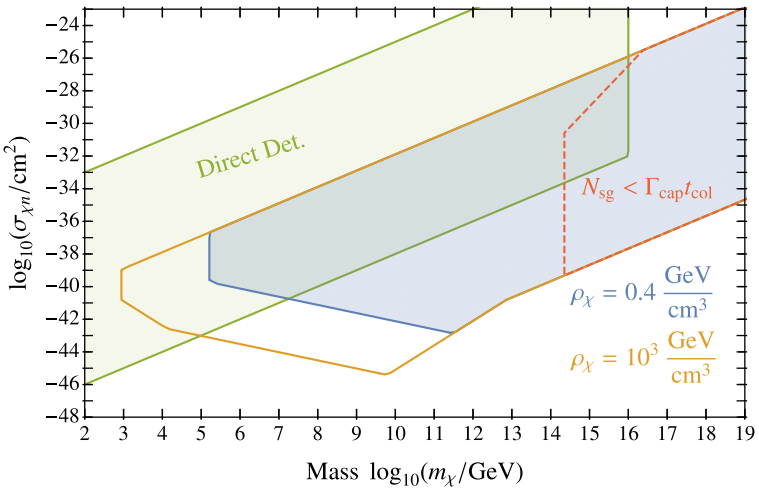


Figure 3.1: Parameter space $\{m_\chi, \sigma_{\chi n}\}$ of asymmetric DM in which a DM core forms and collapses within $\tau_{WD} \approx 5$ Gyr in a WD of local DM density $\rho_\chi$. See text for details.

As described above, the thermalizing DM constitutes a number density of DM throughout the WD volume. Depletion of this in-falling DM is dominated by the total rate of annihilations near the thermal radius:

$$\Gamma_{infall} \sim \frac{(\Gamma_{cap} t_2)^2}{R_{th}^3} \sigma_{\chi\chi} v_{th}. \tag{3.40}$$

Therefore a DM core at $R_{th}$ will steadily collect at a rate roughly $\Gamma_{cap}$ as long as

$$\Gamma_{infall} < \Gamma_{cap}, \quad \text{(steady DM collection)}. \tag{3.41}$$

Of course this collecting DM core is also depleting via annihilations, and will at most reach an equilibrium number

$$N_{eq} \sim \left( \frac{\Gamma_{cap} R_{th}^3}{\sigma_{\chi\chi} v_{th}} \right)^{1/2}. \tag{3.42}$$

This results in a more stringent condition for self-gravitation:

$$N_{sg} < \min[N_{life}, N_{eq}], \quad \text{(core self-gravitates)}. \tag{3.43}$$

If $N_{sg} > N_{life}$ or $N_{sg} > N_{eq}$, the DM core has either saturated at a number $N_{eq}$ or is still continuing to collect at a number $N_{life}$, whichever comes first. In either case if the core does not reach self-gravitation (i.e. (3.43) is not satisfied), we found that the total rate of annihilations within a core subregion of volume $\lambda_T^3 \ll R_{th}^3$ is much too small to ignite a SN.

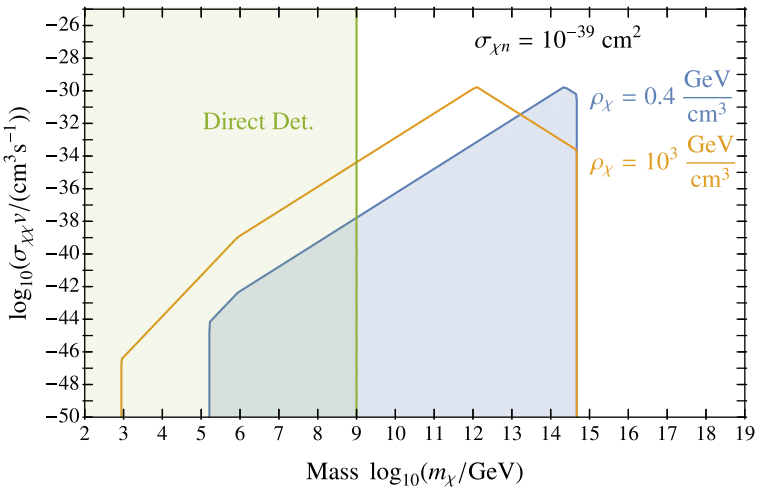


Figure 3.2: Parameter space $\{m_\chi, \sigma_{\chi\chi} v\}$ of annihilating DM in which a DM core forms and collapses within $\tau_{\rm WD} \approx 5$ Gyr in a WD of local DM density $\rho_\chi$. We take a fixed value of the DM-nuclei scattering cross section $\sigma_{\chi n} = 10^{-39}$ cm$^2$. See text for details.

We thus turn to core collapse, during which annihilations become more rapid as the core shrinks. The conditions (3.19), (3.41) and (3.43) on the $\{m_\chi, \sigma_{\chi\chi} v\}$ parameter space for which a collapse takes place are depicted in Fig. 3.2. Here we have taken a fixed fiducial value of the scattering cross section $\sigma_{\chi n} = 10^{-39}$ cm$^2$, though the allowed parameter space of collapse in the case of annihilating DM exists for any $\sigma_{\chi n}$ within the region shown in Fig. 3.1. We have checked that there are no existing constraints at these low DM annihilation cross sections, for instance from DM annihilations in the galactic halo contributing to the observed cosmic ray flux.

As before, a self-gravitating DM core shrinks at a rate set by cooling (3.26). However the core is also annihilating so that $N(r)$ is decreasing from its initial value $N_{\rm col}$ (3.28). When the DM core is at a radius $r$, the total rate of annihilations is:

$$\Gamma_{\chi\chi} \sim \frac{N^2}{r^3} \sigma_{\chi\chi} v_{\rm col}, \tag{3.44}$$

The collapse will initially proceed unscathed, with the number of collapsing particles roughly constant $N(r) \approx N_{\rm col}$, until the characteristic annihilation time $\frac{N}{\Gamma_{\chi\chi}}$ is of order the collapse time $t_{\rm col}$. The size of the core at this stage is an important scale, which we denote as $R_{\chi\chi}$. Note that $R_{\chi\chi}$ as defined is trivially smaller than $R_{\rm th}$ if conditions (3.41) and (3.43) are satisfied. The expression for $R_{\chi\chi}$ depends on whether this takes place during the "viscous" or "inertial" drag regimes, or in the inelastic scattering regime (3.27). Written in terms of

the annihilation cross-section $\sigma_{\chi\chi} v_{\rm col}$, this scales as:

$$R_{\chi\chi} \propto \begin{cases} (\sigma_{\chi\chi} v_{\rm col})^{1/3} & v_{\rm col} < v_{\rm ion} \text{ or } 2 \cdot 10^{-2} < v_{\rm col} \\ (\sigma_{\chi\chi} v_{\rm col})^{2/5} & v_{\rm ion} < v_{\rm col} < 2 \cdot 10^{-2} \end{cases} . \tag{3.45}$$

Note that $v_{\rm col}$ is to be evaluated at $R_{\chi\chi}$ in these expressions.

Once the DM core collapses to within $R_{\chi\chi}$, it begins depleting appreciably. We call this an annihilation burst. Once $r \lesssim R_{\chi\chi}$, the continued evolution of the DM core is driven by two competing effects: scatters with the stellar matter drive the core to collapse to smaller radii, as before, but at the same time annihilations drive the core to expand by weakening the gravitational potential. We do not work out this detailed evolution, but rather conservatively consider the constraints only for $r \gtrsim R_{\chi\chi}$.

For DM masses (3.31), if $R_{\chi\chi} > R_{\rm QM}$ then the core effectively annihilates before any quantum statistics become significant. On the other hand, if $R_{\chi\chi} < R_{\rm QM}$ then the core remains roughly intact and can form a fermi degenerate core or BEC, as in the asymmetric DM case. We examine the subsequent evolution of the core in the case $R_{\chi\chi} < R_{\rm QM}$, but with the added presence of annihilations.

**Fermionic DM** If DM is a fermion, a fermi degenerate core will continue to collect DM particles and shrink (and thus the rate of annihilations increases). During this stage, the degenerate DM core can saturate at an equilibrium $N^{\rm f}_{\chi\chi}$ when the annihilation rate $\Gamma_{\chi\chi}$ is of order the shrinking rate set by DM capture $\Gamma_{\rm cap}$. If $N^{\rm f}_{\chi\chi} \lesssim N_{\rm sg}$, the fermi degenerate core saturates while still roughly at $R_{\rm QM}$ (3.29). If $N^{\rm f}_{\chi\chi} \gtrsim N_{\rm sg}$, the core substantially shrinks before saturating at a number:

$$N^{\rm f}_{\chi\chi} \sim \frac{\Gamma_{\rm cap}^{1/3}}{G m_\chi^3 (\sigma_{\chi\chi} v_{\rm col})^{1/3}}, \quad N^{\rm f}_{\chi\chi} > N_{\rm sg}. \tag{3.46}$$

Of course, for sufficiently low annihilation cross section a saturated core may never form in the WD lifetime $N_{\rm life} < N^{\rm f}_{\chi\chi}$ or before forming a BH $N^{\rm f}_{\rm Cha} < N^{\rm f}_{\chi\chi}$.

**Bosonic DM** If DM is a boson the core will condense particles into a BEC. As the non-condensed core collapse proceeds at constant density, it will never burst as the rate of annihilations in the enveloping sphere only decreases. However the BEC can saturate at an equilibrium number when the annihilation rate in the compact region becomes of order the condensation rate given by (3.36). We have checked that this saturation is never reached before the BEC self-gravitates at a number (3.35). Subsequently the BEC adds particles from the core and shrinks (and the rate of annihilations in the BEC increases). The self-gravitating BEC then either saturates at a number

$$N^{\rm b}_{\chi\chi} \sim \left( \frac{N_{\rm sg}}{t_{\rm col}(R_{\rm QM}) G^3 m_\chi^9 \sigma_{\chi\chi} v_{\rm BEC}} \right)^{1/5}, \quad N^{\rm b}_{\chi\chi} > N_{\rm BEC,\,sg}. \tag{3.47}$$

or first reaches $N^{\rm b}_{\rm Cha}$ when annihilations are negligible and forms a BH.

### Endgame

There are many possible outcomes of the DM core collapse in a WD.For asymmetric DM the core can collapse to a mini BH, either directly or by first forming a fermi degenerate core or populating a BEC.As detailed in Sec. 3.4, such a BH can ignite a SN by emission of Hawking radiation or, as we motivate, possibly even during its accretion. For annihilating DM the core annihilates at an increasing rate until collapsing to $R_{\chi\chi}$, at which point it is effectively annihilating an $\mathcal{O}(1)$ fraction. As detailed in Sec. 3.5, this large number of rapid annihilations can even ignite a SN before the core reaches $R_{\chi\chi}$.

It is also the case that the DM core is directly heating the WD via nuclear scatters. This may be sufficient to ignite a SN, as first calculated by [25]. We estimate the total energy deposited by a collapsing core of size $r$ inside a trigger region $\lambda_T^3$ during a time $\tau_{\rm diff}$ as:

$$\mathcal{E}_{\chi A}(r) \sim N_{\rm col} m_\chi v_{\rm col}^2 \left(\frac{\tau_{\rm diff}}{t_{\rm col}}\right) \cdot \min\left[1, \left(\frac{\lambda_T}{r}\right)^3\right]. \tag{3.48}$$

In considering this process, [25] additionally required that (1) the DM core be self-thermalized (e.g., due to DM-DM self interactions) and (2) the core must uniformly heat a trigger region $\lambda_T^3$, thus restricting the analysis to core sizes $r \gtrsim \lambda_T$. Neither of these requirements are necessary, however. While a deposited energy well inside the trigger region may not immediately ignite a conductive flame as per [21], it will eventually if the energy is sufficiently large (3.2) once the heat has diffused out to a size $\sim \lambda_T$ (see [5] for a more detailed discussion of this evolution). This observation allows the derived constraints of [25] to be extended to larger DM masses: we simply require $\mathcal{E}_{\chi A} \gtrsim \mathcal{E}_{\rm boom}$ satisfies the condition (3.2) in order for scattering to ignite a SN.

We emphasize that the heat deposited in the stellar matter during a DM collapse would be drastically affected by the presence of an additional cooling mechanism which drives the collapse, e.g., emitting dark radiation. In particular, if such a cooling mechanism is present and efficient in a collapsing core, ignition due to heating by nuclear scatters as in [25] might not occur. As we show in Sec. 3.4 and Sec. 3.5, however, most collapsing DM cores would still ignite a SN from BH formation or annihilations. For this reason, while we show the extended constraints on DM-nuclear scatters from (3.48), we will also consider and show the consequences of core collapse to smaller radii, below the size at which nuclear scatters (as the sole cooling mechanism) would deposit sufficient energy to be constrained.

## 3.4 Black hole-induced SN

As described in Sec. 3.3, a BH formed by DM collapse will have an initial mass (shown in Fig. 3.3):

$$M_{\rm BH} \sim \begin{cases} N_{\rm Cha}^{\rm f} m_\chi & m_\chi \lesssim 10^9 \text{ GeV} \quad \text{fermionic DM} \\ N_{\rm Cha}^{\rm b} m_\chi & m_\chi \lesssim 10^9 \text{ GeV} \quad \text{bosonic DM} \\ G N_{\rm col} m_\chi & m_\chi \gtrsim 10^9 \text{ GeV} \end{cases}. \tag{3.49}$$

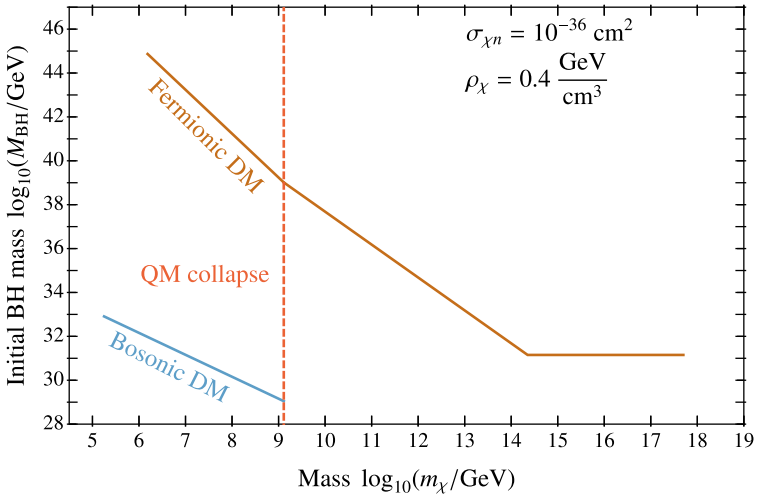


Figure 3.3: Initial black hole mass formed by DM core collapse in a WD. We take a representative value of the scattering cross section, though $M_{\rm BH}$ is independent of $\sigma_{\chi n}$ except for large DM masses where $N_{\rm sg} < \Gamma_{\rm cap} t_{\rm col}$. As plotted $M_{\rm BH}$ cuts-off at points where a DM core does not even form or collapse, or where a fermi degenerate core does not have time to collect a Chandrasekhar number $N^{\rm f}_{\rm Cha}$.

Note that any such BH will necessarily have some angular momentum. The DM core initially inherits its angular velocity from the rotating WD, though loses angular momentum to the stellar medium as it cools and collapses. We find the dimensionless spin parameter of the initial BH is always small $\frac{J_{\rm BH}}{G M_{\rm BH}^2} \lesssim 10^{-2}$, assuming a WD angular velocity of $\Omega_{\rm WD} \approx 0.01$ Hz. Thus the newly formed BH is approximately Schwarzschild, and has a radius:

$$R_{\rm BH} = 2GM_{\rm BH} \approx 3 \cdot 10^{-5}\ \text{cm} \left(\frac{M_{\rm BH}}{10^{47}\ \text{GeV}}\right). \tag{3.50}$$

## Fate of a BH

It is generally believed [91] that BHs have a temperature

$$T_{\rm BH} = \frac{1}{4\pi R_{\rm BH}} \approx 6\ \text{MeV} \left(\frac{M_{\rm BH}}{10^{39}\ \text{GeV}}\right)^{-1}, \tag{3.51}$$

and lose mass by emitting particles at a rate

$$\left(\frac{dM_{\rm BH}}{dt}\right)_{\rm HR} = \frac{\alpha}{G^2 M_{\rm BH}^2}, \tag{3.52}$$

where $\alpha(M_{\rm BH})$ encodes the different particle emission rates, roughly increasing as the BH temperature exceeds the mass threshold of a new species. Detailed calculation [92] finds $\alpha \approx 2.8 \cdot 10^{-4}$ for $T_{\rm BH} \lesssim$ MeV, accounting for emission of photons, gravitons, and three neutrino species. Counting only experimentally verified SM degrees of freedom, the emission rate effectively asymptotes to $\alpha \approx 4.1 \cdot 10^{-3}$ for $T_{\rm BH} \gtrsim 100$ GeV [93]. Thus an evaporating BH (by this we mean a BH which only Hawking radiates without any accretion)[3] has a lifetime less than $\tau_{\rm WD} \approx 5$ Gyr if:

$$M_{\rm BH} \lesssim 2 \cdot 10^{38}\ \text{GeV} \quad (\text{evaporate in } \tau_{\rm WD}). \tag{3.53}$$

The BH primarily accretes nuclear matter and additional DM particles: which dominates depends on the BH mass, or more precisely the DM parameters. In the hydrodynamic spherical so-called Bondi approximation, the former is given by

$$\left(\frac{dM_{\rm BH}}{dt}\right)_{\rm WD} = 4\pi\lambda \left(\frac{GM_{\rm BH}}{c_s^2}\right)^2 \rho_{\rm WD} c_s, \tag{3.54}$$

where $c_s \approx 2 \cdot 10^{-2}$ is the sound speed (approximated from numerical calculations in [95]), and $\lambda \sim \mathcal{O}(1)$ [96].

The accretion of DM potentially has two contributions. Under the influence of the BH gravitational potential, individual DM particles will continue reducing their orbit size below the thermal radius by scattering with the stellar medium. Once it crosses the angular momentum barrier $4GM_{\rm BH}$, the DM will rapidly fall into the BH [96]. A steady state is soon achieved after the BH is formed where DM feeds the BH at a rate set by the capture rate:

$$\left(\frac{dM_{\rm BH}}{dt}\right)_{\chi} = \Gamma_{\rm cap} m_\chi \tag{3.55}$$

There may also be large overdensity of DM particles in the vicinity of the newly formed BH, which is likely if the DM core collapses with non-uniform density. In the collisionless spherical approximation [96], a DM population with density $\rho_\infty$ and velocity $v_\infty$ far from the BH accretes at a rate:

$$\left(\frac{dM_{\rm BH}}{dt}\right)_{\chi} = \frac{16\pi\rho_\infty G^2 M_{\rm BH}^2}{v_\infty}. \tag{3.56}$$

Such accretion is especially relevant for bosonic DM if the BH is formed from a compact BEC within an enveloping non-condensed DM core [66]. For our purposes we will only consider (3.56) in this scenario, where $\rho_\infty$ is given by the very large density (3.30) and $v_\infty$ is given by (3.37).

The fate of a BH is determined by:

$$\frac{dM_{\rm BH}}{dt} = -\left(\frac{dM_{\rm BH}}{dt}\right)_{\rm HR} + \left(\frac{dM_{\rm BH}}{dt}\right)_{\rm WD} + \left(\frac{dM_{\rm BH}}{dt}\right)_{\chi}. \tag{3.57}$$

[3] An evaporating BH loses angular momentum rapidly and has a decreasing spin parameter—thus rotation is negligible throughout the evaporation [94].

We first consider BHs that are not formed from a BEC. Without DM accretion, we find Hawking evaporation beats Bondi accretion, i.e., $\left(\frac{dM_{\rm BH}}{dt}\right)_{\rm HR} > \left(\frac{dM_{\rm BH}}{dt}\right)_{\rm WD}$ at masses:

$$M_{\rm BH} \lesssim 10^{38}\ {\rm GeV}, \quad \text{(Hawking beats Bondi)}. \tag{3.58}$$

Including the steady accretion of DM (3.55), we find Hawking evaporation beats the largest possible DM accretion, i.e., $\left(\frac{dM_{\rm BH}}{dt}\right)_{\rm HR} > \left(\frac{dM_{\rm BH}}{dt}\right)_{\chi}$ when $\Gamma_{\rm cap} = \Gamma_{\rm trans}$ at masses

$$M_{\rm BH} \lesssim 2 \cdot 10^{35}\ {\rm GeV}, \quad \text{(Hawking beats DM)}, \tag{3.59}$$

where Hawking also clearly beats Bondi. The critical mass $M_{\rm crit}$ at which $dM_{\rm BH}/dt = 0$ depends on the strength of the steady DM accretion (3.55), and for the relevant DM parameter space lies in the range:

$$M_{\rm crit} \approx 2 \cdot 10^{35} - 10^{38}\ {\rm GeV}, \tag{3.60}$$

where the upper end of this range holds when Bondi dominates the accretion, and all lower values apply when steady DM accretion (3.55) dominates.

We now consider the timescales involved in accreting or evaporating, which can estimated by the characteristic time:

$$\tau_{\rm BH} \sim \frac{M_{\rm BH}}{dM_{\rm BH}/dt}. \tag{3.61}$$

If the BH is evaporating, $\tau_{\rm BH} \propto M_{\rm BH}^3$ and is set by the time spent at the largest BH mass, i.e. the initial BH mass. If the BH is dominantly accreting by Bondi then $\tau_{\rm BH} \propto M_{\rm BH}^{-1}$ is set by the time spent at the smallest BH mass, If, however, the BH is dominantly accreting by DM (3.55) then $\tau_{\rm BH} \propto M_{\rm BH}$ is instead set by the time spent at the largest BH mass—this is the BH mass at which Bondi accretion takes over $10^{38} \lesssim M_{\rm BH} \lesssim 10^{41}$ GeV (depending on the capture rate $\Gamma_{\rm cap}$). Miraculously, we find $\tau_{\rm BH} \approx$ Gyr for BH masses $M_{\rm BH} \approx 10^{38}$ GeV, coinciding with the upper end of (3.60) where Bondi accretion becomes of order the Hawking evaporation. This can also be seen from the fact that $M_{\rm crit}$ (3.60) lies *just* below the BH mass necessary to evaporate within $\tau_{\rm WD} \approx 5$ Gyr in the absence of any accretion (3.53). Thus it is clear that whether the BH is evaporating or accreting, it will necessarily do so in a characteristic time less than a Gyr.

Returning to the case of BHs formed from a BEC, we find that the DM accretion of the non-condensed enveloping DM core (3.56) in fact beats Hawking evaporation over the entire DM mass range of interest. Note that this outcome is strikingly different from the analogous process in a NS, where it has been found that such BHs always dominantly evaporate [66]. The difference arises from the fact that the density of the DM core (3.30) is significantly smaller at NS densities/temperatures and at the lower DM masses considered by [66].

We now briefly address the question: is Bondi always a valid estimate for the accretion of nuclear matter onto the BH? As is well-known, accretion could be in the Eddington-limited regime: this occurs when the radiation produced by in-falling matter exerts a significant

pressure so as to back-react on the accretion. In the spherical approximation, this yields a maximum luminosity:

$$L_{\rm edd} = \frac{4\pi G M_{\rm BH} m_{\rm ion}}{\sigma}, \tag{3.62}$$

where $\sigma$ is the dominant interaction by which outgoing radiation transfers momentum to the in-falling matter. Assuming photon energies near the horizon $\omega \gtrsim$ MeV, this is either set by hard Compton scattering off electrons $\sigma \sim \frac{\alpha^2}{m_e \omega} \sim 100 \text{ mb} \left(\frac{\omega}{\text{MeV}}\right)^{-1}$ or inelastic photo-nuclear interactions off ions $\sigma \sim$ mb (see [5] for details). Accretion is Eddington-limited if $\epsilon \cdot (dM_{\rm BH}/dt)_{\rm WD}$ exceeds $L_{\rm edd}$, where $\epsilon$ is the radiation efficiency. If we conservatively take $\epsilon \sim 0.1$, we find Bondi accretion is not Eddington-limited for BH masses less than $M_{\rm BH} \lesssim 10^{40}$ GeV. Note that even if the accretion is Eddington-limited at larger BH masses, the timescale $\tau_{\rm BH}$ then becomes independent of $M_{\rm BH}$ and is still much less than a Gyr.

The accretion could also be stalled by the stellar rotation: this occurs when the in-falling matter possesses excess angular momentum that must be dissipated to accrete, e.g., by viscous stresses during a slow phase of disk accretion [96]. [68] examines the effect of rotations for mini BHs in NSs, concluding that kinematic viscosity can maintain Bondi spherical accretion as long as the BH mass is sufficiently small. Based on the analysis of [68], we crudely estimate that Bondi accretion would hold for $M_{\rm BH} \lesssim 10^{46}$ GeV, assuming a (conservative choice of) WD viscosity [97]. Even if the BH accretion is stalled beyond this point we suspect the accretion timescale is still much smaller than a Gyr, though a detailed understanding is beyond the scope of this work.

## Constraints

**Hawking.** The Hawking radiation emitted by a BH will ignite a SN if

$$\mathcal{E}_{\rm BH} \sim \frac{\alpha}{G^2 M_{\rm BH}^2} \cdot \min[\tau_{\rm diff}, \tau_{\rm BH}] \tag{3.63}$$

satisfies the condition (3.2) $\mathcal{E}_{\rm BH} \gtrsim \mathcal{E}_{\rm boom}$. If the BH is evaporating, then $\tau_{\rm BH}$ is just its remaining lifetime (which is greater than $\tau_{\rm diff}$ for BH masses $M_{\rm BH} \gtrsim 10^{29}$ GeV). Even if a BH is technically accreting, it is possible to ignite a SN by the large amount of Hawking radiation emitted during its infancy. In this case, one can check that (3.63) still approximates the dominant contribution to the total energy emitted during a time $\tau_{\rm diff}$.

Assuming $\tau_{\rm diff} \ll \tau_{\rm BH}$, applicable for all starting BH masses we consider, Hawking is explosive at BH masses:

$$M_{\rm BH,\ boom} \approx 2 \cdot 10^{35} \text{ GeV}. \tag{3.64}$$

Of course, any DM core that results in a BH initially less than $M_{\rm BH,\ boom}$ ignites a SN upon formation. In addition, DM cores that result in a BH initially greater than $M_{\rm BH,\ boom}$ but less than the critical threshold $M_{\rm crit}$ evaporate and eventually ignite a SN within a Gyr. Coincidentally, any BH initially greater than $M_{\rm crit}$ will not ignite a SN via Hawking but will instead accrete—this is evident from the fact that (3.64) lies just below the lower end of

the critical threshold (3.60). However this is notably not the case for accreting BHs formed from a BEC: we have checked that all BHs formed from a BEC *immediately* ignite a SN by Hawking despite the large accretion rate from the large enveloping DM density.

**Accretion.** Finally, we comment on the final outcome of an accreting BH. It is conservative to suppose that such a BH simply eats the star. However, it is plausible that accreting BHs in WDs ignite SN once they grow sufficiently large. We can think of at least two potential mechanisms for this:

(1) The flow of stellar matter into the BH leads to the formation of a sonic horizon $R_s \sim GM_{\rm BH}/c_s^2 \sim 10^4\ R_{\rm BH}$, with supersonic flow as the matter enters free-fall near the BH. The kinetic energy of a carbon ion at the sonic horizon is $m_{\rm ion}c_s^2 \sim$ MeV, increasing as it falls inward. It is reasonable to suppose that the flow inside the sonic horizon is not perfectly radial, in which case this violent swarm of carbon ions may ignite thermonuclear fusion. BH masses $M_{\rm BH} \gtrsim 10^{43}$ GeV have sonic horizons $R_s \gtrsim \lambda_T$. Assuming substantial non-radial flow, such BHs may then have carbon ions colliding at large enough energies to overcome the coulomb barrier and initiate fusion over a large region. As this fusion is happening within the sonic horizon, a resulting fusion front would need to propagate out as a supersonic shockwave (e.g., a so-called detonation front [32]) in order to ignite the rest of the star.

(2) Inflow onto the BH also increases the density of stellar matter near the BH, for instance by roughly a factor $\sim 10 - 100$ at the sonic horizon [96]. This increased density may be sufficient, even at low temperatures, to ignite the star outside the sonic horizon through pycnonuclear fusion without the need for a supersonic shockwave (or inside the sonic horizon, with an accompanying supersonic fusion front.) Runaway pycnonuclear fusion begins when a sufficiently large region of carbon achieves a critical density $\sim 10^{10}$ g/cm$^3$ [32], which is a factor $\sim 30$ greater than our chosen central density. Note that the corresponding pycnonuclear trigger size $\lambda_P$ may be different from the thermonuclear trigger size $\lambda_T$ as the rates of fusion and diffusion depend on density and temperature, and both may be modified by dynamics near the BH. However, if we simply assume $\lambda_P \sim \lambda_T \sim 10^{-5}$ cm, then large BH masses $M_{\rm BH} \gtrsim 10^{44}$ GeV would have a sonic horizon $R_s \gg \lambda_P$, and could thus potentially ignite a SN via subsonic fusion front.

To confirm either of these mechanisms leads to ignition would require more detailed numerical calculations, which we do not attempt here. In any case, whether an accreting BH eats the star or ignites a SN, we are able to constrain any such BHs by the existence of observed WDs given that the accretion timescale is less than a Gyr.

To summarize, BHs formed by DM core collapse will either ignite a SN by Hawking radiation, or accrete and subsequently eat the star or ignite a SN. The resulting constraints on DM parameters are shown in Fig. 3.4 (fermionic DM) and Fig. 3.5 (bosonic DM). For fermionic DM these constraints extend well beyond those previously derived which consider BH formation/accretion in NSs, and are thus complementary. For bosonic DM these constraints are entirely new—in the DM mass range of interest, there are in fact no bounds due to BH formation in NSs (see [66] for details). We also show the constraints from DM-nuclei

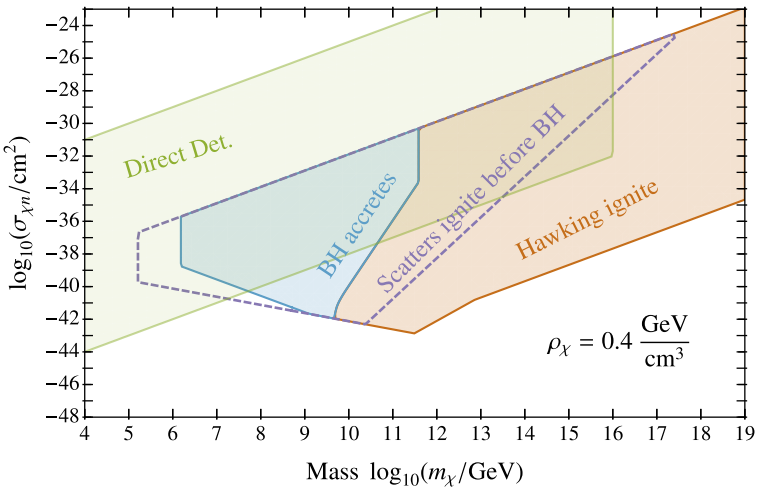


Figure 3.4: Constraints on fermionic asymmetric DM which forms a DM core and collapses to a mini black hole in a WD. The black hole either ignites a supernova via Hawking emission (red) or accretes and eats the star (or possibly ignites a supernova) (blue). Also shown (purple) are the constraints on DM-nuclei scatters igniting a supernova during core collapse before formation of a black hole.

scatters igniting a SN during core collapse at any point before formation of a BH (or a fermi degenerate core or BEC).

## 3.5 Annihilation-induced SN

A collapsing core of annihilating DM has an increasing annihilation rate, and effectively depletes $\mathcal{O}(1)$ ("bursts") upon shrinking to a size $r \sim R_{\chi\chi}$. However, even while $r \gtrsim R_{\chi\chi}$ and the DM core roughly retains its initial number $N(r) \approx N_{\text{col}}$, the energy deposited by a small fraction of the core may be significant. We estimate the energy deposited in the large number of annihilations within a trigger region $\lambda_T^3$ and diffusion time $\tau_{\text{diff}}$ for $r \gtrsim R_{\chi\chi}$:

$$\mathcal{E}_{\chi\chi}(r) \sim m_\chi \frac{N_{\text{col}}^2}{r^3} \sigma_{\chi\chi} v_{\text{col}} \tau_{\text{diff}} \cdot \min\left[1, \left(\frac{\lambda_T}{r}\right)^3\right]. \tag{3.65}$$

This is sufficient to ignite a SN if it satisfies $\mathcal{E}_{\chi\chi} \gtrsim \mathcal{E}_{\text{boom}}$ (3.2).

As expected, the annihilating core deposits energy more and more rapidly as it shrinks to smaller radii. We can also evaluate the deposited energy (3.65) at the bursting point $r \sim R_{\chi\chi}$. Interestingly for $R_{\chi\chi} < \lambda_T$, we find $\mathcal{E}_{\chi\chi}(R_{\chi\chi})$ scales inversely with annihilation cross section $\mathcal{E}_{\chi\chi}(R_{\chi\chi}) \propto (\sigma_{\chi\chi} v_{\text{col}})^{-1/5}$ in the regime $v_{\text{ion}} < v_{\text{col}}(R_{\chi\chi}) < 2 \cdot 10^{-2}$, i.e. the DM core is more explosive for *lower* annihilation cross section. This is basically a result of the

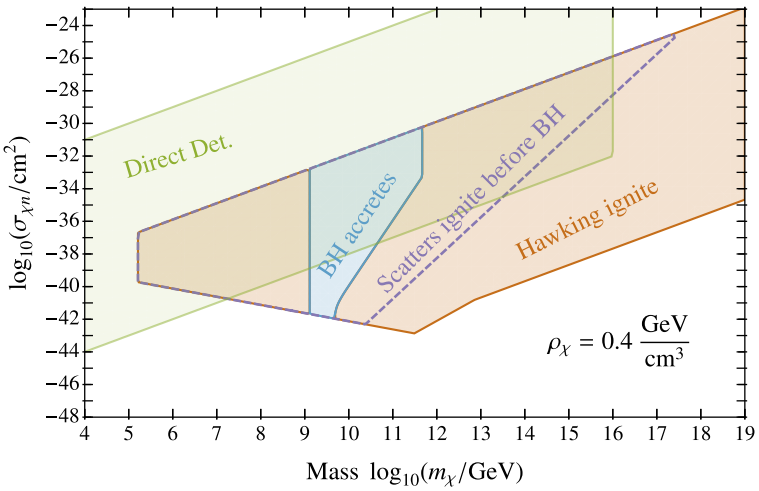


Figure 3.5: Constraints on bosonic asymmetric DM which forms a DM core and collapses to a mini black hole in a WD. The black hole either ignites a supernova via Hawking emission (red) or accretes and eats the star (or possibly ignites a supernova) (blue). Also shown (purple) are the constraints on DM-nuclei scatters igniting a supernova during core collapse before formation of a black hole.

collapsing core focusing and becoming more dense before annihilating $\mathcal{O}(1)$, thus making this energy deposition at $r \sim R_{\chi\chi}$ more violent. It is also interesting that $\mathcal{E}_{\chi\chi}(R_{\chi\chi})$ scales inversely with DM mass—this is just a result of the greater number of collapsing particles at lower DM masses. Similarly, in the regimes $v_{\rm col}(R_{\chi\chi}) < v_{\rm ion}$ or $v_{\rm col}(R_{\chi\chi}) > 2 \cdot 10^{-2}$ we find $\mathcal{E}_{\chi\chi}(R_{\chi\chi})$ is *independent* of annihilation cross section $\sigma_{\chi\chi} v_{\rm col}$, i.e. the ignition condition $\mathcal{E}_{\chi\chi}(R_{\chi\chi}) \gtrsim \mathcal{E}_{\rm boom}$ simply corresponds to an upper bound on DM mass. This variation in the dependence of $\mathcal{E}_{\chi\chi}$ on $\sigma_{\chi\chi} v_{\rm col}$ for different regimes of $v_{\rm col}(R_{\chi\chi})$ is responsible for the change in slope of the constrained regions of Figure 3.6 and 3.7 for $10^{11}$ GeV $\lesssim m_\chi \lesssim 10^{12}$ GeV.

If the core has not yet ignited a SN by the time it collapses to $R_{\chi\chi}$, could it do so afterwards? Although the number of collapsing particles at this point is depleting appreciably, the shrinking of the core may still drive the total rate of annihilations to increase; if so, there is the possibility of igniting a SN at sizes $r \lesssim R_{\chi\chi}$. We have estimated that this is not the case. However, as described in Sec. 3.3, the evolution of the annihilating DM core here is somewhat complicated and requires more detailed study—thus we only consider the constraints on annihilations while the DM core is still at sizes $r \gtrsim R_{\chi\chi}$.

Of course, the DM core may never annihilate efficiently if it first collapses to a BH $G N_{\rm col} m_\chi \gtrsim R_{\chi\chi}$, though the energy deposited by annihilations before the core shrinks to within the Schwarzschild radius may still be sufficient to ignite a SN. Similarly, if the DM core first reaches the size at which QM effects become important before efficiently annihilating, $R_{\rm QM} \gtrsim R_{\chi\chi}$, then the energy deposited by annihilations at or before this point may still be

sufficient to ignite a SN. We have included both of these constraints.

We now consider annihilations igniting SN after formation of a fermi degenerate core or a BEC. As shown in Sec. 3.3, a fermi degenerate core shrinks by capturing additional DM and can saturate once the capture rate is of order the annihilation rate. If this saturation occurs before the core has a chance to shrink much below $R_{\rm QM}$, then it does not ignite a SN. On the other hand if saturation occurs at a number (3.46) much greater than the initial collapsing number, then annihilations in the fermi degenerate core can ignite a SN at a number $N \lesssim N^{\rm f}_{\chi\chi}$. The energy deposited in a trigger region $\lambda_T^3$ and a diffusion time $\tau_{\rm diff}$ is:

$$\mathcal{E}^{\rm f}_{\chi\chi}(N) \sim m_\chi \frac{N^2}{r^3}\sigma_{\chi\chi} v_{\rm col}(r)\tau_{\rm diff} \cdot \min\left[1, \left(\frac{\lambda_T}{r}\right)^3\right], \quad r \sim \frac{1}{G m_\chi^3 N^{1/3}}. \tag{3.66}$$

Thus a shrinking fermi degenerate core ignites a SN through annihilations if (3.66) satisfies $\mathcal{E}^{\rm f}_{\chi\chi} \gtrsim \mathcal{E}_{\rm boom}$ (3.2). Of course this assumes that $N \lesssim N_{\rm life}$ and that the core has not yet collapsed to a BH first $N \lesssim N^{\rm f}_{\rm Cha}$.

Similarly, a self-gravitating BEC that is collecting particles from the enveloping non-condensed core will saturate at a number (3.47). This highly compact BEC can ignite a SN at any number $N \lesssim N^{\rm b}_{\chi\chi}$. The energy deposited by annihilations in the BEC within a time $\tau_{\rm diff}$ (or (3.36), whichever is shorter) is simply:

$$\mathcal{E}^{\rm f}_{\chi\chi}(N) \sim m_\chi \frac{N^2}{r^3}\sigma_{\chi\chi} v_{\rm BEC}(r)\tau_{\rm diff} \cdot \min\left[1, \left(\frac{\lambda_T}{r}\right)^3\right], \quad r \sim \frac{1}{G m_\chi^3 N}. \tag{3.67}$$

and will ignite a SN if it is satisfies $\mathcal{E}^{\rm b}_{\chi\chi} \gtrsim \mathcal{E}_{\rm boom}$ (3.2). Of course this also assumes that the BEC has not yet collapsed to a BH $N \lesssim N^{\rm b}_{\rm Cha}$. Note that the DM annihilation cross section must be extremely small for a shrinking BEC to have not ignited a SN before formation of a BH: the requirement $\mathcal{E}^{\rm b}_{\chi\chi}(N^{\rm b}_{\rm Cha}) \gtrsim \mathcal{E}_{\rm boom}$ implies cross sections as low as $\sigma_{\chi\chi} v_{\rm BEC} \gtrsim \frac{\mathcal{E}_{\rm boom}}{M_{\rm pl}^4 \tau_{\rm diff}} \sim 10^{-90}$ cm$^3$/s would ignite a SN through annihilations in the BEC.

To summarize, a collapsing DM core can ignite a SN by a large number of rapid annihilations. These constraints are valid regardless of the nature of the annihilation products as long as they deposit their energy within a trigger sized region. The resulting constraints on DM parameters are shown in Fig. 3.6 (fermionic DM) and Fig. 3.7 (bosonic DM), taking a fixed value of the scattering cross section $\sigma_{\chi n} = 10^{-39}$ cm$^2$. This roughly corresponds to the interaction strength for $Z$ boson exchange, i.e., heavy hyper-charged DM (or "WIMPzilla") [98, 99, 100, 101]. We also show the constraint from DM-nuclei scatters igniting a SN during core collapse at any point before DM annihilations would have done so. Note that the particular shape of the bounded regions in Fig. 3.6 and Fig. 3.7 results from the expressions for the energy released in annihilations, e.g. as in (3.65).

For an explicit DM model $\sigma_{\chi\chi} v$ is typically related to the DM mass in a calculable way, e.g. s-wave annihilation of hyper-charged DM $\sigma_{\chi\chi} v \sim \alpha_2^2/m_\chi^2$, $\alpha_2$ is the $SU(2)_L$ gauge coupling. As shown in Fig. 3.6 and Fig. 3.7, we constrain annihilation cross sections many

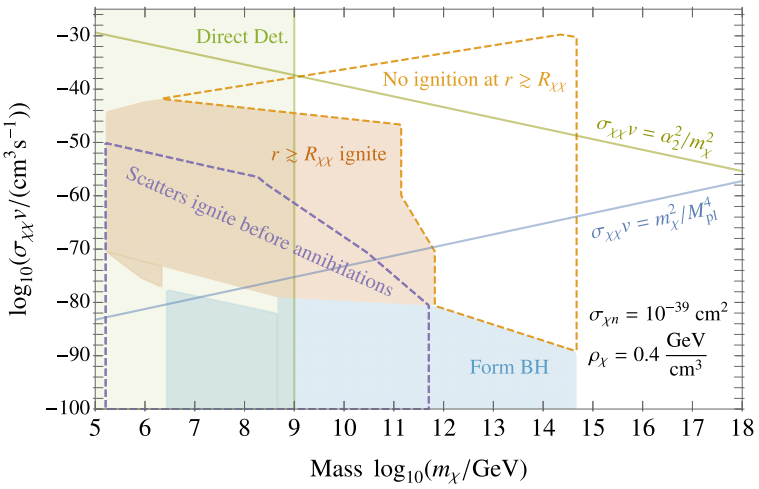


Figure 3.6: Constraints on fermionic DM which forms a DM core and ignites a supernova through annihilations (red). For sufficiently small $\sigma_{\chi\chi} v$ the core first collapses to a black hole (blue), and is otherwise constrained, see Fig. 3.4. Also shown (purple) are the constraints on DM-nuclei scatters igniting a supernova during core collapse before annihilations could do so.

orders of magnitude smaller than this naive estimate. However, this estimate is based upon annihilations of DM its antiparticle $\chi\bar{\chi} \to$ SM, with both existing in roughy equal abundances today. It is straightforward to imagine a scenario in which essentially no $\bar{\chi}$ particles remain today, and yet $\chi$ is capable of annihilating itself through a parametrically suppressed interaction. To demonstrate, an explicit DM model of this sort is hypercharged DM with a large vector-like mass and an additional small dimension-5 Majorana mass term. We emphasize though that any DM candidate which can annihilate itself through higher dimension operators may have $\sigma_{\chi\chi} v$ small enough to be constrained by our results e.g., annihilation to SM fermions through a Planck-suppressed cross section $\sigma_{\chi\chi} v \sim m_\chi^2/M_{\rm pl}^4$.

## 3.6 Discussion

We have studied the possibility of DM core collapse triggering type Ia SN in sub-Chandrasekhar WDs, following up on previous work [5]. Collapse of asymmetric DM can lead to the formation of a mini BH which ignites a SN by the emission of Hawking radiation, and collapse of annihilating DM can lead to large number of rapid annihilations which also ignite a SN. Such processes allow us to place novel constraints on DM parameters, as shown in Fig. 3.4, Fig. 3.5, Fig. 3.6, and Fig. 3.7. These constraints improve on the limits set by terrestrial experiments, and they are complementary to previous considerations of DM capture in compact objects.

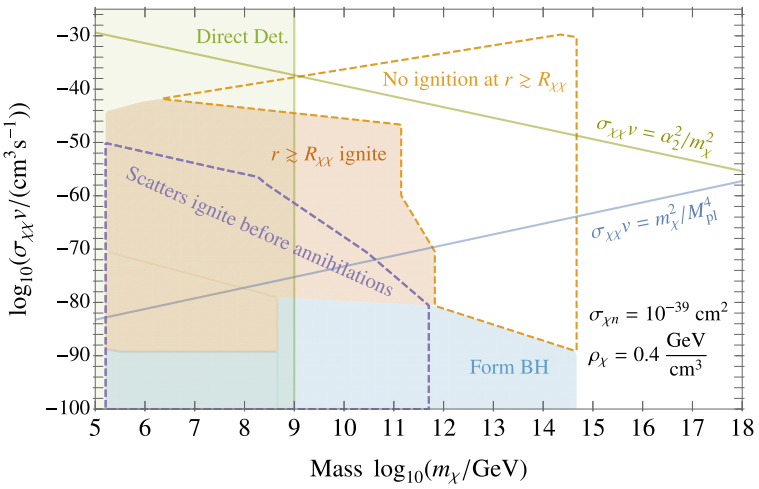


Figure 3.7: Constraints on bosonic DM which forms a DM core and ignites a supernova through annihilations (red). For sufficiently small $\sigma_{\chi\chi} v$ the core first collapses to a black hole (blue), and is otherwise constrained, see Fig. 3.5. Also shown (purple) are the constraints on DM-nuclei scatters igniting a supernova during core collapse before annihilations could do so.

It is interesting to contemplate that the ignition of type Ia SN through the evaporation of mini black holes represents a potential observable signature of Hawking radiation. Further, it also interesting that the extremely tiny annihilation cross sections constrained in this work, which to our knowledge have no other observable consequences, can nonetheless be capable of igniting a SN.

The processes studied here present a number of opportunities for future work. The DM constraints presented in this paper are based on the existence known, heavy WDs. It would also be interesting to calculate the constraints on DM core collapse scenarios arising from the observed galactic SN rate—these may depend more sensitively on the timescale to form a core, or in the case of BH formation, the evaporation time. In addition, we have restricted our attention here and in [5] to DM candidates which interact with the SM through short-range, elastic nuclear scatters. It would be interesting to broaden our scope to relics with qualitatively different interactions, such as inelastic scatters or radiative processes. DM which can cool via emission of dark radiation will be more susceptible to collapse, and is likely to be more strongly constrained than models possessing only elastic cooling. Another particularly interesting case is electrically charged particles [102] or magnetic monopoles. Ultra-heavy monopoles and anti-monopoles could be captured in a WD and subsequently annihilate, igniting SN—we estimate that such a process can be used to place constraints on the flux of galactic monopoles exceeding current limits [103].

Finally, though we have not touched upon it here, there are many puzzles in our under-

standing of the origin of type Ia SN and other WD events, such as Ca-rich transients. It is plausible (e.g., see the discussion in [5]) that DM is responsible for a fraction of these events. To this end, it is important to identify the distinguishing features of SN that would originate from DM core collapse (e.g. the lack of a stellar companion) in order to observationally test such tantalizing possibilities.

*Note added:* While this paper was in the final stages of preparation, [104] appeared which has some overlap with this work.

# Bibliography

[1] Matteo Nori, Riccardo Murgia, Vid Iršič, Marco Baldi, and Matteo Viel. Lyman-$\alpha$ forest and non-linear structure characterization in Fuzzy Dark Matter cosmologies. *Monthly Notices of the Royal Astronomical Society*, 482(3):3227–3243, January 2019. arXiv: 1809.09619.

[2] D. P. Quinn, M. I. Wilkinson, M. J. Irwin, J. Marshall, A. Koch, and V. Belokurov. On the Reported Death of the MACHO Era. *Monthly Notices of the Royal Astronomical Society: Letters*, 396(1):L11–L15, June 2009. arXiv: 0903.1644.

[3] E. Aprile et al. Dark Matter Search Results from a One Ton-Year Exposure of XENON1T. *Phys. Rev. Lett.*, 121(11):111302, 2018.

[4] Peter W. Graham, Igor G. Irastorza, Steven K. Lamoreaux, Axel Lindner, and Karl A. van Bibber. Experimental Searches for the Axion and Axion-Like Particles. *Ann. Rev. Nucl. Part. Sci.*, 65:485–514, 2015.

[5] Peter W. Graham, Ryan Janish, Vijay Narayan, Surjeet Rajendran, and Paul Riggins. White Dwarfs as Dark Matter Detectors. *Phys. Rev.*, D98(11):115027, 2018.

[6] Ryan Janish, Vijay Narayan, and Paul Riggins. Type Ia supernovae from dark matter core collapse. *Phys. Rev.*, D100(3):035008, 2019.

[7] D. S. Akerib et al. Results from a search for dark matter in the complete LUX exposure. *Phys. Rev. Lett.*, 118(2):021303, 2017.

[8] R. Agnese et al. Results from the Super Cryogenic Dark Matter Search Experiment at Soudan. *Phys. Rev. Lett.*, 120(6):061802, 2018.

[9] Kim Griest, Agnieszka M. Cieplak, and Matthew J. Lehner. Experimental Limits on Primordial Black Hole Dark Matter from the First 2 yr of Kepler Data. *Astrophys. J.*, 786(2):158, 2014.

[10] Peter W. Graham, Surjeet Rajendran, and Jaime Varela. Dark Matter Triggers of Supernovae. *Phys. Rev.*, D92(6):063007, 2015.

[11] D. Maoz and F. Mannucci. Type-ia supernova rates and the progenitor problem: A review. *Publications of the Astronomical Society of Australia*, 29(4):447–465, 2012.

[12] R. Scalzo et al. Type Ia supernova bolometric light curves and ejected mass estimates from the Nearby Supernova Factory. *Mon. Not. Roy. Astron. Soc.*, 440(2):1498–1518, 2014.

[13] R. A. Scalzo, A. J. Ruiter, and S. A. Sim. The ejected mass distribution of type Ia supernovae: A significant rate of non-Chandrasekhar-mass progenitors. *Mon. Not. Roy. Astron. Soc.*, 445(3):2535–2544, 2014.

[14] Sean L. McGee and Michael L. Balogh. Constraints on intragroup stellar mass from hostless type ia supernovae. *Monthly Notices of the Royal Astronomical Society: Letters*, 403(1):L79–L83, Mar 2010.

[15] Ryan J. Foley, P. J. Challis, R. Chornock, M. Ganeshalingam, W. Li, G. H. Marion, N. I. Morrell, G. Pignata, M. D. Stritzinger, J. M. Silverman, and et al. Type iax supernovae: A new class of stellar explosion. *The Astrophysical Journal*, 767(1):57, Mar 2013.

[16] Mansi M. Kasliwal, S. R. Kulkarni, Avishay Gal-Yam, Peter E. Nugent, Mark Sullivan, Lars Bildsten, Ofer Yaron, Hagai B. Perets, Iair Arcavi, Sagi Ben-Ami, and et al. Calcium-rich gap transients in the remote outskirts of galaxies. *The Astrophysical Journal*, 755(2):161, Aug 2012.

[17] S. E. Woosley and Daniel Kasen. Sub-chandrasekhar mass models for type ia supernovae. *The Astrophysical Journal*, 734(1):38, May 2011.

[18] M. Fink, W. Hillebrandt, and F. K. Roepke. Double-detonation supernovae of sub-Chandrasekhar mass white dwarfs. *Astron. Astrophys.*, 2007. [Astron. Astrophys.476,1133(2007)].

[19] R. Pakmor, M. Kromer, and S. Taubenberger. Helium-ignited violent mergers as a unified model for normal and rapidly declining Type Ia Supernovae. *Astrophys. J.*, 770:L8, 2013.

[20] P. H. Sell, T. J. Maccarone, R. Kotak, C. Knigge, and D. J. Sand. Calcium-Rich Gap Transients: Tidal Detonations of White Dwarfs? *Mon. Not. Roy. Astron. Soc.*, 450(4):4198–4206, 2015.

[21] F. X. Timmes and S. E. Woosley. The conductive propagation of nuclear flames. i. degenerate c + o and o + ne + mg white dwarfs. *Astrophysical Journal*, 396(2):649–667, 1992.

[22] Gianfranco Bertone and Malcolm Fairbairn. Compact Stars as Dark Matter Probes. *Phys. Rev.*, D77:043515, 2008.

[23] Matthew McCullough and Malcolm Fairbairn. Capture of Inelastic Dark Matter in White Dwarves. *Phys. Rev.*, D81:083520, 2010.

[24] S. C. Leung, M. C. Chu, L. M. Lin, and K. W. Wong. Dark-matter admixed white dwarfs. *Phys. Rev.*, D87(12):123506, 2013.

[25] Joseph Bramante. Dark matter ignition of type Ia supernovae. *Phys. Rev. Lett.*, 115(14):141301, 2015.

[26] L. R. Gasques, A. V. Afanasjev, E. F. Aguilera, M. Beard, L. C. Chamon, P. Ring, M. Wiescher, and D. G. Yakovlev. Nuclear fusion in dense matter: Reaction rate and carbon burning. *Phys. Rev.*, C72:025806, 2005.

[27] F. X. Timmes. http://cococubed.asu.edu/code_pages/coldwd.shtml.

[28] Raj Gandhi, Chris Quigg, Mary Hall Reno, and Ina Sarcevic. Neutrino interactions at ultrahigh-energies. *Phys. Rev.*, D58:093009, 1998.

[29] J. A. Formaggio and G. P. Zeller. From eV to EeV: Neutrino Cross Sections Across Energy Scales. *Rev. Mod. Phys.*, 84:1307–1341, 2012.

[30] William H. Press and David N. Spergel. Capture by the sun of a galactic population of weakly interacting massive particles. *Astrophys. J.*, 296:679–684, 1985. [,277(1985)].

[31] Andrew Gould. Resonant Enhancements in WIMP Capture by the Earth. *Astrophys. J.*, 321:571, 1987.

[32] Rudolf Kippenhahn and Alfred Weigert. *Stellar Structure and Evolution*. Springer, New York, 2007.

[33] Sandro Mereghetti. RX J0648.0–4418: the fastest-spinning white dwarf. In *Proceedings, 13th Marcel Grossmann Meeting on Recent Developments in Theoretical and Experimental General Relativity, Astrophysics, and Relativistic Field Theories (MG13): Stockholm, Sweden, July 1-7, 2012*, pages 2459–2461, 2015.

[34] S. O. Kepler, S. J. Kleinman, A. Nitta, D. Koester, B. G. Castanheira, O. Giovannini, A. F. M. Costa, and L. Althaus. White Dwarf Mass Distribution in the SDSS. *Mon. Not. Roy. Astron. Soc.*, 375:1315–1324, 2007.

[35] Kerstin Perez, Charles J. Hailey, and et al. Bauer, Franz E. Extended hard-x-ray emission in the inner few parsecs of the galaxy. *Nature*, 520:646 EP –, 04 2015.

[36] Fabrizio Nesti and Paolo Salucci. The Dark Matter halo of the Milky Way, AD 2013. *JCAP*, 1307:016, 2013.

[37] Subrahmanyan Chandrasekhar. *An Introduction to the Study of Stellar Structure*. University of Chicago Press, 1939.

[38] Cora Dvorkin, Kfir Blum, and Marc Kamionkowski. Constraining Dark Matter-Baryon Scattering with Linear Cosmology. *Phys. Rev.*, D89(2):023519, 2014.

[39] Tracy R. Slatyer, Nikhil Padmanabhan, and Douglas P. Finkbeiner. CMB Constraints on WIMP Annihilation: Energy Absorption During the Recombination Epoch. *Phys. Rev.*, D80:043526, 2009.

[40] Tracy R. Slatyer and Chih-Liang Wu. General Constraints on Dark Matter Decay from the Cosmic Microwave Background. *Phys. Rev.*, D95(2):023010, 2017.

[41] Nikhil Padmanabhan and Douglas P. Finkbeiner. Detecting dark matter annihilation with CMB polarization: Signatures and experimental prospects. *Phys. Rev.*, D72:023508, 2005.

[42] Alexander Aab et al. The Pierre Auger Cosmic Ray Observatory. *Nucl. Instrum. Meth.*, A798:172–213, 2015.

[43] Gregory D. Mack, John F. Beacom, and Gianfranco Bertone. Towards Closing the Window on Strongly Interacting Dark Matter: Far-Reaching Constraints from Earth's Heat Flow. *Phys. Rev.*, D76:043523, 2007.

[44] E. Aprile et al. First Dark Matter Search Results from the XENON1T Experiment. *Phys. Rev. Lett.*, 119(18):181301, 2017.

[45] M. Ambrosio et al. Final results of magnetic monopole searches with the MACRO experiment. *Eur. Phys. J.*, C25:511–522, 2002.

[46] David M. Jacobs, Glenn D. Starkman, and Bryan W. Lynn. Macro Dark Matter. *Mon. Not. Roy. Astron. Soc.*, 450(4):3418–3430, 2015.

[47] Sidney R. Coleman. Q Balls. *Nucl. Phys.*, B262:263, 1985. [Erratum: Nucl. Phys.B269,744(1986)].

[48] Alexander Kusenko and Mikhail E. Shaposhnikov. Supersymmetric Q balls as dark matter. *Phys. Lett.*, B418:46–54, 1998.

[49] Alexander Kusenko, Vadim Kuzmin, Mikhail E. Shaposhnikov, and P. G. Tinyakov. Experimental signatures of supersymmetric dark matter Q balls. *Phys. Rev. Lett.*, 80:3185–3188, 1998.

[50] Michael Dine and Alexander Kusenko. The Origin of the matter - antimatter asymmetry. *Rev. Mod. Phys.*, 76:1, 2003.

[51] A. Bottino, G. Fiorentini, N. Fornengo, B. Ricci, S. Scopel, and F. L. Villante. Does solar physics provide constraints to weakly interacting massive particles? *Phys. Rev.*, D66:053005, 2002.

[52] Daniel T. Cumberbatch, Joyce.A. Guzik, Joseph Silk, L. Scott Watson, and Stephen M. West. Light WIMPs in the Sun: Constraints from Helioseismology. *Phys. Rev.*, D82:103503, 2010.

[53] Mads T. Frandsen and Subir Sarkar. Asymmetric dark matter and the sun. *Phys. Rev. Lett.*, 105:011301, Jul 2010.

[54] Ilidio Lopes and Joseph Silk. Solar constraints on asymmetric dark matter. *Astrophys. J.*, 757:130, 2012.

[55] Jordi Casanellas and Ilidio Lopes. First asteroseismic limits on the nature of dark matter. *Astrophys. J.*, 765:L21, 2013.

[56] Fredrik Sandin and Paolo Ciarcelluti. Effects of mirror dark matter on neutron stars. *Astropart. Phys.*, 32:278–284, 2009.

[57] Paolo Ciarcelluti and Fredrik Sandin. Have neutron stars a dark matter core? *Phys. Lett.*, B695:19–21, 2011.

[58] Ang Li, Feng Huang, and Ren-Xin Xu. Too massive neutron stars: The role of dark matter? *Astropart. Phys.*, 37:70–74, 2012.

[59] I. Goldman, R. N. Mohapatra, S. Nussinov, D. Rosenbaum, and V. Teplitz. Possible Implications of Asymmetric Fermionic Dark Matter for Neutron Stars. *Phys. Lett.*, B725:200–207, 2013.

[60] Itzhak Goldman and Shmuel Nussinov. Weakly interacting massive particles and neutron stars. *Phys. Rev. D*, 40:3221–3230, Nov 1989.

[61] Andrew Gould, Bruce T. Draine, Roger W. Romani, and Shmuel Nussinov. Neutron Stars: Graveyard of Charged Dark Matter. *Phys. Lett.*, B238:337–343, 1990.

[62] Chris Kouvaris and Peter Tinyakov. Constraining asymmetric dark matter through observations of compact stars. *Phys. Rev. D*, 83:083512, Apr 2011.

[63] Chris Kouvaris and Peter Tinyakov. Excluding light asymmetric bosonic dark matter. *Phys. Rev. Lett.*, 107:091301, Aug 2011.

[64] Samuel D. McDermott, Hai-Bo Yu, and Kathryn M. Zurek. Constraints on Scalar Asymmetric Dark Matter from Black Hole Formation in Neutron Stars. *Phys. Rev.*, D85:023519, 2012.

[65] Alan O. Jamison. Effects of gravitational confinement on bosonic asymmetric dark matter in stars. *Phys. Rev.*, D88:035004, 2013.

[66] Chris Kouvaris and Peter Tinyakov. (not)-constraining heavy asymmetric bosonic dark matter. *Phys. Rev. D*, 87:123537, Jun 2013.

[67] Joseph Bramante, Keita Fukushima, and Jason Kumar. Constraints on bosonic dark matter from observation of old neutron stars. *Phys. Rev.*, D87(5):055012, 2013.

[68] Chris Kouvaris and Peter Tinyakov. Growth of Black Holes in the interior of Rotating Neutron Stars. *Phys. Rev.*, D90(4):043512, 2014.

[69] Nicole F. Bell, Andrew Melatos, and Kalliopi Petraki. Realistic neutron star constraints on bosonic asymmetric dark matter. *Phys. Rev. D*, 87:123507, Jun 2013.

[70] Chris Kouvaris. Limits on self-interacting dark matter from neutron stars. *Phys. Rev. Lett.*, 108:191301, May 2012.

[71] Joseph Bramante, Keita Fukushima, Jason Kumar, and Elan Stopnitzky. Bounds on self-interacting fermion dark matter from observations of old neutron stars. *Phys. Rev.*, D89(1):015010, 2014.

[72] Joseph Bramante and Tim Linden. Detecting Dark Matter with Imploding Pulsars in the Galactic Center. *Phys. Rev. Lett.*, 113(19):191301, 2014.

[73] Joseph Bramante, Tim Linden, and Yu-Dai Tsai. Searching for dark matter with neutron star mergers and quiet kilonovae. *Phys. Rev.*, D97(5):055016, 2018.

[74] Raghuveer Garani, Yoann Genolini, and Thomas Hambye. New Analysis of Neutron Star Constraints on Asymmetric Dark Matter. *JCAP*, 1905(05):035, 2019.

[75] Matthew McCullough and Malcolm Fairbairn. Capture of inelastic dark matter in white dwarves. *Phys. Rev. D*, 81:083520, Apr 2010.

[76] Dan Hooper, Douglas Spolyar, Alberto Vallinotto, and Nickolay Y. Gnedin. Inelastic dark matter as an efficient fuel for compact stars. *Phys. Rev. D*, 81:103531, May 2010.

[77] Chris Kouvaris. Wimp annihilation and cooling of neutron stars. *Phys. Rev. D*, 77:023006, Jan 2008.

[78] Arnaud de Lavallaz and Malcolm Fairbairn. Neutron stars as dark matter probes. *Phys. Rev. D*, 81:123521, Jun 2010.

[79] Chris Kouvaris and Peter Tinyakov. Can neutron stars constrain dark matter? *Phys. Rev. D*, 82:063531, Sep 2010.

[80] Gianfranco Bertone and Malcolm Fairbairn. Compact stars as dark matter probes. *Phys. Rev. D*, 77:043515, Feb 2008.

[81] Masha Baryakhtar, Joseph Bramante, Shirley Weishi Li, Tim Linden, and Nirmal Raj. Dark Kinetic Heating of Neutron Stars and An Infrared Window On WIMPs, SIMPs, and Pure Higgsinos. *Phys. Rev. Lett.*, 119(13):131801, 2017.

[82] Nirmal Raj, Philip Tanedo, and Hai-Bo Yu. Neutron stars at the dark matter direct detection frontier. *Phys. Rev. D*, 97:043006, Feb 2018.

[83] Richard Brito, Vitor Cardoso, and Hirotada Okawa. Accretion of dark matter by stars. *Phys. Rev. Lett.*, 115:111301, Sep 2015.

[84] Richard Brito, Vitor Cardoso, Caio F. B. Macedo, Hirotada Okawa, and Carlos Palenzuela. Interaction between bosonic dark matter and stars. *Phys. Rev.*, D93(4):044045, 2016.

[85] Richard H. Helm. Inelastic and elastic scattering of 187-mev electrons from selected even-even nuclei. *Phys. Rev.*, 104:1466–1475, Dec 1956.

[86] E. Aprile et al. Constraining the spin-dependent WIMP-nucleon cross sections with XENON1T. *Phys. Rev. Lett.*, 122(14):141301, 2019.

[87] Joseph Bramante, Antonio Delgado, and Adam Martin. Multiscatter stellar capture of dark matter. *Phys. Rev.*, D96(6):063002, 2017.

[88] S. Nussinov. Technocosmology: Could a technibaryon excess provide a 'natural' missing mass candidate. *Phys. Lett.*, 165B:55–58, 1985.

[89] Kathryn M. Zurek. Asymmetric Dark Matter: Theories, Signatures, and Constraints. *Phys. Rept.*, 537:91–121, 2014.

[90] Monica Colpi, Stuart L. Shapiro, and Ira Wasserman. Boson stars: Gravitational equilibria of self-interacting scalar fields. *Phys. Rev. Lett.*, 57:2485–2488, Nov 1986.

[91] S. W. Hawking. Particle Creation by Black Holes. *Commun. Math. Phys.*, 43:199–220, 1975.

[92] Don N. Page. Particle Emission Rates from a Black Hole: Massless Particles from an Uncharged, Nonrotating Hole. *Phys. Rev.*, D13:198–206, 1976.

[93] T. N. Ukwatta, D. R. Stump, J. T. Linnemann, J. H. MacGibbon, S. S. Marinelli, T. Yapici, and K. Tollefson. Primordial Black Holes: Observational Characteristics of The Final Evaporation. *Astropart. Phys.*, 80:90–114, 2016.

[94] Don N. Page. Particle emission rates from a black hole. ii. massless particles from a rotating hole. *Phys. Rev. D*, 14:3260–3273, Dec 1976.

[95] Shmuel Balberg and Stuart L. Shapiro. The Properties of matter in white dwarfs and neutron stars. 2000.

[96] Stuart L. Shapiro and Saul A. Teukolsky. *Black Holes, White Dwarfs, and Neutron Stars*. Wiley, New York, 1983.

[97] Simone Dall'Osso and Elena Maria Rossi. Constraining white dwarf viscosity through tidal heating in detached binary systems. *Mon. Not. Roy. Astron. Soc.*, 443(2):1057–1064, 2014.

[98] Daniel J. H. Chung, Patrick Crotty, Edward W. Kolb, and Antonio Riotto. Gravitational production of superheavy dark matter. *Phys. Rev. D*, 64:043503, Jul 2001.

[99] Daniel J. H. Chung, Edward W. Kolb, and Antonio Riotto. Superheavy dark matter. *Phys. Rev. D*, 59:023501, Nov 1998.

[100] Brian Feldstein, Masahiro Ibe, and Tsutomu T. Yanagida. Hypercharged Dark Matter and Direct Detection as a Probe of Reheating. *Phys. Rev. Lett.*, 112(10):101301, 2014.

[101] Keisuke Harigaya, Tongyan Lin, and Hou Keong Lou. GUTzilla Dark Matter. *JHEP*, 09:014, 2016.

[102] Michael A. Fedderke, Peter W. Graham, and Surjeet Rajendran. White Dwarf Bounds on CHAMPs. 2019.

[103] Ryan Janish, Jacob Leedom, and Vijay Narayan. *to appear.*

[104] Javier F. Acevedo and Joseph Bramante. Supernovae Sparked By Dark Matter in White Dwarfs. *Phys. Rev.*, D100(4):043020, 2019.

[105] Stefaan Tavernier. *Experimental Techniques in Nuclear and Particle Physics*. Springer, Berlin, Germany, 2010.

[106] T.-S. H. Lee and R. P. Redwine. Pion-nucleus interactions. *Annual Review of Nuclear and Particle Science*, 52(1):23–63, 2002.

[107] Lisa Gerhardt and Spencer R. Klein. Electron and Photon Interactions in the Regime of Strong LPM Suppression. *Phys. Rev.*, D82:074017, 2010.

[108] Spencer Klein. Suppression of Bremsstrahlung and pair production due to environmental factors. *Rev. Mod. Phys.*, 71:1501–1538, 1999.

[109] H. Bethe and W. Heitler. On the Stopping of fast particles and on the creation of positive electrons. *Proc. Roy. Soc. Lond.*, A146:83–112, 1934.

[110] John David Jackson. *Classical electrodynamics; 2nd ed.* Wiley, New York, NY, 1975.

[111] B. Rossi. *High Energy Particles*. Prentice-Hall, Inc., Englewood Cliffs, NJ, 1952.

# Appendix A

# Particle Stopping in a White Dwarf

Here we provide a more detailed analysis of the stopping power (energy loss per distance traveled) of high-energy SM particles in a carbon-oxygen WD due to strong and electromagnetic interactions. We consider incident electrons, photons, pions, and nucleons with kinetic energy greater than an MeV.

## A.1 WD Medium

For the WD masses that we consider, the stellar medium consists of electrons and fully-ionized carbon nuclei with central number densities in the range $n_e = Z n_{\rm ion} \sim 10^{31} - 10^{33}$ cm$^{-3}$ where $Z = 6$. The internal temperature is $T \sim$ keV [32]. The electrons are a degenerate and predominantly relativistic free gas, with Fermi energy

$$E_F = (3\pi^2 n_e)^{1/3} \sim 1 - 10 \text{ MeV}. \tag{A.1}$$

The carbon ions, however, are non-degenerate and do not form a free gas. The plasma frequency due to ion-ion Coulomb interactions is given by

$$\Omega_p = \left( \frac{4\pi n_{\rm ion} Z^2 \alpha}{m_{\rm ion}} \right)^{1/2} \sim 1 - 10 \text{ keV}, \tag{A.2}$$

where $m_{\rm ion}$ is the ion mass. Finally, the medium also contains thermal photons, though these are never significant for stopping particles as the photon number density $n_\gamma \sim T^3$ is much smaller than that of electrons or ions.

## A.2 Nuclear Interactions

**Elastic Scattering of Hadrons.** Hadrons with energy less than the nuclear binding energy $E_{\rm nuc} \sim 10$ MeV will predominantly stop due to elastic nuclear scatters with ions. These

are hard scatters, resulting in a stopping power

$$\frac{dE}{dx} \sim n_{\rm ion}\sigma_{\rm el}\left(\frac{m}{m_{\rm ion}}\right)E \tag{A.3}$$

for a hadron of mass $m \ll m_{\rm ion}$ and kinetic energy $E$. $\sigma_{\rm el}$ is the elastic nuclear scattering cross section, which is of order $\sigma_{\rm el} \approx$ b at these energies and drops to $\sigma_{\rm el} \approx 0.1$ b above 10 MeV [105], ignoring the nontrivial effect of nuclear resonances in the intermediate regime $1 - 10$ MeV.

**Inelastic Scattering of Hadrons.** For energies above $E_{\rm nuc}$, the stopping of hadrons is dominated by inelastic nuclear scatters. In such a collision, an incoming hadron interacts with one or more nucleons to produce a $\mathcal{O}(1)$ number of additional hadrons which approximately split the initial energy. At incident energy greater than $\sim$ GeV, the majority of secondary hadrons are pions with transverse momenta $\sim 100$ MeV [105]. Below $\sim$ GeV, it is found that roughly equal fractions of protons, neutrons, and pions are produced in each collision [106]. We will thus have a roughly collinear shower terminating at an energy $\sim 10$ MeV which consists of pions for most of the shower's development and converts to an mix of pions and nucleons in the final decade of energy. This cascade is described by a radiative stopping power

$$\frac{dE}{dx} \sim n_{\rm ion}\sigma_{\rm inel}E, \tag{A.4}$$

where the inelastic nuclear cross section is given by $\sigma_{\rm inel} \approx 100$ mb and roughly constant in energy [105]. The total length of the shower is only logarithmically dependent on the initial hadron energy $E$,

$$X_{\rm had} \sim \frac{1}{n_{\rm ion}\sigma_{\rm inel}}\log\left(\frac{E}{E_{\rm nuc}}\right). \tag{A.5}$$

**Photonuclear Interactions.** Photons of energy greater than 10 MeV can also strongly interact with nuclei through the production of virtual quark-antiquark pairs. This is the dominant mode of photon energy loss at high energy. The photonuclear scatter destroys the photon and fragments the nucleus, producing secondary hadrons in a shower analogous to that described above. The photonuclear cross section $\sigma_{\gamma A}$ is roughly given by $\sigma_{\gamma A} \approx \alpha\sigma_{\rm inel}$, again ignoring the nuclear resonances that occur for $E \lesssim$ GeV [105]. For $E \gtrsim$ GeV, $\sigma_{\gamma A}$ is likely a slowly increasing function of energy due to the coherent interaction of the photon over multiple nucleons [107], however, instead of extrapolating this behavior we conservatively take a constant photonuclear cross section $\sigma_{\gamma A} \approx 1$ mb.

**Electronuclear Interactions.** Electrons can similarly lose energy to nuclei by radiating a virtual photon that undergoes a photonuclear scatter, which indeed provides the dominant energy loss for high energy electrons. The cross section for this process is roughly given by

the photonuclear cross section, scaled by a factor representing the probability to radiate such a photon. This can be estimated with the Weizsacker-Williams approximation, which gives a stopping power that is suppressed from the photonuclear result by $\alpha$ but enhanced by an $\mathcal{O}(10)$ logarithmic phase space factor [107]:

$$\frac{dE}{dx} \sim \alpha \, n_{\text{ion}} \sigma_{\gamma A} E \log\left(\frac{E}{m_e}\right). \tag{A.6}$$

Unlike the photonuclear interaction, the electronuclear event is a radiative process that preserves the original electron while leaving hadronic showers in its wake.

## A.3 Radiative Processes

Electromagnetic showers due to successive bremsstrahlung and pair production events off carbon ions are the dominant stopping mechanisms for intermediate-energy electrons and photons. Both of these processes result in radiative stopping powers, derived semi-classically as [108]

$$\frac{dE}{dx} \sim \frac{E}{X_0}, \qquad X_0^{-1} = 4 n_{\text{ion}} Z^2 \frac{\alpha^3}{m_e^2} \log\Lambda. \tag{A.7}$$

$X_0$ is the well-known radiation length, and $\log\Lambda$ is a Coulomb form factor given by the range of effective impact parameters $b$:

$$\Lambda = \frac{b_{\text{max}}}{b_{\text{min}}}. \tag{A.8}$$

The maximal impact parameter is set by the plasma screening length (see A.4) and the minimum by the electron mass, below which the semi-classical description breaks down. Note that for the highest WD densities $\Lambda \lesssim 1$, in which case (A.7) ought be replaced by a fully quantum mechanical result as in [109]. This still results in a radiative stopping power, and so for simplicity we employ (A.7) with $\log\Lambda \sim \mathcal{O}(1)$ for all WD densities.

**LPM Suppression** A radiative event involving momentum transfer $q$ to an ion must, quantum mechanically, occur over a length $\sim q^{-1}$. All ions within this region contribute to the scattering of the incident particle, and for sufficiently small $q$ this results in a decoherence that suppresses the formation of photons or electron-positron pairs. This is the "Landau-Pomeranchuk-Midgal" (LPM) effect. The momentum transfer $q$ in a given event decreases with increasing incident particle energy, and so the LPM effect will suppress radiative processes for energies greater than some scale $E_{\text{LPM}}$. This can be calculated semi-classically [108],

$$E_{\text{LPM}} = \frac{m_e^2 X_0 \alpha}{4\pi} \approx 1 \text{ MeV} \left(\frac{10^{32}\text{cm}^{-3}}{n_{\text{ion}}}\right). \tag{A.9}$$

which is quite small due to the high ion density in the WD. The stopping power for bremsstrahlung and pair production in the regime of LPM suppression $E > E_{\rm LPM}$ is

$$\frac{dE}{dx} \sim \frac{E}{X_0}\left(\frac{E_{\rm LPM}}{E}\right)^{1/2} \qquad E > E_{\rm LPM}. \tag{A.10}$$

In addition to the LPM effect, soft bremsstrahlung may be suppressed in a medium as the emitted photon acquires an effective mass of order the plasma frequency $\Omega_p$. However, for high-energy electrons this dielectric suppression only introduces a minor correction to (A.10), in which soft radiation is already suppressed [108].

## A.4 Elastic EM Scattering

**Electron Coulomb Scattering off Ions.** Coulomb collisions with ions are the mechanism by which electrons of energy $1-10$ MeV ultimately thermalize ions. In this scenario we may treat the ions as stationary and ignore their recoil during collisions. The nuclear charge will be screened by the mobile electrons of the medium, so incident particles scatter via a potential

$$V(\mathbf{r}) = \frac{Z\alpha}{r}e^{-r/\lambda_{\rm TF}}. \tag{A.11}$$

The screening length $\lambda_{\rm TF}$ is given in the Thomas-Fermi approximation by [96]:

$$\lambda_{\rm TF}^2 = \frac{E_F}{6\pi\alpha n_e} \sim \frac{1}{\alpha E_F^2}. \tag{A.12}$$

This plasma screening suppresses scatters with momentum transfers below $\sim \lambda_{\rm TF}^{-1}$, corresponding to a minimal energy transfer of $\omega_{\rm min} = \lambda_{\rm TF}^{-2}/2m_{\rm ion}$. Ions may in principle also cause screening through lattice distortion, however this may be ignored as the sound speed of the lattice $c_s \sim 10^{-2}$ is much smaller than the speed of an incident relativistic electron. From the Born approximation, the cross section for energy transfer $\omega$ is

$$\frac{d\sigma}{d\omega} = \frac{2\pi Z^2\alpha^2}{m_{\rm ion}v_{\rm in}^2}\frac{1}{(\omega+\omega_{\rm min})^2}, \tag{A.13}$$

where $v_{\rm in}$ is the incident velocity. Thus the stopping power is

$$\frac{dE}{dx} = \int_0^{\omega_{\rm max}} d\omega\, n_{\rm ion}\frac{d\sigma}{d\omega}\omega \approx \frac{2\pi\, n_{\rm ion}Z^2\alpha^2}{m_{\rm ion}v_{\rm in}^2}\log\left(\frac{\omega_{\rm max}}{\omega_{\rm min}}\right), \tag{A.14}$$

where the second line is valid if $\omega_{\rm max} \gg \omega_{\rm min}$. $\omega_{\rm max}$ is the maximum possible energy transfer. This may be due to 4-momentum conservation, or in the case of incident electrons, the

impossibility of scattering to a final energy less than $E_F$. 4-momentum conservation sets an upper bound $\omega_{\rm kin}$, which for a stationary target is

$$\omega_{\rm kin} = \frac{2m_{\rm ion}p^2}{m_{\rm ion}^2 + m^2 + 2Em_{\rm ion}}, \tag{A.15}$$

with $p$, $E$ the incoming momentum and energy. The Fermi upper bound is $\omega_F = E - E_F$ so for incident electrons we take $\omega_{\rm max} = \min\{\omega_{\rm kin}, \omega_F\}$.

For scatters that transfer energy less than the plasma frequency $\Omega_p$, one may be concerned about phonon excitations. This occurs for incident electrons with energy below $\sim 10$ MeV. We estimate this stopping power treating each ion as an independent oscillator with frequency $\Omega_p$ (an Einstein solid approximation) and compute the stopping power due to scatters which excite a single oscillator quanta. There are two key differences between this and the free ion case: incident particles must transfer an energy $\Omega_p$, and the cross section to transfer momentum $q$ is suppressed by a factor $q^2/2m_{\rm ion}\Omega_p = \omega_{\rm free}/\Omega_p$. $\omega_{\rm free}$ is the energy transfer that would accompany a free ion scatter with momentum transfer $q$. The resulting stopping power is unchanged from the free case (A.14), as the increased energy transfer compensates for the suppressed cross section.

As electrons transfer their energy at the rate (A.14), they occasionally experience a hard scatter with mean free path

$$\lambda_{\rm hard} \approx \frac{p^2 v_{\rm in}^2}{\pi n_{\rm ion} Z^2 \alpha^2}. \tag{A.16}$$

For sufficiently small incident energies, the electron experiences several hard scatters before it has deposited its energy by elastic scatters, and the stopping length is reduced by the resulting random walk. This effect is not significant for incident pions due to their larger mass.

Finally, we note that for highly energetic incident particles the cross section (A.13) should be modified to account for the recoil of the ion. However, at such energies the dominant stopping power will be from hadronic or electromagnetic showers anyway, so we do not include these recoil effects.

**Relativistic Coulomb Scattering off Electrons.** The scattering of incident electrons off degenerate electrons determines the termination energy of electromagnetic showers. This calculation demands two considerations not present when scattering off ions: the targets are not stationary and they require a threshold energy transfer in order to be scattered out of the Fermi sea. However for relativistic incident particle, with momentum $p \gg p_F$, the stopping power off electrons is ultimately of the same form as the stopping power off ions (A.14). In this limit, all particle velocities and the relative velocity is $\mathcal{O}(1)$, and the deflection of the incident particle will generally be small. It is reasonable then that scattering proceeds, up to $\mathcal{O}(1)$ factors, as though a heavy incident particle is striking a light, stationary target. The

cross section is given by the usual result,

$$\frac{d\sigma}{d\omega} \approx \frac{2\pi\alpha^2}{E_F}\frac{1}{\omega^2}, \tag{A.17}$$

where we have accounted for the target's motion by replacing its mass with its relativistic inertia $\approx E_F$. This is equivalent to a boost of the cross section from the rest frame of the target into the WD frame. Note that plasma screening can be ignored in this case, as Pauli-blocking will provide a more stringent cutoff on soft scatters. Scatters which transfer an energy $\omega \leq E_F$ will have a suppressed contribution to the stopping power as they can only access a fraction of the Fermi sea. In this limit it is sufficient to ignore these suppressed scatters:

$$\frac{dE}{dx} = \int_{E_F}^{\omega_{\rm max}} d\omega\, n_e \frac{d\sigma}{d\omega}\omega \approx \frac{2\pi\, n_e\alpha^2}{E_F}\log\left(\frac{\omega_{\rm max}}{E_F}\right) \tag{A.18}$$

where, as described above, $\omega_{\rm max} = \min\{\omega_{\rm kin}, \omega_F\}$. This derivation is admittedly quite heuristic, and so it has been checked with a detailed numerical calculation accounting fully for the target's motion and degeneracy. Equation (A.18) is indeed a good approximation to the stopping power for incident energies larger than the Fermi energy.

**Non-Relativistic Coulomb Scattering off Electrons** For non-relativistic incident particles, the Coulomb stopping off electrons becomes strongly suppressed due to degeneracy. Stopping in this limit appears qualitatively different than in the typical case—the slow incident particle is now bombarded by relativistic electrons from all directions. Note that only those scatters which slow the incident particle are allowed by Pauli-blocking.

As the electron speeds are much faster than the incident, a WD electron with momentum $p_F$ will scatter to leading order with only a change in direction, so the momentum transfer is $|\vec{q}| \sim p_F$. We again take the incident momentum $p \gtrsim p_F$, which is valid for all incident particles we consider. This results in an energy transfer

$$\omega = \left|\frac{p^2}{2m} - \frac{(\vec{p}-\vec{q})^2}{2m}\right| \sim v_{\rm in} E_F. \tag{A.19}$$

For $v_{\rm in} \ll 1$ the energy transfer is less than Fermi energy, so Pauli-blocking will be important. The incident particle is only be able to scatter from an effective electron number density

$$n_{\rm eff} = \int_{E_F-\omega}^{E_F} g(E)\, dE \approx 3 n_e \frac{\omega}{E_f}, \tag{A.20}$$

where $g(E)$ is the Fermi density of states. At leading order the electron is not aware of the small incident velocity, so the cross section is given by relativistic Coulomb scattering off a stationary target $\sigma \sim \alpha^2/q^2$ [110]. The incident particle thus loses energy to degenerate electrons at a rate:

$$\frac{dE}{dt} \sim n_{\rm eff}\, \sigma\, \omega \sim n_e \frac{\alpha^2}{E_F} v_{\rm in}^2. \tag{A.21}$$

Note that this includes a factor of the relative velocity which is $\mathcal{O}(1)$. As a result, the stopping power is parametrically

$$\frac{dE}{dx} = \frac{1}{v_{\rm in}}\frac{dE}{dt} \sim n_e \frac{\alpha^2}{E_F} v_{\rm in}. \tag{A.22}$$

As above, this heuristic result has been verified with a full integration of the relativistic cross section.

We can compare (A.22) to the stopping power of non-relativistic, heavy particles off roughly stationary, non-degenerate electrons $\frac{dE}{dx} \sim n_e \frac{\alpha^2}{m_e v_{\rm in}^2}$, which is the familiar setting of stopping charged particles in a solid due to ionization [111]. Evidently, the analogous stopping in a WD is parametrically suppressed by $v_{\rm in}^3 m_e/E_F$. One factor of $v_{\rm in}$ is due to Pauli blocking, while the other factors are kinematic, due to the relativistic motion of the targets.

**Compton Scattering** Compton scattering off degenerate electrons is the dominant interaction for photons of incident energy $k \leq E_F$. As we will show, this stopping power is parametrically different from that of high-energy photons due to Pauli-blocking and the motion of the electron. For $k > E_F$, the effect of Pauli-blocking is negligible and the stopping power is simply:

$$\frac{dk}{dx} \sim \frac{\pi\alpha^2 n_e}{E_F} \log\left(\frac{k}{m_e}\right), \tag{A.23}$$

where again we have (partially) applied the heuristic $m_e \to E_F$ replacement to boost the usual result for stationary electrons while avoiding divergence at the Fermi energy. This, along with the low-energy estimate below, matches a full integration of the relativistic cross section well.

We now turn to the regime of interest, $k < E_F$. Only those electrons near the top of the Fermi sea are available to scatter, so the photon interacts with only the effective electron density (A.20). In addition, Compton scatters will only occur off electrons moving roughly collinear with the photon momentum - a head-on collision would result in an energy loss for the electron, which is forbidden by Pauli exclusion. In the electron rest frame these collinear scatters are Thompson-like, and the photon energy loss is dominated by backward scatters. For relativistic electrons near the Fermi surface, these scatters transfer an energy

$$\omega \sim k\left(1 - \frac{m_e^2}{4E_F^2}\right) \approx k. \tag{A.24}$$

The cross section can be taken in the electron rest frame $\sigma \sim \alpha^2/m_e^2$, along with an 'aiming' factor $1/4\pi$ to account for the restriction to initially parallel trajectories. This gives a stopping power

$$\frac{dk}{dx} \approx \frac{\alpha^2 n_e k^2}{4\pi m_e^2 E_F}. \tag{A.25}$$

# Appendix B

# Dark Matter Capture

Here we give a more detailed discussion of DM capture in a WD and its subsequent evolution. For the remainder of this section all numerical quantities are evaluated at a central WD density $\rho_{\rm WD} \sim 3 \times 10^8 \frac{\rm g}{\rm cm^3}$ ($n_{\rm ion} \sim 10^{31}$ cm$^{-3}$), for which the relevant WD parameters are [27]: $M_{\rm WD} \approx 1.25\, M_\odot$, $R_{\rm WD} \approx 4000$ km, and $v_{\rm esc} \approx 2 \times 10^{-2}$. Depending on the context, the relevant density may be the average value which we take to be $\sim 10^{30}$ cm$^{-3}$. We also assume an average value of the WD temperature $T_{\rm WD} \sim$ keV.

## B.1 Capture Rate

Consider spin-independent DM elastic scattering off ions with cross section $\sigma_{\chi A}$. This is related to the per-nucleon cross section

$$\sigma_{\chi A} = A^2 \left(\frac{\mu_{\chi A}}{\mu_{\chi n}}\right)^2 F^2(q) \sigma_{\chi n} = A^4 F^2(q) \sigma_{\chi n}, \tag{B.1}$$

where $F^2(q)$ is the Helm form factor [85]. If the DM is at the WD escape velocity, the typical momentum transfer to ions is $q \sim \mu_{\chi A} v_{\rm esc} \sim 200$ MeV. As this $q$ is less than or of order the inverse nuclear size, DM scattering off nuclei will be coherently enhanced. We find $F^2(q) \approx 0.1$ for $q \sim 200$ MeV.

For the DM to ultimately be captured, it must lose energy $\sim m_\chi v^2$, where $v$ is the DM velocity (in the rest frame of the WD) asymptotically far away. Since typically $v \ll v_{\rm esc}$, the DM has velocity $v_{\rm esc}$ while in the star and must lose a fraction $(v/v_{\rm esc})^2$ of its kinetic energy to become captured. Properly, the DM velocity is described by a boosted Maxwell distribution peaked at the galactic virial velocity $v_{\rm halo} \sim 10^{-3}$. However, this differs from the ordinary Maxwell distribution by only $\mathcal{O}(1)$ factors [31], and we can approximate it by (ignoring the exponential Boltzmann tail):

$$\frac{dn_\chi}{dv} \approx \begin{cases} \frac{\rho_\chi}{m_\chi} \left(\frac{v^2}{v_{\rm halo}^3}\right) & v \le v_{\rm halo} \\ 0 & v > v_{\rm halo} \end{cases}. \tag{B.2}$$

The DM capture rate is given by an integral of the DM transit rate weighted by a probability for capture $P_{\rm cap}$

$$\Gamma_{\rm cap} \sim \int dv \frac{d\Gamma_{\rm trans}}{dv} P_{\rm cap}(v), \tag{B.3}$$

where the (differential) transit rate is

$$\frac{d\Gamma_{\rm trans}}{dv} \sim \frac{dn_\chi}{dv} R_{\rm WD}^2 \left(\frac{v_{\rm esc}}{v}\right)^2 v. \tag{B.4}$$

$P_{\rm cap}$ depends on both the *average* number of scatters in a WD

$$\overline{N}_{\rm scat} \sim n_{\rm ion} \sigma_{\chi A} R_{\rm WD}, \tag{B.5}$$

and the number of scatters *needed* for capture

$$N_{\rm cap} \sim \max\left\{1, \frac{m_\chi v^2}{m_{\rm ion} v_{\rm esc}^2}\right\}, \tag{B.6}$$

and is most generally expressed as a Poisson sum

$$P_{\rm cap} = 1 - \sum_{n=0}^{N_{\rm cap}-1} \exp(-\overline{N}_{\rm scat}) \frac{(\overline{N}_{\rm scat})^n}{n!}. \tag{B.7}$$

For our purposes we will approximate the sum as follows:

$$P_{\rm cap} \approx \begin{cases} 1 & \overline{N}_{\rm scat} > N_{\rm cap} \\ \overline{N}_{\rm scat} & \overline{N}_{\rm scat} < N_{\rm cap} \text{ and } N_{\rm cap} = 1 \\ 0 & \text{else} \end{cases}. \tag{B.8}$$

Here we ignore the possibly of capture if $\overline{N}_{\rm scat} < N_{\rm cap}$ except in the special case that only one scatter is needed for capture. If $\overline{N}_{\rm scat} > N_{\rm cap}$, we assume all DM is captured. Most accurately, this capture rate should be computed numerically, e.g. see [87]. However with the above simplifications we find that the capture rate is of order

$$\Gamma_{\rm cap} \sim \Gamma_{\rm trans} \cdot \min\left\{1, \overline{N}_{\rm scat} \min\{B, 1\}\right\}, \quad B \equiv \frac{m_{\rm ion} v_{\rm esc}^2}{m_\chi v_{\rm halo}^2}. \tag{B.9}$$

$B$ here encodes the necessity of multiple scattering for capture. For ultra-heavy DM $m_\chi > 10^{15}$ GeV, $B \ll 1$ and essentially multiple scatters are always needed.

## B.2 Thermalization and Collapse

Once DM is captured, it thermalizes to an average velocity

$$v_{\rm th} \sim \sqrt{\frac{T_{\rm WD}}{m_\chi}} \approx 10^{-11} \left(\frac{m_\chi}{10^{16}\ {\rm GeV}}\right)^{-1/2}, \tag{B.10}$$

and settles to the thermal radius

$$R_{\rm th} \sim \left(\frac{T_{\rm WD}}{G m_\chi \rho_{\rm WD}}\right)^{1/2} \approx 0.1\ {\rm cm} \left(\frac{m_\chi}{10^{16}\ {\rm GeV}}\right)^{-1/2},$$

where its kinetic energy balances against the gravitational potential energy of the (enclosed) WD mass. This thermalization time can be explicitly calculated for elastic nuclear scatters [62]. The stopping power due to such scatters is

$$\frac{dE}{dx} \sim \rho_{\rm WD} \sigma_{\chi A}\, v\, \max\{v, v_{\rm ion}\}, \tag{B.11}$$

where $v_{\rm ion} \sim \sqrt{T_{\rm WD}/m_{\rm ion}}$ is the thermal ion velocity. The max function indicates the transition between "inertial" and "viscous" drag, as the DM velocity $v$ slows to below $v_{\rm ion}$. DM first passes through the WD many times on a wide orbit until the size of its orbit decays to become contained in the star. The timescale for this process is

$$\begin{aligned} t_1 &\sim \left(\frac{m_\chi}{m_{\rm ion}}\right)^{3/2} \frac{R_{\rm WD}}{v_{\rm esc}} \frac{1}{\overline{N}_{\rm scat}} \frac{1}{\max\{\overline{N}_{\rm scat}, 1\}^{1/2}} \\ &\approx 7 \times 10^{16}\ {\rm s} \left(\frac{m_\chi}{10^{16}\ {\rm GeV}}\right)^{3/2} \left(\frac{\sigma_{\chi A}}{10^{-35}\ {\rm cm}^2}\right)^{-3/2}. \end{aligned} \tag{B.12}$$

Subsequently, the DM completes many orbits within the star until dissipation further reduces the orbital size to the thermal radius. The timescale for this process is

$$\begin{aligned} t_2 &\sim \left(\frac{m_\chi}{m_{\rm ion}}\right) \frac{1}{n_{\rm ion} \sigma_{\chi A}} \frac{1}{v_{\rm ion}} \\ &\approx 10^{14}\ {\rm s} \left(\frac{m_\chi}{10^{16}\ {\rm GeV}}\right) \left(\frac{\sigma_{\chi A}}{10^{-35}\ {\rm cm}^2}\right)^{-1}. \end{aligned} \tag{B.13}$$

There is an additional $\mathcal{O}(10)$ logarithmic enhancement of the timescale once the DM velocity has slowed below $v_{\rm ion}$. Note that time to complete a single orbit is set by the gravitational free-fall timescale:

$$t_{\rm ff} \sim \sqrt{\frac{1}{G\rho_{\rm WD}}} \approx 0.5\ {\rm s}. \tag{B.14}$$

In the above description, we have assumed that the DM loses a negligible amount of energy during a single transit:

$$\frac{\sigma_{\chi A}}{m_\chi} \ll \frac{1}{\rho_{\rm WD} R_{\rm WD}}. \tag{B.15}$$

This also ensures that the dynamics of DM within the star is that of Newtonian gravity along with a small drag force. In the opposite regime, the qualitative evolution of captured DM differs from the picture presented in detail below. In this case there is no stage of external orbital motion corresponding to $t_1$—DM will instead rapidly thermalize to a speed $v_{\rm th}$ after entering the star. The internal motion now proceeds as a gravitationally-biased random walk, with a net drift of DM towards the center of the star. For sufficiently large $\sigma_{\chi A}$, DM will collect at a radius $r_{\rm c}$ which is larger than $r_{\rm th}$ given above, due to a balance of gravity with outward Brownian diffusion. This may delay the onset of self-gravitation, possibly beyond $\tau_{\rm WD}$, as we now require the collection of a larger mass $\rho_{\rm WD} r_{\rm c}^3$. It is important to note that the differences between the Brownian and orbital regimes are immaterial for constraints on the decay of captured DM (e.g., Fig. 2.11), which cares only about the quantity of DM present in the star. For annihilation constraints, however, the internal evolution of DM is quite important. For the largest unconstrained cross sections $\sigma_{\chi A}$ (see Fig. 2.9), one can check that captured DM is distributed across a large fraction of the star due to Brownian motion and does not collapse. This DM population still yields a strong constraint on $\sigma_{\chi\chi}$, similar to but somewhat weaker than the constraints which can be placed on DM that undergoes self-gravitational collapse after capture (e.g., Fig. 2.10).

When Brownian motion is insignificant, the DM will begin steadily accumulating at $R_{\rm th}$ after a time $t_1 + t_2$. Once the collected mass of DM at the thermal radius exceeds the WD mass within this volume, there is the possibility of self-gravitational collapse. The time to collect a critical number $N_{\rm sg}$ of DM particles is

$$t_{\rm sg} \sim \frac{N_{\rm sg}}{\Gamma_{\rm cap}} \sim \frac{\rho_{\rm WD} R_{\rm th}^3}{m_\chi \Gamma_{\rm cap}} \approx 10^{10}\ {\rm s} \left(\frac{m_\chi}{10^{16}\ {\rm GeV}}\right)^{-1/2} \left(\frac{\sigma_{\chi A}}{10^{-35}\ {\rm cm}^2}\right)^{-1} \tag{B.16}$$

Typically, the timescale for collapse is then set by the DM sphere's ability to cool and shed gravitational potential energy. This is initially just $t_2$, while the time to collapse at any given radius $r$ decreases once the DM velocity rises again above $v_{\rm ion}$:

$$t_{\rm cool} \sim t_2 {\rm min}\{v_{\rm ion}/v_\chi, 1\}, \quad v_\chi \sim \sqrt{\frac{GNm_\chi}{r}}, \tag{B.17}$$

where $N$ is the number of collapsing DM particles. Note that when $m_\chi > 10^{21}$ GeV, the number of particles necessary for self-gravitation $N_{\rm sg}$ as defined in (B.16) is less than 2. In this case we should formally take $N_{\rm sg} = 2$.

Finally, there is a further subtlety that arises in the growing of DM cores for the large DM masses $m_\chi$ of interest to us. The time $t_{\rm sg}$ to collect a self-gravitating number of particles decreases for larger DM masses. However, the dynamics of the collapse are set by the cooling time, which is initially $t_{\rm cool} \propto m_\chi$. For $m_\chi > 10^{15}$ GeV, the collection time may be shorter than the cooling time $t_{\rm sg} < t_{\rm cool}$ (depending on the cross section). In fact, the collection time may even be shorter than the dynamical time $t_{\rm ff}$. If $t_{\rm ff} < t_{\rm sg} < t_{\rm cool}$, the DM core will be driven to shrink because of the gravitational potential of the over-collecting DM. The timescale for the shrinking is set by the capture rate of DM. Ultimately, the collapsing DM

core will consist of $N_{\rm sg}$ enveloped in a "halo" of $\Gamma_{\rm cap} t_{\rm cool} \gg N_{\rm sg}$ particles, which will also proceed to collapse. If instead $t_{\rm sg} < t_{\rm ff} < t_{\rm cool}$, the DM core will rapidly accumulate to this large number before dynamically adjusting. For the purpose of the collapse constraints on DM annihilation, if $t_{\rm sg} < t_{\rm cool}$ we will simply assume a number of collapsing particles $N = \Gamma_{\rm cap} t_{\rm cool}$. This is the case for the constraints plotted in Fig. 2.10.